2: ☐ Analysis ☐ Engineering

3. ☒ Model

☐ Performance Assessment

☐ Scientific

☒ Conceptual Model Documentation

☒ Model Documentation

☒ Model Validation Documentation

4. Title:

Seepage Calibration Model and Seepage Testing Data

5. Document Identifier (including Rev. No. and Change No., if applicable):

MDL-NBS-HS-000004 REV00

6. Total Attachments:

2

7. Attachment Numbers - No. of Pages in Each:

Attachment I-12

Attachment II-8

		Printed Name	Signature	Date
8.	Originator	S. Finsterle	*V. Finsterle*	1/28/00
		R.C. Trautz	*R.C. Trautz*	1/28/00
9.	Checker	R. Stover	*R Stover*	1/28/00
		T.M. Bandurraga	*Bo Bo... for McG Bodvarsson*	1/28/00
10.	Lead/Supervisor	G.S. Bodvarsson	*Bo Bo...*	1/28/00
11.	Responsible Manager	D. Hoxie	*Hoxie*	01-31-00

12. Remarks:

Block 8: This AMR was prepared by S. Finsterle except for Section 6.2, which was prepared by R.C. Trautz.

Block 9: This AMR was checked by R. Stover, except for Sections 5.3, 6.3, 6.4, and 6.5, which were checked by T.M. Bandurraga.

INFORMATION COPY

LAS VEGAS DOCUMENT CONTROL

NMSS07

2. Analysis or Model Title:

Seepage Calibration Model and Seepage Testing Data

3. Document Identifier (including Rev. No. and Change No., if applicable):

MDL-NBS-HS-000004 REV00

4. Revision/Change No.	5. Description of Revision/Change
00	Initial Issue

DISCLAIMER

This contractor document was prepared for the U.S. Department of Energy (DOE), but has not undergone programmatic, policy, or publication review, and is provided for information only. The document provides preliminary information that may change based on new information or analysis, and represents a conservative treatment of parameters and assumptions to be used specifically for Total System Performance Assessment analyses. The document is a preliminary lower level contractor document and is not intended for publication or wide distribution.

Although this document has undergone technical reviews at the contractor organization, it has not undergone a DOE policy review. Therefore, the views and opinions of authors expressed may not state or reflect those of the DOE. However, in the interest of the rapid transfer of information, we are providing this document for your information per your request.

CONTENTS

Page

INTENTIONALLY LEFT BLANK

FIGURES

FIGURES (Continued)

Page

TABLES

Page

INTENTIONALLY LEFT BLANK

ACRONYMS

2D	two-dimensional, two dimensions
3D	three-dimensional, three dimensions
ACC	Accession Number
AEP	Air-Entry Pressure
AMR	Analysis/Model Report
AP	Administrative Procedure (DOE)
BL	bottom left
BR	bottom right
cdf	cumulative distribution function
CFR	Code of Federal Regulations
DFM	Discrete Feature Model
DFNM	Discrete Fracture Network Model
DIRS	Document Input Reference Sheet
DOE	Department of Energy
DTN	Data Tracking Number
ESF	Exploratory Studies Facility
FCM	Fracture Continuum Model
FY	Fiscal Year
kg	kilogram
L	left
LBNL	Lawrence Berkeley National Laboratory
m	meters
M	middle
ML	middle left
mm	millimeters
MR	middle right
M&O	Management and Operating Contractor
OCRWM	Office of Civilian Radioactive Waste Management
Pa	Pascal
PA	Performance Assessment
Q	Qualified
QA	Quality Assurance
QAP	Quality Administrative Procedure (M&O)

ACRONYMS (Continued)

QARD	Quality Assurance Requirements and Description
QIP	Quality Implementing Procedure
R	right
s	second
SCM	Seepage Calibration Model
SN	Scientific Notebook
STN	Software Tracking Number
TBD	To Be Determined
TBV	To Be Verified
TDMS	Technical Data Management System
TSw	Topopah Spring welded unit
UL	upper left
UM	upper middle
UR	upper right
U.S.	United States
UZ	Unsaturated Zone
YMP	Yucca Mountain Site Characterization Project

1. PURPOSE

The purpose of this Analysis/Model Report (AMR) is to document the development of the Seepage Calibration Model (SCM) based on available seepage testing data. The SCM is a template fracture continuum model that is developed based on air-permeability and liquid-release test data from the experiments performed in Niche 3650 of the Exploratory Studies Facility (ESF) at Yucca Mountain, Nevada. The SCM provides a methodological and conceptual basis for the subsequent development of drift-scale seepage models.

Specific objectives of this work activity are to evaluate inflow rates into drifts and seepage thresholds based on seepage testing data from the niche studies. The potential of an underground opening to act as a capillary barrier, which limits or precludes seepage of water into drifts, is also evaluated. Inverse modeling is used to calibrate the SCM and to estimate seepage-relevant, model-related parameters. The accuracy of the derived parameters is estimated based on the goodness-of-fit to the observed data and the sensitivity of calculated seepage with respect to the parameters of interest. The SCM is validated against liquid-release test data that were not used for the calibration of the model. Linear uncertainty propagation analyses and Monte Carlo simulations are performed to evaluate prediction uncertainty.

The scope of this AMR is limited to an analysis of liquid-release test data from Niche 3650. The parameters estimated and seepage percentages predicted by the SCM are therefore only applicable to an uncollapsed excavation with the geometry of Niche 3650 under ambient temperature conditions. Moreover, these parameters are restricted to the middle nonlithophysal zone of the Topopah Spring Tuff at Yucca Mountain.

This AMR is written in accordance with the Development Plan (CRWMS M&O 1999c) in support of the following project activities:

- Performance Assessment (PA)

- Seepage Model for PA

- Drift-Scale Coupled Processes Models

- Abstraction of Drift Seepage and Drift-Scale Coupled Processes

- Process Model Report (PMR) for the 3D site-scale unsaturated zone flow and transport model of Yucca Mountain, Nevada (UZ Model)

INTENTIONALLY LEFT BLANK

2. QUALITY ASSURANCE

This AMR was developed in accordance with AP-3.10Q, *Analyses and Models*. Other applicable Department of Energy (DOE) Office of Civilian Radioactive Waste Management (OCRWM) Administrative Procedures (APs) and YMP-LBNL Quality Implementing Procedures (QIPs) are identified in the AMR Development Plan (CRWMS M&O 1999c).

The activities documented in this AMR were evaluated with other related activities in accordance with QAP-2-0, *Conduct of Activities*, and were determined to be subject to the requirements of the U.S. DOE Office of Civilian Radioactive Waste Management (OCRWM) *Quality Assurance Requirements and Description* (QARD) (DOE 1998). This evaluation is documented in CRWMS 1999a, b; and Wemheuer 1999 (*Activity Evaluation for Work Package WP 1401213UM1*).

Scientific Notebooks (SN) used for the modeling activities described in this AMR are listed in Table 1.

Table 1. Scientific Notebooks

Scientific Notebook	Page numbers	Owner	YMP M&O SNR	Accession number
YMP-LBNL-SAF-1	1–150	S. Finsterle	SN-LBNL-SCI-087-V1	MOL.19990723.0301
YMP-LBNL-SAF-2	1–27	S. Finsterle	SN-LBNL-SCI-171-V1	MOL.19990812.0357
YMP-LBNL-RCT-DSM-1	1–37	R.C. Trautz	SN-LBNL-SCI-157-V1	MOL.19990923.0302

INTENTIONALLY LEFT BLANK

3. COMPUTER SOFTWARE AND MODEL USAGE

The software codes and routines listed in Table 2 were used in support of this AMR. The software codes iTOUGH2, SISIM, GAMV2, and EXT are obtained from software configuration management in accordance with AP-SI.1Q, *Software Management*. The software is appropriate for the intended application, and was used only within the range of validation in accordance with applicable software procedures. The software routines are documented in the records listed by accession number in Table 2.

All computer codes listed in Table 2 were installed on hydra, a Sun SPARC multiprocessor workstation running under Unix operating system Solaris. Installation is documented in YMP-LBNL-SAF-1, p. 5. The QA status of the software codes and software routines listed in Table 2 is indicated on the Document Input Reference Sheet (DIRS), Attachment I.

Table 2. Code Names, Versions, Traceability

Software Name	Version	Software Tracking Number or Accession Number
iTOUGH2	4.0	10003-4.0-00
GSLIB Module SISIM	1.203	10001-1.0MSISIMV1.203-00
GSLIB Module GAMV2	1.201	10087-1.0MGAMV2V1.201-00
EXT	1.0	10047-1.0-00
Routines:		
MoveMesh	1.0	ACC: MOL.19990721.0552
AddBound	1.0	ACC: MOL.19990721.0553
Perm2Mesh	1.0	ACC: MOL.19990721.0554
DelMatrix	1.0	ACC: MOL.19990721.0555
Eos9Eos3	1.0	ACC: MOL.19990721.0556
CutNiche	1.1	ACC: MOL.19990721.0557
userobs	1.01	ACC: MOL.19990721.0558

The software iTOUGH2 (iTOUGH2, V4.0, 10003-4.0-00) provides forward and inverse modeling capabilities for unsaturated and multiphase flow in fractured-porous media, and is used in this AMR for calibration, validation, and prediction runs (Sections 5.3, 6.3–6.6). The GSLIB module SISIM (SISIM, V1.203, 10001-1.0MSISIMV1.203-00) generates three-dimensional, spatially correlated random fields based on sequential indicator simulations, and is used in this AMR to generate permeability fields (Sections 5.3.2, 6.3.2). The GSLIB module GAMV2 (GAMV2, V1.201, 10087-1.0MGAMV2V1.201-00) analyzes spatial correlation of two-dimensional, irregularly spaced datasets, and is used in this AMR for the analysis of post-excavation air-permeability data (Section 6.2.3). The software EXT (EXT, V1.0, 10047-1.0-00) is used to extract data from iTOUGH2 output files for visualization with Tecplot V7.0-8-0; Tecplot visualizations are shown in Sections 5.3 and 6. The routine MoveMesh (MoveMesh, V1.0, ACC: MOL.19990721.0552) moves coordinates of a mesh file (Section 5.3, 6.3). The routine AddBound (AddBound, V1.0, ACC: MOL.19990721.0553) adds boundary elements to a mesh file (Sections 5.3, 6.3). The routine Perm2Mesh (Perm2Mesh, V1.0, ACC:

MOL.19990721.0554) maps the permeability field generated using SISIM onto a mesh file (Sections 5.3, 6.3). The routine DelMatrix (DelMatrix, V1.0, ACC: MOL.19990721.0555) reassigns permeabilities to low-permeability matrix elements (Section 5.3). The routine Eos9Eos3 (Eos9Eos3, V1.0, ACC: MOL.19990721.0556) reformats an unsaturated flow output file SAVE to a two-phase flow initial condition file INCON (Section 5.3). The routine CutNiche (CutNiche, V1.1, ACC: MOL.19990721.0557) cuts a niche from the mesh file (Sections 5.3, 6.3). The routine userobs (userobs, V1.01, ACC: MOL.19990721.0558) provides a user-specified observation type needed to estimate semivariogram parameters (Section 6.3.2).

In addition to the above, commercially available standard spreadsheet and visual display graphics programs that are exempt from software quality assurance requirements were used. EXCEL 97-SR-1 was used for spreadsheet calculations and calculations of basic statistics. Tecplot V7.0-8-0 was used for plotting and visualization of analysis results in figures shown in this report.

4. INPUTS

4.1 DATA AND PARAMETERS

The input parameters and data needed for the development of the Seepage Calibration Model are obtained from the TDMS. Specific input data sets and associated Data Tracking Numbers (DTNs) are summarized in Table 3. The QA status of the inputs listed in Table 3 is indicated on the DIRS, Attachment I.

Table 3. DTNs of Inputs Used for the Development of the Seepage Calibration Model

Data Description	DTN
Air-permeability data from air-injection testing in Niche 3650	LB980001233124.002
Liquid-release test data from Niche 3650	LB980001233124.003
Base-case hydrologic parameter set	LB997141233129.001

Reports documenting past experimental and numerical work related to drift seepage at Yucca Mountain as well as other pertinent documents are listed in Section 8.5, Supporting Bibliography. This bibliography is for information only, and this AMR does not directly rely on any of the listed documents

4.2 CRITERIA

At this time, no specific criteria (e.g., System Description Documents) have been identified as applying to this analysis and modeling activity in project requirements documents. However, this AMR provides information required in specific subparts of the proposed U.S. Nuclear Regulatory Commission rule 10 CFR 63 (see Federal Register for February 22, 1999, 64 FR 8640). It supports the site characterization of Yucca Mountain (Subpart B, Section 15), the compilation of information regarding the hydrology of the site in support of the License Application (Subpart B, Section 21(c)(1) (ii)), and the definition of hydrologic parameters used in performance assessment (Subpart E, Section 114(1)).

The DOE interim guidance (Dyer 1999), requiring the use of specified subparts of the proposed NRC high-level waste rule, 10 CFR Part 63 (64 FR 8640), was released after completion of the work documented in this AMR; it has no impact on this work activity.

4.3 CODES AND STANDARDS

No specific, formally established standards have been identified as applying to this analysis and modeling activity.

INTENTIONALLY LEFT BLANK

5. ASSUMPTIONS

5.1 INTRODUCTION

In this section, we discuss the basic assumptions of the Seepage Calibration Model (SCM). The section is structured as follows:

Section 5.2 contains a list of assumptions. Each statement of an assumption is immediately followed by the rationale as to why the assumption is considered valid or reasonable. The justification for making the continuum assumption (Assumption No. 1) required a more extensive study, which is presented in Section 5.3. This synthetic modeling study confirms that the continuum assumption is valid. At the same time, it outlines the approach and provides guidelines for deriving values of key parameters affecting seepage. This approach is followed in Section 6 where the SCM is developed and actual liquid-release test data are analyzed.

5.2 GENERAL MODELING ASSUMPTIONS

The basic assumptions of the SCM must be consistent with those of the "UZ Flow and Transport Model" and the "Seepage Model for PA," because the concepts and parameters derived with the SCM are only valid and useful for subsequent seepage calculations if they refer to similar conceptual models.

The assumptions for the SCM are stated below, followed by the basis or rationale for using them.

1. *Assumption:* It is assumed that the continuum approach is a valid concept to calculate percolation flux and drift seepage at Yucca Mountain. *Rationale:* The rationale for this assumption is presented in Section 5.3.

2. *Assumption:* Adopting the continuum approach, water flow under unsaturated conditions is assumed to be governed by Richards' equation (Richards 1931, pp. 218–233). *Rationale:* This general concept is believed reasonable for unsaturated water flow through both porous matrix and fractures. Richards' equation simply states that water flows under the combined effect of gravitational and capillary forces, and that flow resistance is a function of saturation.

3. *Assumption:* Permeabilities determined from air-injection tests are assumed to be representative of the hydraulic conductivity of the formation. *Rationale:* The assumption is believed to hold for the purposes of the current application, where air-permeability estimates are only used to condition the generation of a spatially correlated, random permeability field. Potential inaccuracies in this assumption are compensated for through the estimation of the van Genuchten $1/\alpha$ parameter (Luckner et al. 1989, pp. 2191–2192), which is correlated to permeability.

4. *Assumption:* Relative permeability and capillary pressure are assumed to be described as continuous functions of effective liquid saturation, following the expressions given by the van Genuchten-Mualem model (Luckner et al. 1989, pp. 2191–2192) as implemented in the iTOUGH2 code (Finsterle 1997, p. 224). *Rationale:* The van Genuchten-Mualem

model is the standard model used in the suite of UZ flow and transport models; it was chosen here for consistency. Furthermore, the applicability of relative permeability and capillary pressure functions is consistent with the continuum assumption and seems appropriate also for fractures, which are likely to be rough and/or partially filled with porous material.

5. *Assumption:* For heterogeneous models, the van Genuchten parameter $1/\alpha$ is assumed to be correlated to absolute permeability according to the Leverett scaling rule (Leverett 1941, p. 159; Finsterle 1997, p. 224). *Rationale:* Continuum permeability is partly related to fracture aperture. An increase in permeability is therefore associated with a decrease in capillary strength.

6. *Assumption:* Water removal from the formation and the capture system by vapor diffusion and evaporation is assumed to be small. *Rationale and discussion:* Under isothermal conditions, potential evaporation is small compared to the amount of water being released and given the relatively short time period of the experiments. This assumption may not be valid for injection tests performed at lower rates. In these cases, the amount of water collected in the capture system does not accurately reflect the seepage percentage as a result of evaporation. No relative humidity or evaporation-rate measurements are available from Niche 3650, and thus no correction has been made to the seepage-percentage data. ("Seepage percentage" is defined as the mass of water that dripped into the capture system divided by the mass of water released into the borehole interval during a liquid-release test event.) It is important to realize that prescribing a 100% relative humidity boundary condition in a seepage prediction model is a conservative assumption. While such a model underestimates vapor flow, it yields the maximum liquid-phase influx, which is defined here as drift seepage. The underestimation of vapor flow is irrelevant, since the assumption of 100% relative humidity already implies that the moisture content in the drift environment is at its maximum. However, the assumption is not conservative if used in an inverse model because parameters are adjusted such that the model reproduces the observed seepage percentage, which is likely to be too small. We suggest to address this issue in future experiments by monitoring relative humidity in the niche and directly measuring evaporation rates.

7. *Assumption:* Background percolation flux is assumed to be constant at 3 mm/year during the course of the experiment. *Rationale:* The background percolation flux is appropriate and of little impact on the simulation of liquid-release tests, which involve much higher rates.

8. *Assumption:* Matrix imbibition is assumed to be small and is thus not explicitly modeled in the SCM. *Rationale:* Matrix permeability is low, and matrix imbibition is reflected in the effective porosity estimated by inverse modeling. Porosity estimates are irrelevant in the subsequent simulations of seepage under natural flow conditions, which are near steady state.

All these assumptions are used throughout this report. They do not require further confirmation.

5.3 FRACTURE-CONTINUUM ASSUMPTION

5.3.1 Objective

We performed a synthetic modeling study to examine the appropriateness of using a Fracture Continuum Model (FCM), i.e., a model that is based on the continuum assumption, for predictive seepage calculations. Seepage into underground openings is dominated by water accumulation in a boundary layer at the apex of the opening and subsequent dripping from discrete fractures. Seepage threshold is determined by the capability of individual fractures to hold water by capillary forces and by the permeability and connectivity of the fracture network, which allows water to be diverted around the drift.

Simulation studies of unsaturated flow and transport at Yucca Mountain are usually based on the continuum approach, in which fractures and matrix are modeled as continua for which averaged properties are provided. The continuum approach has been questioned to be suitable for describing certain flow phenomena at Yucca Mountain (see, for example, Pruess (1999)), and specifically for predicting drift seepage, which apparently exhibits strong discrete effects.

In this section, we examine the appropriateness of using a heterogeneous fracture-continuum model as the basis for drift-scale seepage calculations. We consider the continuum approach appropriate for seepage studies if it is capable of predicting seepage threshold and seepage percentages for a drift in a fractured formation. On account of the simplifying assumptions and the limited amount of characterization data typically available, there will be differences between the seepage rates predicted by the FCM and the actual seepage rates. Therefore, the uncertainty of the model prediction will be considered. The seepage rates under natural flow conditions are unknown and can currently not be observed in the field. They are thus replaced in this study with synthetically generated seepage rates calculated using a model that exhibits discrete flow and seepage effects. This model is referred to as the Discrete Feature Model (DFM).

We do not attempt to compare the performance of an FCM with that of a discrete fracture network model, which is often cited as a valid alternative to the continuum model. Such a comparison would have to include a detailed discussion of data needs for each of the models, the respective uncertainties in these characterization data, and conceptual uncertainties and their impact on model predictions. Moreover, a computer code capable of accurately simulating unsaturated flow and seepage based on a discrete fracture formulation is currently not available.

The approach used in this synthetic study involves the following steps:

1. A model with a complex network of high-permeability features embedded in a low-permeability matrix is developed. The only purpose of this model is to produce discrete flow behavior and localized seepage events. Unsaturated-flow simulations performed with this discrete-feature model provide synthetic data against which the simplified Fracture Continuum Model (FCM) will be tested.

2. Air-injection tests, liquid-release experiments, and seepage under natural flow conditions are simulated using the DFM to generate synthetic characterization, calibration, and validation data, respectively.

3. A simplified heterogeneous FCM is developed based on the available synthetic characterization data.

4. Effective parameters are determined by calibrating the FCM against the synthetic liquid-release test data.

5. Predictions of seepage threshold and additional liquid-release tests are made with the FCM and compared to results obtained with the DFM for model validation.

It is important to notice that this is a *synthetic* modeling study designed for the specific purpose outlined above. While loosely based on expected conditions encountered during the liquid-release tests performed in the ESF at Yucca Mountain, the parameters used to develop the DFM should not be interpreted as describing actual formation characteristics at Yucca Mountain.

The study described here is documented in detail in Scientific Notebook YMP-LBNL-SAF-1, pp. 30–86, 120–139.

5.3.2   Development of Discrete Feature Model (DFM)

A high-resolution, two-dimensional (2D), vertical model was developed, representing an excavated niche in a fractured-porous formation. The model domain of dimensions 6 × 7 m in horizontal and vertical direction, respectively, was discretized into regular, square gridblocks with a side length of 0.05 m (SN YMP-LBNL-SAF-1, p. 36); the depth of the model is 1 m. The model was selected to be 2D instead of three-dimensional (3D) because effects of discrete fractures intersecting the drift are expected to be stronger in 2D than in 3D, where more opportunities for flow diversion around the opening exist. This was confirmed by 3D fracture-network simulations, which yielded lower seepage rates and a more porous-medium-type flow field (SN YMP-LBNL-SAF-2, p. 9). It is important to recall that the purpose of this study is to create a system behavior that is strongly affected by the discreteness of the fracture network.

In order to generate a complex network of discrete, heterogeneous fractures, a series of four permeability fields generated using sequential indicator simulation (Deutsch and Journel 1992, p. 151) were overlapped. The individual fracture sets of orientation 0, 45, 90, and 135° were created by drawing log-permeability values from discretized bi- and multi-modal cumulative distribution functions (cdf) that yield a high probability for very low values (10^{-17} m^2 or smaller, representing the matrix), a very low probability for intermediate values, and a relatively high probability for very high values (representing the fractures). Each indicator cutoff representing a point of the cdf was assigned its own semivariogram with a very high anisotropy ratio to generate elongated high-permeable features, which were cross-cut with occasional low-permeability obstacles. The resulting permeability field, shown in Figure 1a, is very complex with heterogeneous fractures of variable angle, length, and permeability. The permeability field shown in Figure 1a cannot be described using simple geostatistical parameters. The complexity and relative inaccessibility of the fracture-network characteristics are intentional to mimic a realistic situation where complete information about the geometry and hydrologic properties of a fracture network is not available. The process of fracture-network generation is described in detail in SN YMP-LBNL-SAF-1, pp. 31–35.

The effective vertical permeability of the fracture network was determined by applying constant-pressure conditions at the top and bottom boundaries of the model, running a transient flow simulation to steady state, and using Darcy's law to back out an effective permeability from the simulated steady-state flow rate (SN YMP-LBNL-SAF-1, p. 47). The effective permeability of approximately $4 \cdot 10^{-12}$ m^2 is consistent with fracture permeabilities observed at Yucca Mountain; note, however, that this information is considered unknown and will not be used in the subsequent analysis.

The permeability field was mapped onto the computational grid, and an opening (niche) was cut out from the mesh (SN YMP-LBNL-SAF-1, pp. 37–39). During this process, the fracture permeabilities in the vicinity of the niche were linearly increased within a 1-m-thick skin zone as a function of distance from the niche wall, reaching a factor of 100 at the niche wall. This permeability increase was introduced to mimic the presence of an excavation-disturbed zone, which is believed to exist around the niches in the ESF (Wang and Elsworth 1999, pp. 751–757). It was assumed that the mechanical disturbance mainly affects fractures, i.e., matrix permeability was left unchanged at its original low value. After attaching boundary elements, the final mesh, shown in Figure 1b, consisted of 11,984 elements and 24,005 connections between them.

(a)   (b)
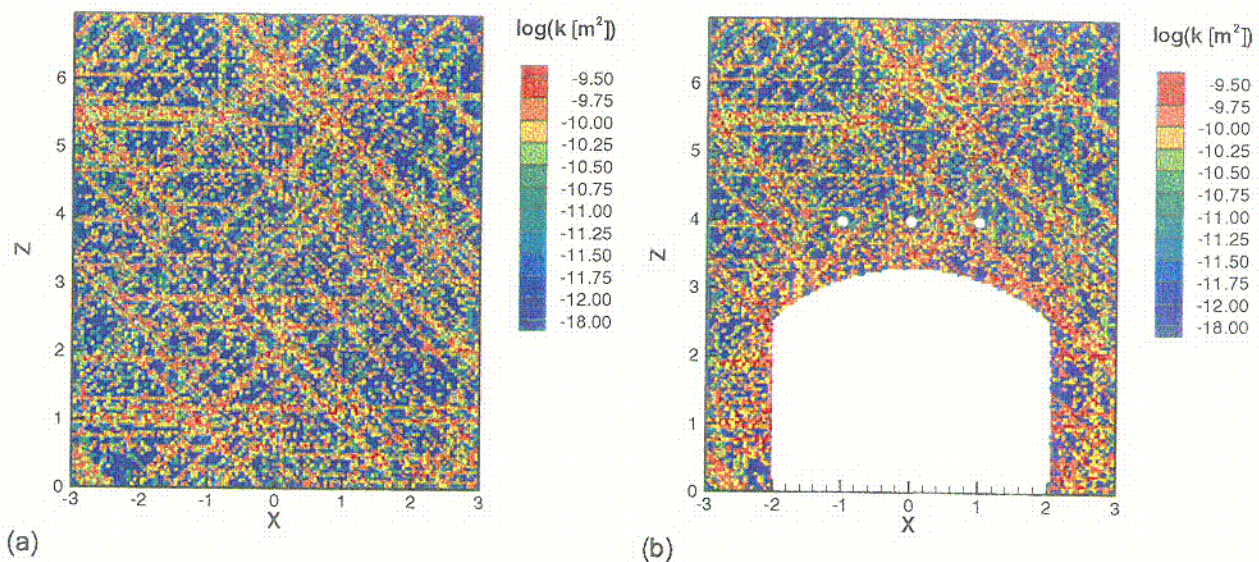
(based on data submitted with this AMR under DTN: LB990831012027.001)

NOTE: The model is used to generate synthetic seepage data.

Figure 1. Permeability Field of the Discrete Feature Model (a) Before and (b) After Niche Insertion

Capillary pressure and relative liquid permeability are described by van Genuchten's function (Luckner et al. 1989, pp. 2191–2192), with the capillary strength parameter $1/\alpha$ correlated to the heterogeneous permeability field shown in Figure 1 according to Leverett's scaling rule (Leverett 1941, p.159; Finsterle 1997, p. 224). The niche is modeled as a domain of zero capillarity,

representing 100% relative humidity. A free-drainage boundary condition (Finsterle 1998, pp. 14-15) is applied at the bottom of the model at Z=0.0 m to avoid an unphysical capillary pressure end effect. A constant percolation flux of 3 mm/year is applied at the top of the model.

The reference value of $1/\alpha$ (sometimes referred to as air-entry pressure, AEP) for the reference permeability of 10^{-12} m^2 was varied, until no seepage occurred under natural, steady-state flow conditions for a percolation flux of 3 mm/year (SN YMP-LBNL-SAF-1, p. 73). The percolation flux was then increased to 300 mm/year, yielding a seepage percentage of 80% (SN YMP-LBNL-SAF-1, p. 74). From that, it can be concluded that with a reference $1/\alpha$ value of 5,000 Pa and a reference permeability of 10^{-12} m^2, a seepage threshold exists somewhere between 3 and 300 mm/year. The actual seepage threshold was determined to be 15 mm/year (see Section 5.3.7).

Figure 2 shows the simulated steady-state flow field and saturation distribution for a percolation flux of 3 mm/year. A moderate saturation build-up in the skin zone is sufficient to divert all the water around the niche; this constitutes the so-called capillary barrier effect. Figure 3 shows the flux distribution across the top and bottom of the model. The constant flux, which is applied uniformly at the top of the model, is immediately redistributed into high-conductivity fractures. Flow diversion around the niche leads to a percolation shadow as well as locally increased fluxes below the niche.
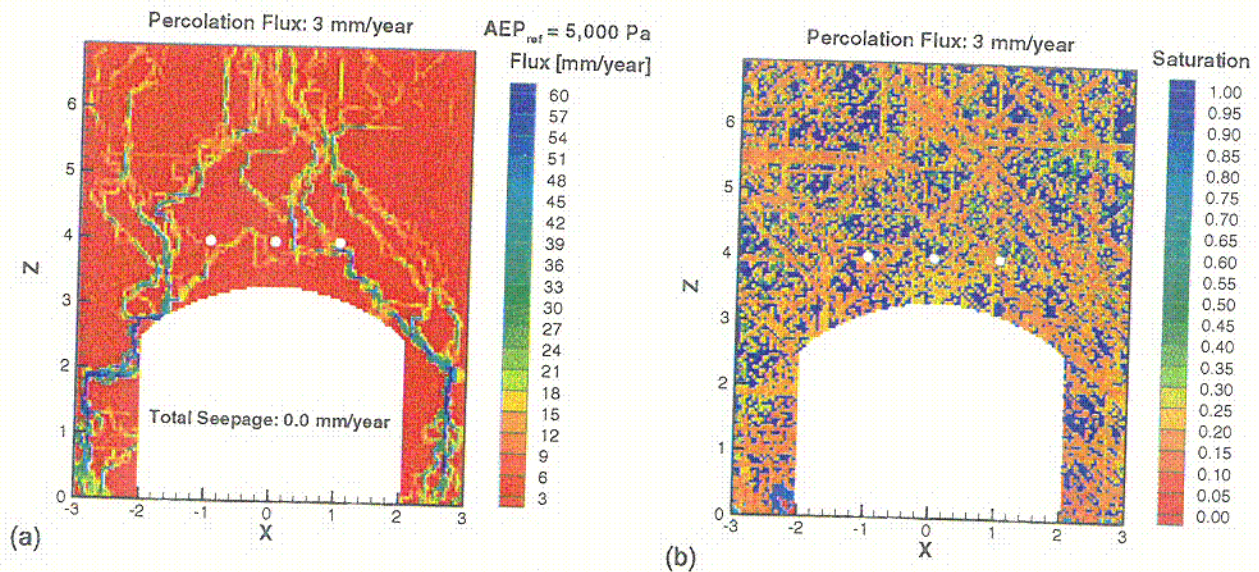
(based on data submitted with this AMR under DTN: LB990831012027.001)

Figure 2. Simulated Steady-State Flow Field (a) and Saturation Distribution (b)

Average Flux: 3 mm/year

(based on data submitted with this AMR under DTN: LB990831012027.001)
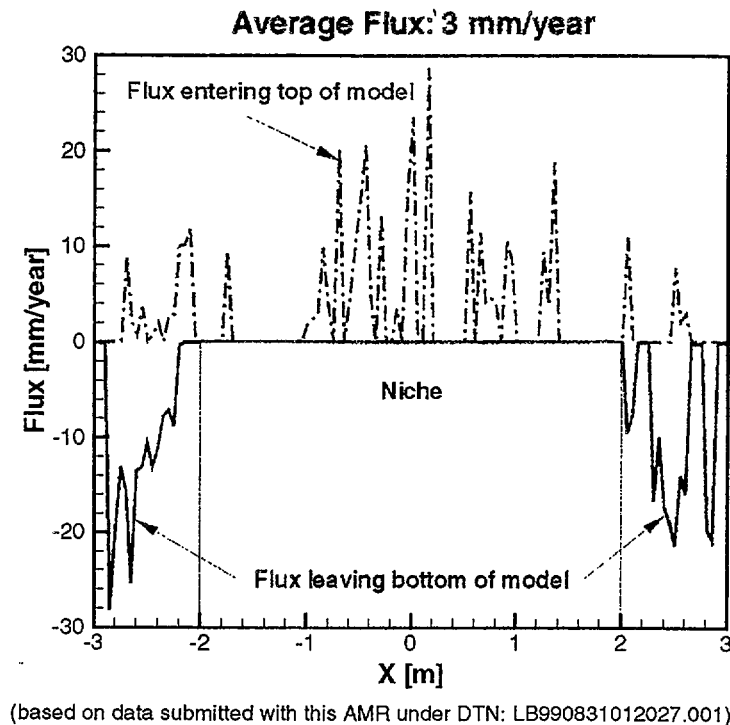
Figure 3. Simulated Steady-State Fluxes Across Top and Bottom of Model Domain, Showing Flow Redistribution as a Result of the Capillary Barrier Effect

5.3.3 Simulation of Air-Injection Tests Using the DFM

Air-injection tests are part of a standard characterization study performed at Yucca Mountain. We therefore simulated air-injection tests in three boreholes and analyzed the steady-state pressure data based on a commonly used analytical solution (LeCain 1995, p. 10). The derived air permeabilities are assumed to be the only data available for the development of a drift-scale seepage model, which will then be calibrated against liquid-release test data.

Air-injection tests were simulated in three boreholes above the niche (shown, for example, in Figure 1b); they are designated L, M, and R, according to their location to the left, middle, and right of the niche crown, respectively. Air is injected at a constant rate of 0.001 kg/s for 120 seconds, followed by a 120-s recovery period. Gas pressure in the niche as well as the top and bottom boundary were kept constant at 1 bar. Figure 4 shows the almost instantaneous pressure build-up in the injection holes as well as the response in the respective observation holes. The pressure at the end of each injection period is taken as the steady-state pressure for the determination of air permeability. A steady-state overpressure of 1430, 1350, and 1890 Pa was obtained for the three boreholes, leading to permeability estimates of $6.9 \cdot 10^{-12}$, $7.4 \cdot 10^{-12}$, and $5.2 \cdot 10^{-12}$ m^2, respectively. No high accuracy is required for these estimates; they will only be used to condition the heterogeneous permeability field of the FCM. Details about the simulation of air-injection tests using the DFM can be found in SN YMP-LBNL-SAF-1, pp. 51–54, 75, 83.
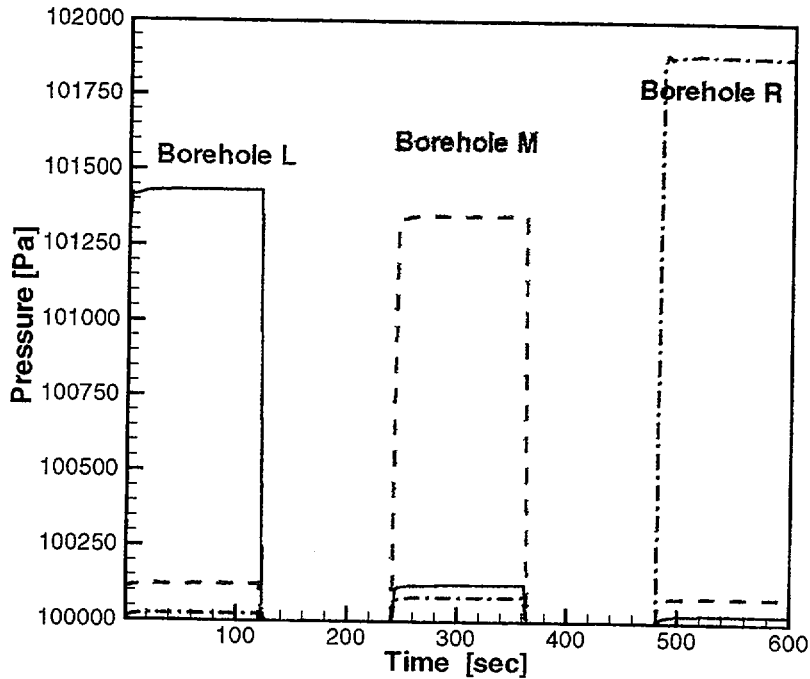
(based on data submitted with this AMR under DTN: LB990831012027.001)

Figure 4. Pressure Response from Simulated Air-Injection Tests Performed in Three Boreholes (Borehole L: Solid Line; Borehole M: Dashed Line; Borehole R: Dash-Dotted Line) Above the Niche

5.3.4 Simulation of Liquid-Release Tests Using the DFM

Three liquid-release tests were simulated from Borehole M. In each event, 3 kg of water were injected at a specified rate. Sufficient time was allowed between individual test events to make sure that seepage into the drift ceases. Nevertheless, subsequent events are likely to exhibit a memory effect, i.e., seepage percentage is expected to increase due to a higher initial saturation in the system as a result of water storage from the previous test. The third event is performed at a lower rate to investigate the dependence of seepage on flux. Table 4 summarizes information about the simulated liquid-release tests. The simulations are described in detail in SN YMP-LBNL-SAF-1, pp. 55–58, 76–79, 84–86.

Table 4. Simulated Liquid-Release Tests

Event	Begin Injection (s)	End Injection (s)	Injection Rate (kg/s)	Water Released (kg)
1	0.0	600.0	0.005	3.0
2	172800.0	173400.0	0.005	3.0
3	345600.0	351600.0	0.0005	3.0

(based on data submitted with this AMR under DTN: LB990831012027.001)

The flow field and saturation distribution after the first test event are visualized in Figure 5, revealing both partial flow diversion around the niche and the saturation build-up at the crown, which eventually breaks the capillary barrier, leading to seepage.
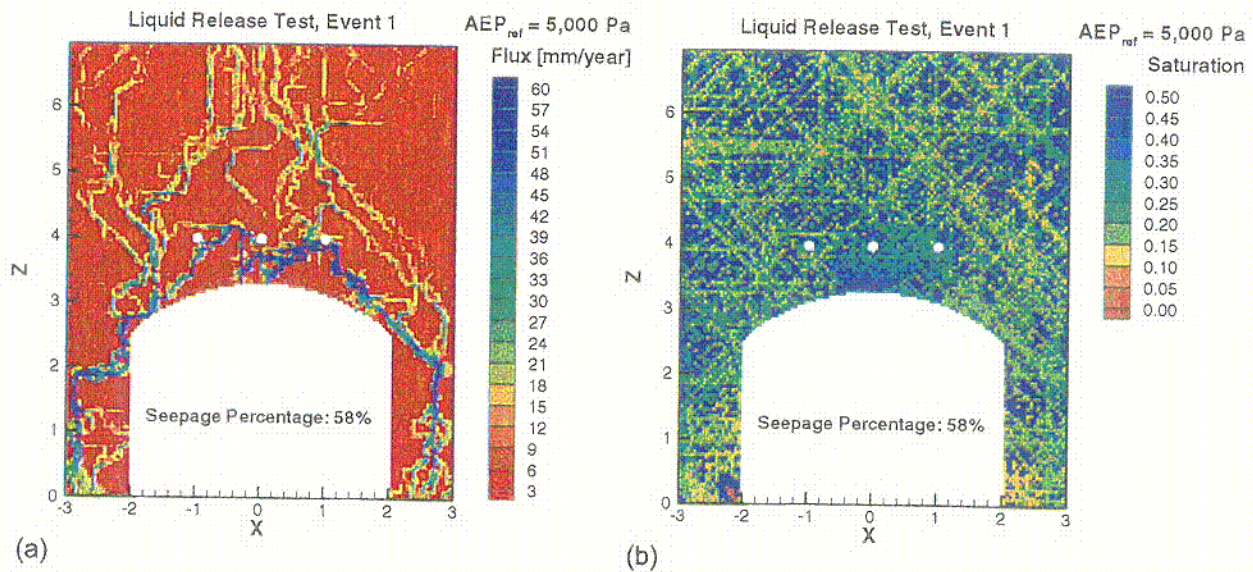
(based on data submitted with this AMR under DTN: LB990831012027.001)

Figure 5. Flow Field (a) and Saturation Distribution (b) After First Liquid-Release Test Event Simulated with DFM

The cumulative amount of water seeping into the niche is recorded as a function of time, separately for each event. The resulting curve of cumulative seepage is shown in Figure 6, which will be the synthetic data used for subsequent calibration of the FCM. Seepage generally stops within a few hours after injection begins. A relatively strong memory effect can be observed for Events 2 and 3, leading to increased seepage (Event 2) despite a reduced injection rate (Event 3). The ratio of the total amount seeped into the niche divided by the amount of water released (3.0 kg) is termed "seepage percentage." The seepage percentages of the three simulated liquid-release tests are 58, 89, and 89%, respectively.
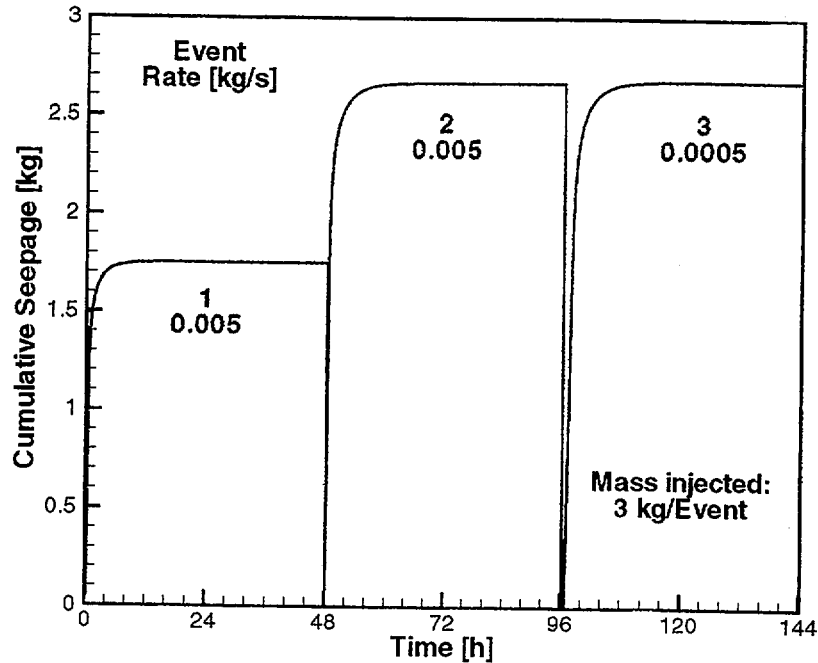
(based on data submitted with this AMR under DTN: LB990831012027.001)

Figure 6. Cumulative Seepage as a Function of Time During Three Simulated Liquid-Release Tests Using the Discrete Feature Model

5.3.5 Development of Fracture Continuum Model (FCM)

The model described in Sections 5.3.2–5.3.4 serves as a hypothetical natural system, in which air-injection and liquid-release tests were performed. It will also be used later to provide synthetic validation data.

In this section, we describe the development of a simplified seepage model that is based on the fracture-continuum approach. The model will be calibrated against synthetic data from liquid-release tests, and predictive simulations of additional liquid-release tests will be performed for validation. Moreover, it will be used to determine the seepage threshold under "natural" flow conditions.

While the characteristics of the fractured system as represented by the DFM are exactly known, only a limited amount of information is assumed to be available for the development of the FCM. The available data include:

- Air-permeability values at the three boreholes L, M, and R (see Section 5.3.3).
- An assumed variance and isotropic correlation structure of the permeability field.
- Cumulative-seepage data from three sequential liquid-release tests (see Figure 6).

Furthermore, the two-dimensionality of the flow field is assumed to be recognized. Finally, the FCM developed here shares some of the simplifying assumptions that apply to the DFM, such as the absence of evaporation effects.

It is important to realize that essentially no information about the fracture network (i.e., fracture density, orientation, aperture distribution, and hydrologic properties) are assumed to be known, and that the purpose of the model is simply to predict seepage percentage and seepage threshold under natural flow conditions.

The development of the FCM can be described as follows:

The FCM is a 2D vertical model, discretized into gridblocks of size 0.1×0.1 m; a niche is cut out from the model. The mesh consists of 3,002 elements and 6,020 connections between them. A heterogeneous permeability field was created using sequential indicator simulation (Deutsch and Journel 1992, p. 151). An arbitrary, uni-modal cumulative distribution function was defined by specifying three discrete cutoff values of 30, 50, and 70% at log-permeability values of -13.0, -12.0, and -11.0, respectively. A spherical semivariogram with a correlation length of 1.0 m, a nugget effect of 0.1, and a sill value of 1.0 was used to generate values ranging over 4 orders of magnitude. While a correlation length of 1.0 m can be considered reasonable—it is of the same order as a potential average fracture length—the choice of the semivariogram function and its parameters was arbitrary, i.e., it was purposely *not* based on a geostatistical analysis of the permeability field shown in Figure 1b. Similarly, the chosen variance of 1.0 is arbitrary but can be considered reasonable. This approach reflects the assumption that no hard data about the fracture network or its hydraulic properties are available. The only information considered available are the three air-permeability values in boreholes L, M, and R (see Section 5.3.3); the permeability field was conditioned on these three values. The log-permeability field of the FCM is shown in Figure 7. Mesh generation and mapping of the spatially correlated permeability field are described in SN YMP-LBNL-SAF-1, pp. 61–67, 75.
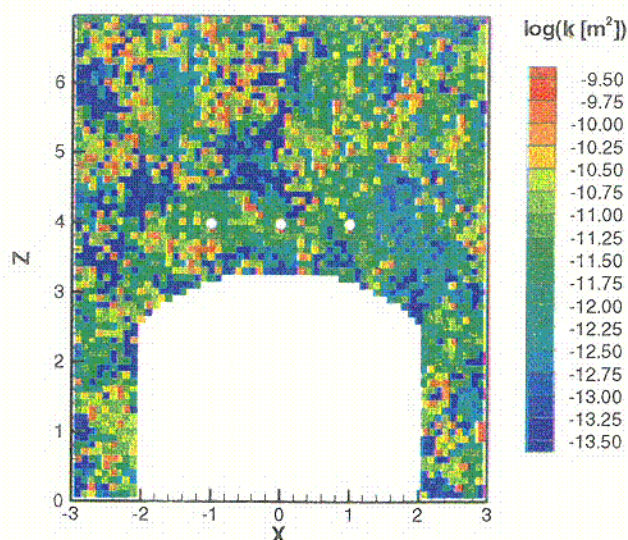
(based on data submitted with this AMR under DTN: LB990831012027.001)

Figure 7. Log-Permeability Field of Fracture Continuum Model

It should be noted that the structure of the FCM described here is by design significantly different from that of the DFM presented in Section 5.3.2. While heterogeneous in nature, the FCM lacks the discrete features, the high resolution, and the low-permeability matrix. Moreover, no excavation-disturbed zone with increased permeability was introduced in the FCM. Since the liquid-release tests were performed within this zone, the estimated parameters will reflect skin-zone properties rather than undisturbed formation characteristics. Using skin-zone parameters for seepage calculations is appropriate because seepage is determined by the properties in the immediate vicinity of the drift wall. Provided that skin-zone properties are used and that the transition between the undisturbed and the excavation-disturbed zone is gradual, no strong impact of the skin zone on seepage is expected. The smooth transition zone implemented in the DFM does not have an visible effect on the flow pattern (see Figure 2a). If properties change abruptly at the skin-zone boundary, however, a partial capillary barrier is formed within the formation. The presence of such a second capillary barrier is likely to further reduce seepage.

In summary, the FCM is an abstracted, highly simplified representation of the fractured-porous system to be studied. It is obvious that such a simplified model cannot accurately reproduce the detailed behavior of the discrete fracture network. It remains to be examined, however, whether the FCM is capable of predicting seepage rates over a large range of percolation fluxes. If so, it fulfills its declared purpose and can be considered acceptable for seepage studies. If not, an alternative conceptual model must be developed, and its appropriateness must be demonstrated in a study similar to that described here. Note that such an alternative model may require different or additional characterization data.

5.3.6 Calibration of FCM Against Synthetic Seepage Data

The FCM can only be successful in predicting seepage if effective parameters can be estimated based on data that reveal seepage-relevant processes. Liquid-release tests are expected to provide this information. The FCM is calibrated against the cumulative-seepage data that were generated with the DFM. Only late-time data are used for calibration, since the early-time transient behavior exhibits distinct effects from the detailed characteristics of the discrete-fracture network. Because the FCM is not expected to be able to match these early-time data, they were excluded from the inversion to reduce the potential bias in the estimates.

In order to avoid overparameterization of the inverse problem, only two parameters were estimated, namely (1) the logarithm of the reference air-entry pressure $1/\alpha$, and (2) the logarithm of porosity ϕ. The van Genuchten parameter $1/\alpha$ is included because seepage is expected to depend on the capillary strength, i.e., the effectiveness of the capillary barrier. Porosity is included as a parameter to be estimated because only a finite, relatively small amount of water is released. Porosity is here an effective parameter that accounts for water storage in the fracture system, potential matrix imbibition, and other transient effects.

The calibration was performed using iTOUGH2. Since changes in the $1/\alpha$ values during the course of the inversion affect the initial saturation distribution, a steady-state run with percolation of 3 mm/year precedes each transient liquid-release test simulation. The misfit between the cumulative seepage calculated by the FCM and the data provided by the DFM is evaluated using the least-squares objective function (Finsterle 1999, p. 33). The objective function is minimized using the Levenberg-Marquardt algorithm (Finsterle 1999, pp. 44–45).

Figure 8 shows the match. The synthetic data are represented by symbols; calibration occurs only against the late-time data, shown as squares. The cumulative seepage predicted with the FCM and an initial parameter guess of $\log(1/\alpha) = 3.0$ and $\log(\phi) = -2.0$ is shown as a dashed line. The best-fit parameter set (1.60/-2.24) is determined after nine Levenberg-Marquardt iterations. The corresponding prediction, which matches the data reasonably well, is shown as a solid line. The flow field and saturation distribution after the first liquid-release event, calculated with the FCM and the best-estimate parameter set, are shown in Figure 9, which can be compared to Figure 5. While the details of the flow pattern are different from that of the DFM, the FCM clearly shows a saturation build-up above the crown, leading to a qualitatively similar capillary barrier effect. Details about the inversion can be found in SN YMP-LBNL-SAF-1, pp. 120–124.
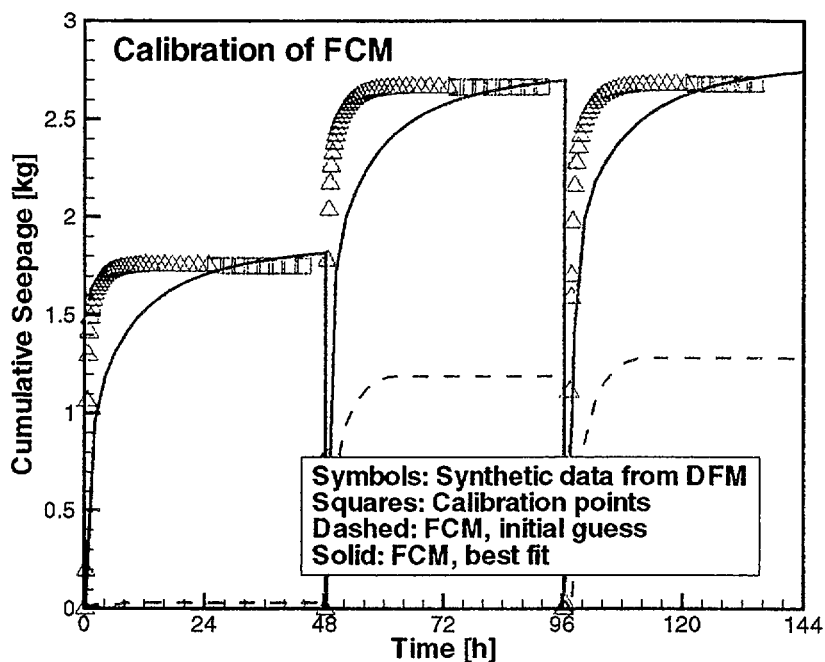
(based on data submitted with this AMR under DTN: LB990831012027.001)

Figure 8. Calibration of FCM Against Late-Time Cumulative-Seepage Data From Three Simulated Liquid-Release Events
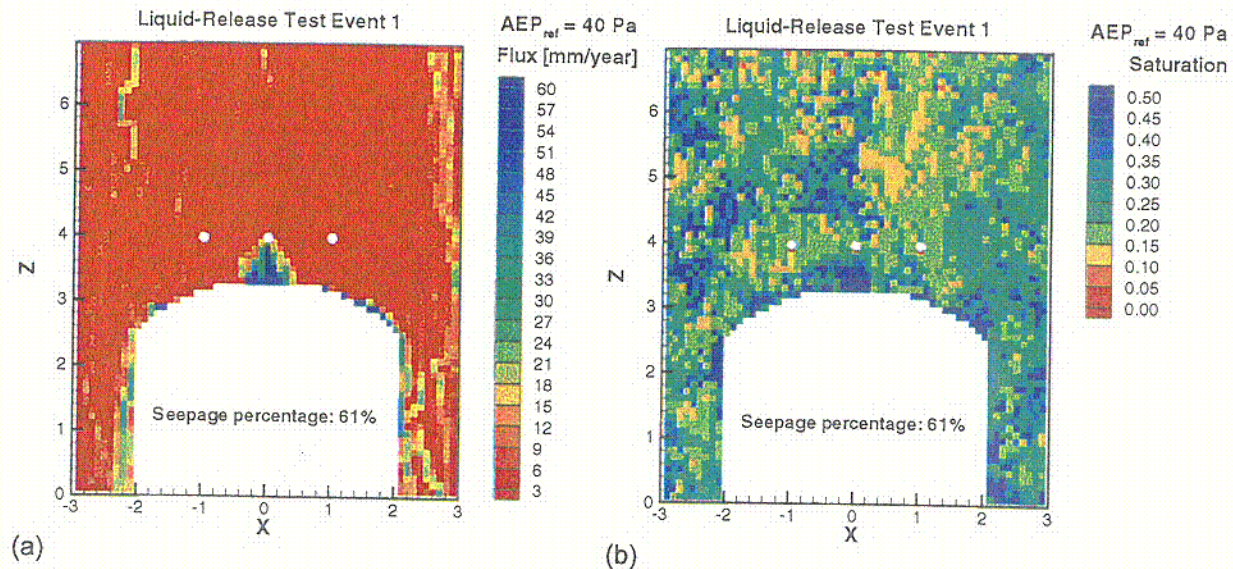
(based on data submitted with this AMR under DTN: LB990831012027.001)

Figure 9. Flow Field (a) and Saturation Distribution (b) After First Liquid-Release Event
Simulated with Calibrated FCM

Next, we discuss the estimated parameters. Since the matrix is not explicitly represented in the FCM, porosity is considered an effective parameter that accounts for water storage in the fracture system as well as matrix imbibition. The total porosity of the excavation-disturbed zone as specified in the DFM is 0.02; about 64% of the pore space is assigned to matrix gridblocks, resulting in a fracture porosity of approximately $0.02 \times (1 - 0.64) = 0.007$. The porosity estimated by calibrating the FCM is 0.006, a value very close to the geometric fracture porosity specified in the DFM. A value larger than the fracture porosity would only be expected if matrix imbibition were a significant process and if all the fractures were available for storage. Apparently, matrix permeability is too small to allow substantial water imbibition during the relatively short testing period. As a result, the porosity estimate reflects the fracture pore space encountered by the injected water from the release point to the drift ceiling. While the porosity estimate is of no importance for steady-state seepage-threshold predictions, the transient nature of the liquid-release tests forced us to estimate porosity concurrently with the van Genuchten parameter $1/\alpha$, to which it is (negatively) correlated. Had it been fixed at a value that is too high (too low), the van Genuchten parameter would have been underestimated (overestimated).

An important result of this study is the finding that a relatively small value $1/\alpha$ is required to match the seepage data. While the reference value used in the DFM is 5,000 Pa, the estimate for the FCM is approximately two orders of magnitude smaller. This discrepancy clearly indicates that the value and interpretation of $1/\alpha$ is strongly related to the conceptual model and its implementation. Two potential reasons explaining the apparent discrepancy can be identified. First, in the DFM, water flows predominantly through high-permeability channels (see Figures 1

and 5), indicating that the observed seepage mass is in fact governed by features that exhibit low capillary suction. The absence of discrete features in the FCM, on the other hand, leads to a more diffusive flow pattern, and the zone encountered by water exhibits more averaged properties (see Figures 7 and 9). To match the data, which are controlled by flow through regions of low capillary suction, the reference capillary strength parameter for the FCM must be lowered accordingly.

The second explanation for the discrepancy focuses on the different degree of connectivity implemented in the two models. Since the FCM provides connections in all directions (allowing water to be easily diverted around the cavity), the capillary-barrier effect is increased and the calculated seepage tends to be small. Consequently, the capillary suction must be reduced to match the data from a discrete system. The van Genuchten parameter is adjusted to compensate for a deficiency in the model structure (here, the lack of discrete features in the FCM). Note that such a compromise is made and considered acceptable whenever a model is built in which certain aspects are simplified and represented by lumped parameters. In our case, the length, connectivity, and hydrologic properties of the fractures intersecting the drift are difficult if not impossible to characterize. A few parameters are chosen to represent the effects of these fractures on seepage, and they are determined by inverse modeling based on seepage-relevant data.

It has been stated that the FCM is devoid of discrete features. A notable exception are the gridblocks adjacent to the drift. Their connections to the element representing the opening have length $\Delta z/2 = 0.05$ m. Since water is diverted horizontally only if capillary suction exceeds 0.05 m, the discretization has an effect similar to that of the discrete fractures that cut into the opening, with an (average) distance to the next fracture intersection of 0.05 m. It should therefore be clear that the estimated $1/\alpha$ value not only depends on the conceptual model, but also on the discretization used in the numerical model.

Such a discretization-dependence of model parameters is well known. For example, since the simulation of contaminant plume spreading is affected by numerical-dispersion effects, the dispersion length that best matches an observed contaminant plume depends on the chosen grid resolution. Similarly, a direct correlation exists between capillarity and gridblock size in unsaturated flow problems involving phase dispersion (Pruess 1991, pp. 272–274). Stronger capillarity leads to increased phase dispersion, as does coarser grid discretization. Consequently, model predictions and thus capillary strength parameters estimated by inverse modeling depend on grid resolution.

Note that the mesh-dependent effects described above counteract each other in seepage calculations. The coarser the grid, the more seepage is induced on account of an increased connection length to the niche element; at the same time, increased phase dispersion leads to a reduction in seepage. It is difficult to assess which of the two effects dominates. However, the effects cancel one another to a certain degree, reducing the overall dependence of seepage calculations on grid resolution.

5.3.7 Synthetic Validation of FCM and Prediction of Seepage Threshold

In order to test the predictability of the FCM, we perform a synthetic validation exercise, in which seepage rates for a new liquid-release experiment are predicted with the calibrated fracture-continuum model. The new injection rate used for the validation run is five times smaller than that used for calibration, and the natural percolation flux is increased to 100 mm/year. The prediction uncertainty is determined by means of Monte Carlo simulations, in which the two estimated parameters $\log(1/\alpha)$ and $\log(\phi)$ are considered uncorrelated and uncertain by a factor of about two, i.e., $\sigma_{\log(1/\alpha)} = 0.3$ and $\sigma_{\log(\phi)} = 0.3$. These standard deviations reflect expected parameter uncertainties, which are based on the estimation uncertainties from the calibration, appropriately increased to account for additional errors and the fact that predictions are made under changed conditions.

Figure 10 shows the model prediction with the best-estimate parameter set (solid line) along with the results from 100 Monte Carlo simulations. The system behavior as calculated by the DFM is shown as a dashed line. The calibrated FCM slightly underpredicts cumulative seepage, mainly because of an error in the early-time behavior. Nevertheless, taking into account the uncertainty of the model prediction as expressed by the Monte Carlo simulations, the model is considered partly validated, i.e., the seepage rate calculated with the DFM lies within the error band predicted by the calibrated FCM. The validation study is described in SN YMP-LBNL-SAF-1, pp. 131–134.

The approach outlined here is also used for the actual validation of the SCM (see Section 6.5).
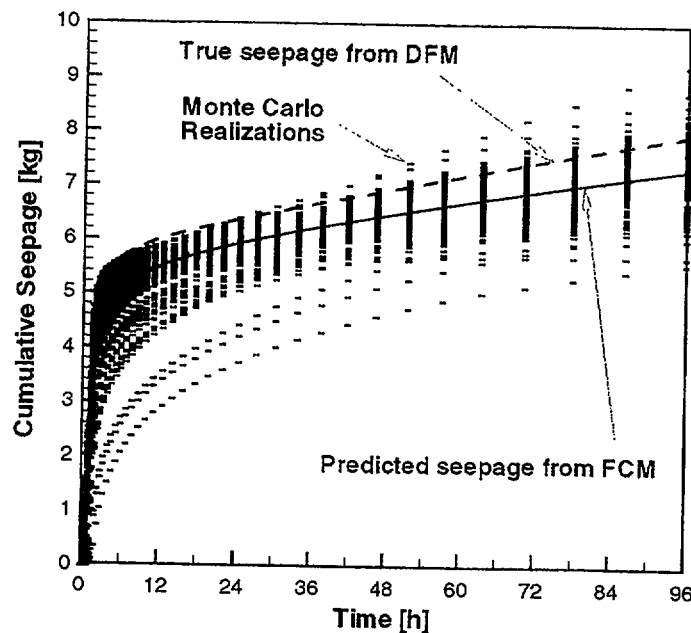
(based on data submitted with this AMR under DTN: LB990831012027.001)

NOTE: Monte Carlo simulations show uncertainty of model predictions.

Figure 10. Validation of Calibrated FCM Against Cumulative Seepage Data

The successful prediction of a transient liquid-release test does not necessarily imply that seepage is accurately predicted for low percolation fluxes under natural steady-state flow conditions. We therefore calculated the seepage percentage using the DFM in the range of percolation fluxes from 3 to 300 mm/year and compared it with FCM predictions.

In Figure 11, the seepage percentage as calculated with the DFM is shown as a dashed line. A seepage threshold of approximately 15 mm/year is obtained. As a result of the discreteness of the fracture network, the flow paths diverting water around the niche change as percolation rate increases, leading to an erratic, but generally increasing seepage-percentage curve. The FCM predicts a seepage threshold of 34 mm/year. Seepage percentage increases monotonically with increasing percolation flux, reaching a maximum value of about 60% for a flux of 300 mm/year (see Figure 11, solid line).

To obtain a measure of uncertainty in the FCM seepage prediction, we performed 500 Monte Carlo simulations with the two estimated parameters assumed to be uncorrelated and uncertain with a standard deviation of 0.3, as above. The percolation flux is sampled uniformly in the interval from 3 to 300 mm/year. The resulting seepage percentages are plotted as short dashes in Figure 11. From the scattering of the Monte Carlo simulations it can be seen that seepage percentage predictions are highly uncertain. The width of the error band is approximately 20% on either side of the result obtained with the calibrated parameter set. The distribution is skewed for low percolation fluxes on account of the physical lower bound of zero seepage. The Monte Carlo simulations for natural percolation fluxes are documented in SN YMP-LBNL-SAF-1, pp. 126-130, 135.
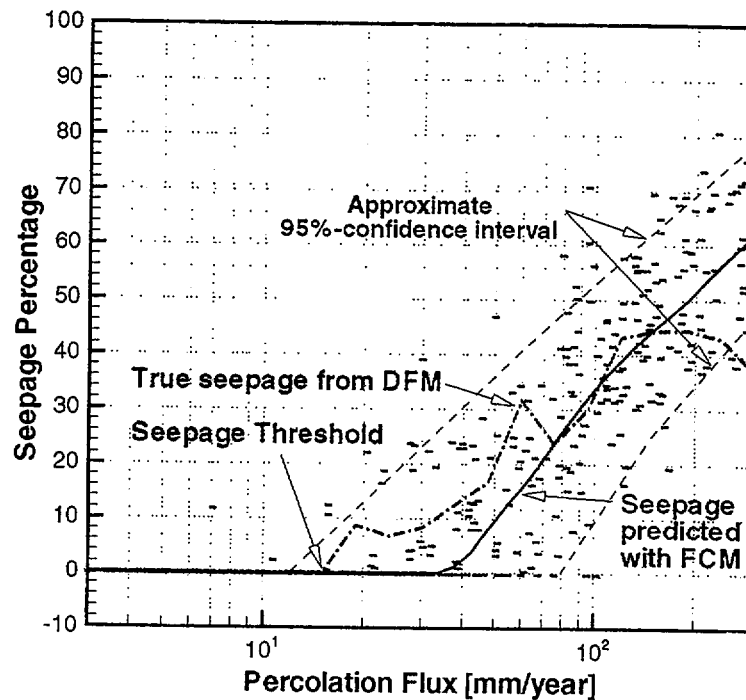
(based on data submitted with this AMR under DTN: LB990831012027.001)

Figure 11. Prediction of Seepage Percentage With Calibrated FCM Including Results From Monte Carlo Simulations and Comparison to Seepage Threshold Provided by the DFM

5.3.8 Summary and Conclusions

In this study, we have demonstrated that simulating seepage into underground openings excavated from a highly fractured formation can be performed using a model that is based on the continuum assumption, provided that the model is calibrated against seepage-relevant data such as data from a liquid-release test.

Synthetically generated data from the DFM, a model that exhibits discrete flow and seepage behavior, were used to calibrate a simplified FCM. The FCM was developed assuming that only minimal information is available. From this study, we conclude that:

1. A calibrated FCM is capable of predicting seepage into an underground opening excavated from a fractured formation.

2. Calibration of the FCM must be performed using data collected from a seepage experiment (e.g., a long-term liquid-release test).

3. The calibration of the FCM yields effective parameters that partially account for the discreteness of the fracture network.

4. For seepage calculations, the calibrated capillary strength parameter (e.g., air-entry pressure or $1/\alpha$) is likely to be small compared to the values obtained for single fractures.

5. Because only limited information is available for model calibration, the estimated parameters and thus the model predictions remain highly uncertain.

6. The interpretation and numerical value of the calibrated parameters are related to the conceptual model used; this is true for any parameter used in any analytical or numerical model.

7. The synthetic exercise presented here should be repeated for alternative conceptual models, e.g., using a discrete fracture network model (DFNM) that is developed based on fracture mapping information. These competing alternatives should be ranked according to their data needs, their ability to pass validation tests, the respective prediction uncertainties, the robustness and stability of the model results, and their computational efficiency.

The study was performed in 2D because effects of discrete fractures on flow and seepage behavior are stronger in two than in three dimensions. A similar study using 3D models is thus expected to yield the same conclusions as those outlined above.

Further investigations of numerical seepage modeling may include the development of a discrete fracture network model or other alternative conceptual models. The prediction uncertainty of these alternative models should be compared to that obtained with the fracture continuum model discussed here. The different data requirements should also be critically evaluated when comparing the performance of alternative modeling approaches.

INTENTIONALLY LEFT BLANK

6. MODEL ANALYSIS

6.1   OBJECTIVES AND OUTLINE

In this section we describe the development, calibration, and validation of the Seepage Calibration Model (SCM). The purpose of the SCM is to present a methodology for the subsequent development of process models that calculate drift seepage for a variety of geologic units, hydrologic property sets, and waste emplacement configurations. The SCM is a template fracture-continuum model that is developed based on air-permeability and liquid-release test data from the experiments performed in Niche 3650 of the ESF at Yucca Mountain, Nevada. It is suggested to use a similar approach when developing seepage models for other units and drift geometries; these models necessarily differ to some extent from the SCM to accommodate particular conditions.

In Section 6.2, we review the data basis—air permeabilities and seepage data from liquid-release tests—used for the development, calibration, and validation of the SCM. The conceptual model as well as details of the SCM are described in Section 6.3, followed by a discussion of its calibration by inverse modeling (Section 6.4). Validation of the SCM is described in Section 6.5. Seepage-threshold predictions with the calibrated SCM are presented in Section 6.6. Alternative conceptual models and sensitivity analyses are briefly discussed in Sections 6.7.1 and 6.7.2, respectively. Conclusions from the analyses presented in this section are summarized in Section 7.

6.2   REVIEW OF DATA USED FOR CALIBRATION AND MODEL VALIDATION

6.2.1   Introduction

The data used for model calibration/validation were collected during the ESF Drift Seepage Test and Niche Moisture Study, an ongoing field-testing program initiated by Lawrence Berkeley National Laboratory (Berkeley Lab) in 1997. The two primary objectives of the field-testing program are:

- Measure *in situ* permeability for use in the Seepage Calibration Model (this AMR) and the Seepage Model for PA.

- Provide a database containing liquid-release and seepage data that can be used to calibrate the drift-scale seepage models.

The objectives of the study described above are realized through field experiments consisting of air-injection and seepage tests. Sections 6.2.2 through 6.2.4 describe the air-injection and liquid-release test data used as input to the SCM described in Sections 6.3 through 6.5 of this AMR.

6.2.2 Site Location and Borehole Configuration at Niche 3650

6.2.2.1 Site Location

Niche 3650 consists of a short drift constructed along the west side of the ESF at the location shown on Figure 12. The niche is located within the middle nonlithophysal zone of the Topopah Spring Tuff in an area of relatively competent rock mass with low fracture density.
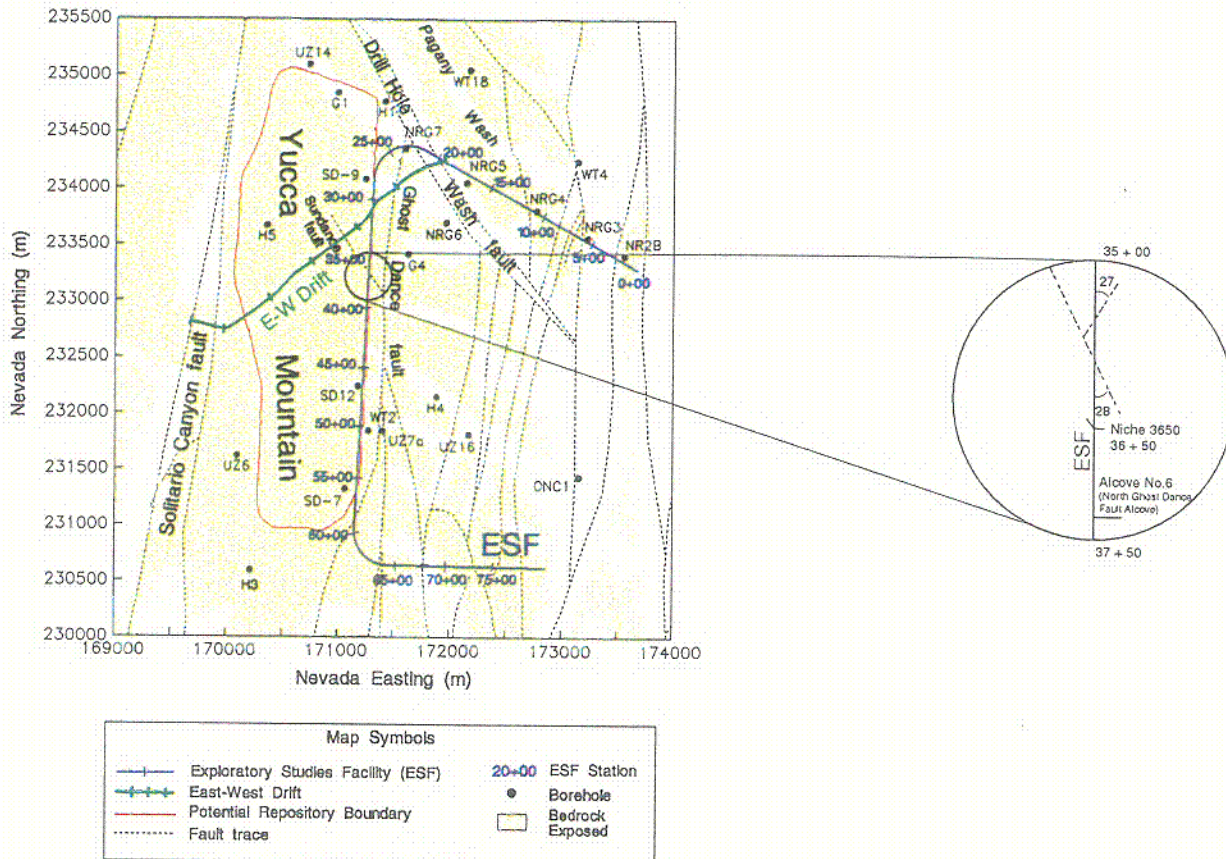
Figure 12. Schematic Showing Approximate Location of Niche 3650

6.2.2.2 Borehole Configuration

Seven short boreholes were drilled at Niche 3650 prior to excavation to gain access to the rock for testing and monitoring purposes. Figures 13 and 14 show the approximate location of the seven borings installed prior to construction of Niche 3650 as well as the idealized shape of the final excavation. Three of the borings, designated UL, UM, and UR (upper left, upper middle, and upper right), were installed above the crown of the niche in a horizontal plane. The remaining boreholes (ML, MR, BL, and BR) were drilled within the limits of the proposed niche and were subsequently mined out during niche construction.

UL 1.0 m UM 1.0 m UR

0.65 m

3.25m

1.15m

0.5 m 0.5 m
ML MR

1.0 m

C̦L

0.5 m 0.5 m
BL BR

Legend

ML Borehole designation
B = Bottom, M= Middle, U=Upper
L = Left, R = Right
*** All measurements are approximate
and do not represent as-built conditions

2.0 m 2.0 m
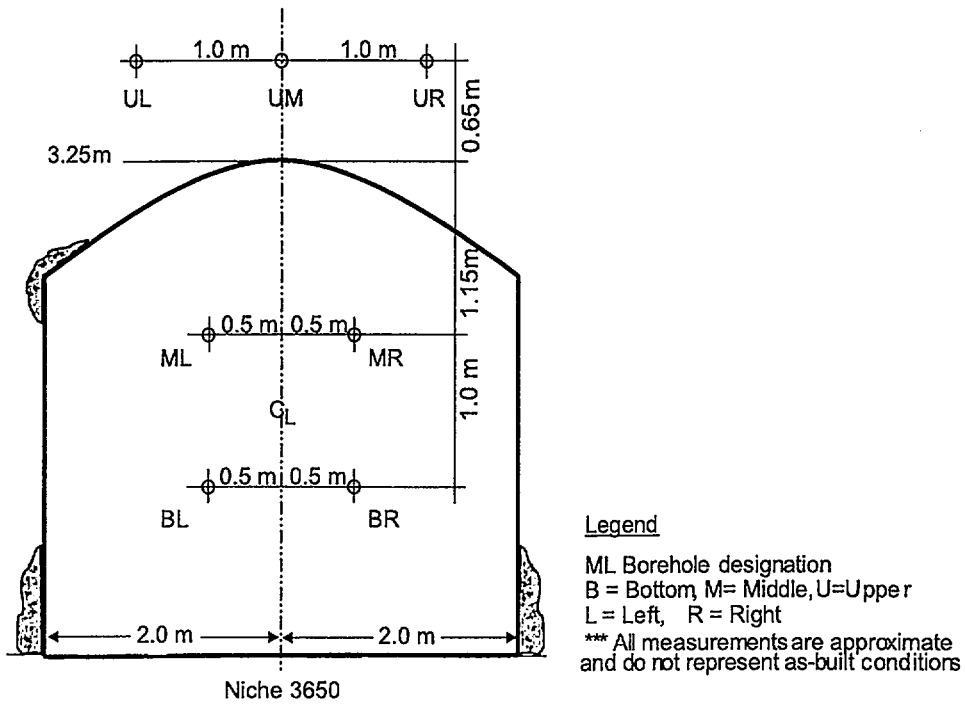
Niche 3650

Figure 13. Schematic of Niche 3650, End View

Legend

Upper Borehole Axis
Bottom & Middle Borehole Axis
UL = Upper Left
UM = Upper Middle
UR = Upper Right
ML = Middle Left
MR = Middle Right
BL = Bottom Left
BR = Bottom Right

ML, BL   MR, BR

UL

UM

UR

z

C̦L

ESF Main Drift

0   1   2 Meters

Approximate Scale: 1 inch = 2 Meters
*** All measurements are approximate and
do not represent as-built conditions.
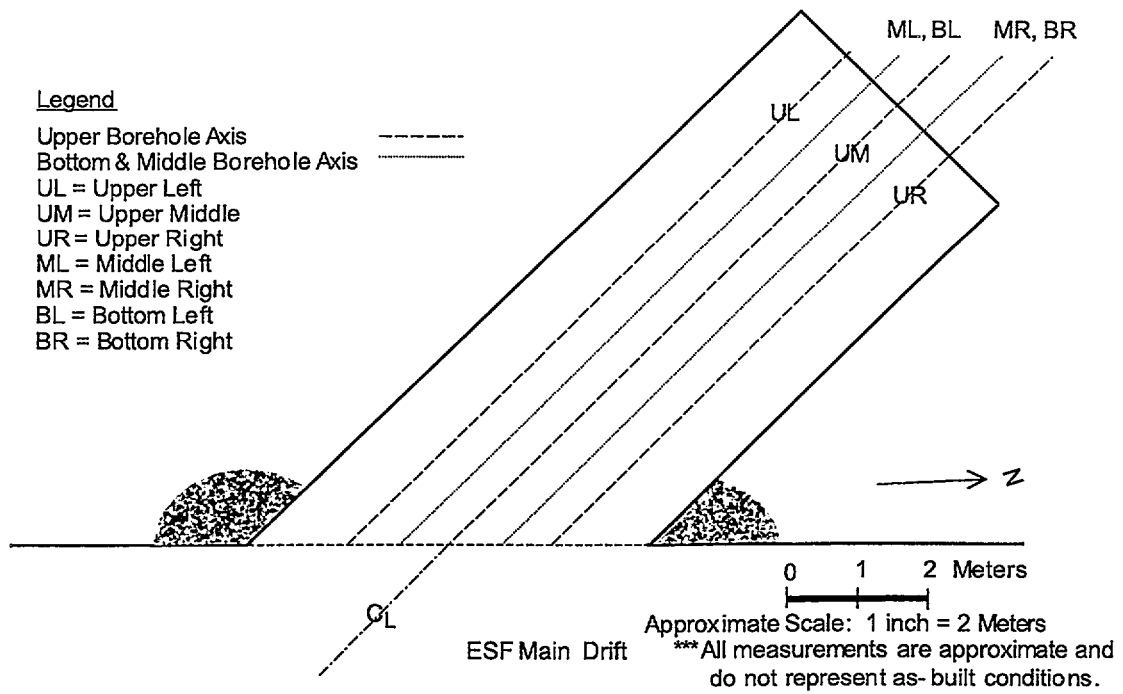
Figure 14. Schematic of Niche 3650, Plan View

6.2.3   Air-Injection Tests

Numerous air-injection tests were performed at Niche 3650 to determine the air-permeability distribution of the rock after niche construction. Air-injection tests were conducted on short test intervals in boreholes UL, UM, and UR. The tests were performed by isolating a short section of borehole using an inflatable packer system and then injecting compressed air at a constant rate into the isolated injection interval. The pressure buildup in the injection interval, as well as in nearby observation intervals, was monitored with time until steady-state conditions were reached, typically occurring within a few minutes of the start of the test. Air injection was terminated after reaching steady-state pressures, and the decline in air pressure was then monitored as it recovered to its initial pre-test condition.

The Niche 3650 air-permeability values were entered into the Technical Database Management System (DTN: LB980001233124.002). The post-excavation air-permeability data for Niche 3650 were extracted from DTN: LB980001233124.002 and the log-transform (logarithm base 10) of these data were calculated and used in this AMR (for details, see SN YMP-LBNL-RCT-DSM-1, p. 11).

The log-transformed values of the post-excavation air-permeability data obtained from boreholes UL, UM, and UR were used as input to GAMV2 (GAMV2, V1.201, 10087-1.0MGAMV2V1.201-00), a software module that is part of the Geostatistical Software Library (GSLIB). GAMV2 is described in detail by Deutsch and Journel (1992, pp. 53–55). GAMV2 calculates the semivariogram of irregularly spaced data in two dimensions. Figure 15 shows the semivariograms calculated for two test cases using a lag distance of 0.3 m. Case 1 includes all the air-permeability data from the post-excavation air-injection tests. The semivariogram shown on Figure 15 for Case 1 (diamonds) is nearly linear with a positive slope, implying unlimited variance and a possible systematic bias in the data set. The semivariogram for Case 2 (triangles) was created by excluding nine data points collected from test intervals located beyond the limits of the excavation (borehole UM, zones 29 through 31 and borehole UR, zones 26 through 31). Removal of these data, which typically have lower air permeabilities than those intervals located immediately above the opening, results in a semivariogram with a finite sill variance. Analyzing only those air-injection tests that were performed on test intervals located immediately above the opening and whose resulting air-permeability values were thus more or less uniformly influenced by the excavation resulted in a reasonable semivariogram devoid of a systematic trend. Data that are located beyond the limits of the excavation and were removed from Case 2 may represent a separate population of air permeabilities performed in an area of relatively undisturbed, lower-permeability rock. More details can be found in SN YMP-LBNL-RCT-DSM-1, pp. 19–25.

The histogram and cumulative distribution function shown in Figure 16 and the descriptive statistics shown in Table 5 were generated using the Case 2 data set described above (for details, see SN YMP-LBNL-RCT-DSM-1, pp. 25–26). The cumulative distribution function, sample statistics, and the semivariogram for the post-excavation air-permeability values will be used in Section 6.3.2 to generate a conditioned heterogeneous permeability field for the SCM.

Table 5. Statistical Summary of Air-Permeability Data

Case 2, Post-Excavation $\log_{10}(k\,[\text{m}^2])$	
Mean	-11.66
Standard deviation	0.72
Standard error	0.08
Median	-11.71
Minimum	-13.84
Maximum	-9.15
Range	4.69
Number of data points	84

(based on data submitted with this AMR under
DTN: LB990831012027.001)
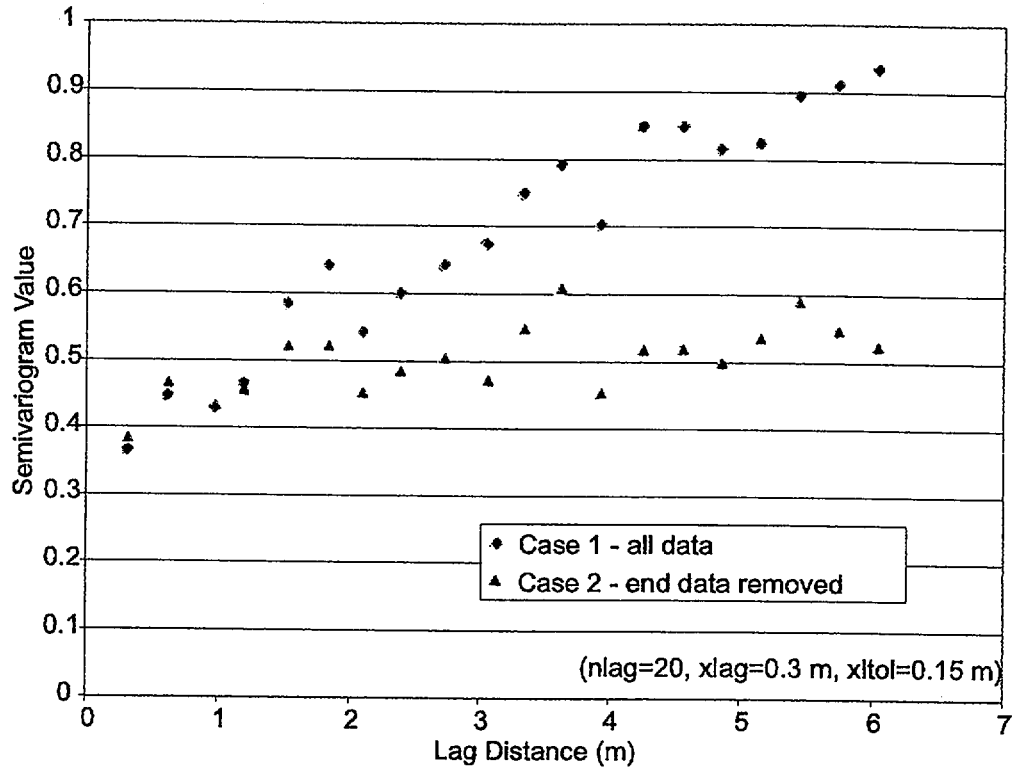
(based on data submitted with this AMR under DTN: LB990831012027.001)

Figure 15. Semivariogram for Post-Excavation Niche 3650 Log-Air-Permeability Values
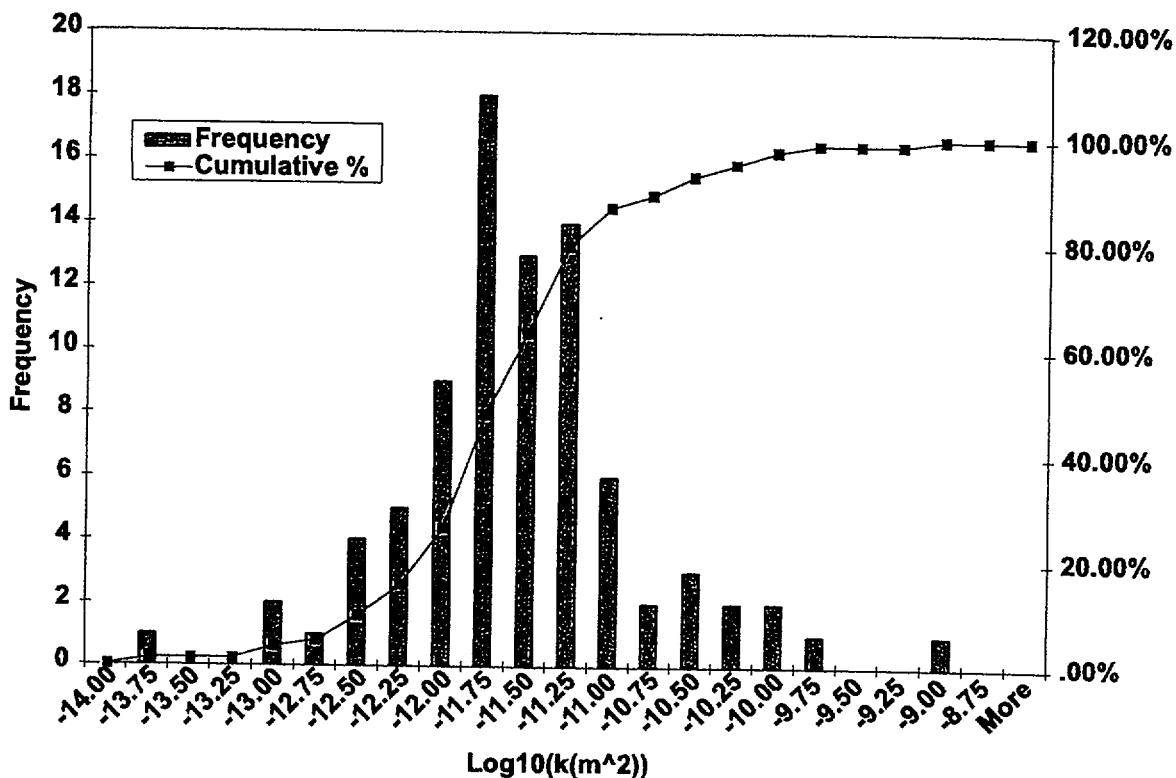
(based on data submitted with this AMR under DTN: LB990831012027.001)

Figure 16. Histogram and Cumulative Distribution Function for Post-Excavation Niche
3650 Log-Air-Permeability Values

6.2.4 Liquid-Release Tests

A series of short-duration liquid-release tests was performed at Niche 3650 to characterize seepage into an underground opening. The seepage tests were conducted after niche excavation by pumping water into select test intervals in boreholes UL, UM, and UR located above the niche. The tests were performed by sealing a short section of borehole using an inflatable packer system and then releasing water at a constant rate into the isolated test interval. Any water that migrated from the borehole to the niche ceiling and dripped into the opening was captured and weighed. The seepage percentage, defined as the mass of water that dripped into the capture system divided by the mass of water released into the borehole interval, was used to quantify seepage into the drift from a localized source of water of known duration and flow rate.

Forty liquid-release tests were performed on 16 test intervals positioned above Niche 3650. Water migrated through the rock and seeped into the niche for 10 out of the 16 zones tested. The seepage and liquid-release data were entered into the Technical Database Management System under DTN: LB980001233124.003.

Seepage-test data collected from two of the 10 intervals (UM 4.27–4.57 m and UM 5.49–5.79 m) were retrieved from DTN: LB980001233124.003 and are used in this AMR to calibrate and test

("validate") the SCM. Table 6 summarizes five separate liquid-release tests conducted at different liquid-release rates in borehole UM at a depth of 4.27 to 4.57 m from the borehole collar. These data are used to calibrate the SCM as described in Section 6.4. Likewise, Table 7 summarizes data from four seepage tests conducted at different liquid-release rates in borehole UM at a depth of 5.49 to 5.79 m from the borehole collar. These data are used to validate the SCM as described in Section 6.5.

Interval UM 4.27–4.57 m was selected because as many as five individual seepage tests were performed at this location (typically, only three or fewer individual tests were conducted per test interval). The liquid-release rate was lowered step-wise to identify a potential seepage threshold. In addition, the seepage percentage for two of the tests (Test #1 12-3-97 and Test #2 12-3-97) were significantly different even though the tests were conducted at nearly the same liquid-release rate. The large difference in seepage percentage was attributed to the effect of wetting history, i.e., the seepage data are believed to exhibit a strong memory effect because the tests were performed only two hours apart. Consequently, residual water remaining in the fractures from the first test (Test #1 12-3-97) influenced the amount of seepage that occurred during the second test (Test #2 12-3-97).

Interval UM 5.49–5.79 m was selected for validation of the SCM because as many as four seepage tests were conducted at different rates, i.e., the calibrated SCM is validated against data from a different location and under variable flow conditions.

Table 6. Summary of Liquid-Release Test Results for Interval UM 4.27–4.57

Event/ Test Name	Elapsed Time					Liquid- Release Rate (kg/s)	Mass Released (kg)	Seepage Mass (kg)	Seepage Percentage %
	Event/ Release Start (sec)	Event/ Release End (sec)	When Wetting Front Arrives (sec)	When Dripping Begins (sec)	When Dripping Ends (sec)				
Test 5 Niche 3650	0	500	409	423	2453	2.019E-03	1.0087	0.2280	22.60
Inactive - no release	500	1720511				0.000E+00			
Test #1 12-3-97	1720511	1722529	1721505	1721804	1724389	5.034E-04	1.0157	0.2354	23.18
Inactive - no release	1722529	1729525				0.000E+00			
Test #2 12-3-97 - start	1729525	1731528	1730015	1730083	1732793	5.057E-04	1.0125	0.5686	56.16
Inactive - no release	1731528	4747330				0.000E+00			
Test #1 1-7-98 - end	4747330	4768628	4755893	4763621	4770213	4.715E-05	1.0042	0.0460	4.58
Inactive - no release	4768628	7690199				0.000E+00			
Test #2 2-10-98 - start	7690199	7760753	7703568	--	--	1.649E-05	1.1633	0	0
Inactive - no release	7760753								

-- Event did not occur

Data Sources:

1. Elapsed times calculated in Excel '97 workbook "Niche 3650 Liq-rel UM4.27-4.57 m-2.xls" in worksheet "Elapsed times" at pp. 32-35 in SN YMP-LBNL-RCT-DSM-1.

2. Liquid-release rate, mass released, seepage mass, seepage percentage, and absolute time of event from DTN: LB980001233124.003.

Table 7. Summary of Liquid-Release Test Results for Interval UM 5.49–5.79

Event/ Test Name	Elapsed Time					Liquid-Release Rate (kg/s)	Mass Released (kg)	Seepage Mass (kg)	Seepage Percentage %
	When Event/ Release Begins (sec)	When Event/ Release Ends (sec)	When Wetting Front Arrives (sec)	When Dripping Begins (sec)	When Dripping Ends (sec)				
Test 4 Niche 3650	0	490	205	327	1385	2.069E-03	1.0134	0.2757	27.21
Inactive - no release	490	1811503				0.000E+00			
Test #2 12-4-97	1811503	1813554	1811905	1812151	1814143	5.040E-04	1.0337	0.2221	21.49
Inactive - no release	1813554	4913288				0.000E+00			
Test #1 1-9-98	4913288	4931265	4916035	4924171	4931765	5.778E-05	1.0387	0.0333	3.21
Inactive - no release	4931265	7773087				0.000E+00			
Test #1 2-11-98	7773087	7849643	7783195	--	--	1.361E-05	1.0417	0.0000	0.00
Inactive - no release	7849643					0.000E+00			

-- Event did not occur

Data Sources:

1. Elapsed times calculated in Excel '97 workbook "Niche 3650 liq-rel UM5.49-5.79 m.xls" in worksheet "Elapsed times" at pp. 35-37 in SN YMP-LBNL-RCT-DSM-1.
2. Liquid-release rate, mass released, seepage mass, seepage percentage and absolute time of event from DTN: LB980001233124.003.

6.3 DEVELOPMENT OF SEEPAGE CALIBRATION MODEL (SCM)

6.3.1 Conceptual Model

The SCM is intended to be a 3D, heterogeneous drift-scale fracture continuum model. The modeling assumptions are described in Section 5.2. The appropriateness of using a fracture-continuum approach for seepage calculations has been demonstrated in Section 5.3. Furthermore, choosing the continuum approach is conceptually consistent with the unsaturated zone site-scale model and submodels thereof, such as the various drift-scale models. This makes it straightforward to embed the SCM into the current modeling framework.

During the step-wise development of the SCM, a number of more simplified models have been tested, including 2D homogeneous, 2D heterogeneous, and 3D homogeneous representations of the SCM.

6.3.2 Generation of Heterogeneous Permeability Field

The geostatistical analysis described in Section 6.2.2 provides an empirical semivariogram of post-excavation air permeabilities at Niche 3650. Different theoretical models are fitted to the empirical semivariogram (SN YMP-LBNL-SAF-1, pp. 89–92, 98). A spherical semivariogram model with a nugget effect of 0.40, a correlation length of 3.87 m, and a sill value of 0.53 best matches the empirical log-permeability semivariogram, as shown in Figure 17. Note that the correlation length is simply a fitting parameter. Its relatively large value should not be misinterpreted as suggesting that the permeability field is strongly correlated. In fact (as clearly shown in Figure 17), the permeability is essentially random without a noticeable spatial correlation. Random, uncorrelated permeability fields are expected to yield similar results as the weakly correlated field used in this study.

The spherical semivariogram of Figure 17 along with the cumulative distribution function shown in Figure 16 is used as input to program SISIM (SISIM, V1.203, 10001-1.0MSISIMV1.203-00). SISIM generates a three-dimensional, spatially correlated permeability field using sequential indicator simulation (Deutsch and Journel 1992, p. 151). The random permeability field is conditioned on the post-excavation air-permeability data measured in various intervals of boreholes UL, UM, and UR. More details about the generation of a heterogeneous permeability field can be found in SN YMP-LBNL-SAF-1, pp. 93–99. The resulting permeability field is mapped onto the numerical grid of the SCM, as described in Section 6.3.3. Van Genuchten's capillary pressure and relative permeability functions (Luckner et al. 1989, pp. 2191–2192) are used in the SCM, where the capillary strength parameter $1/\alpha$ is correlated to the permeability in each grid block according to Leverett's scaling rule (Leverett 1941, p. 159; Finsterle 1997, p. 224).

(based on data submitted with this AMR under DTN: LB990831012027.001)
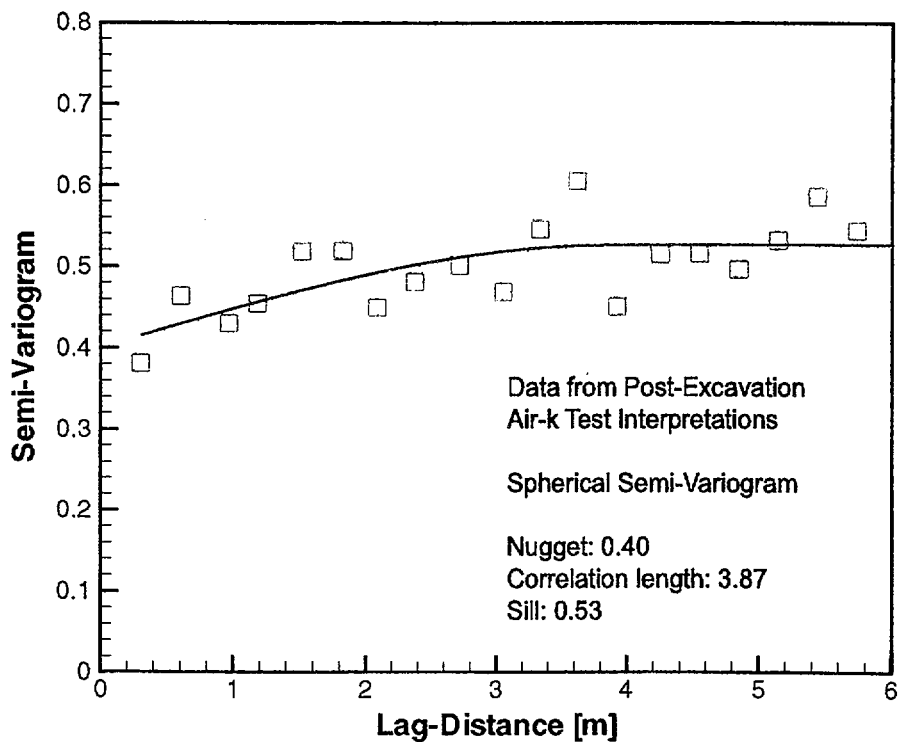
Figure 17. Empirical and Fitted Spherical Semivariogram of Post-Excavation
Air-Permeabilities Used to Generate Permeability Field of Seepage Calibration Model

6.3.3   Mesh Generation

Since the SCM will be calibrated against liquid-release test data, it is discretized to include the
approximate geometry of Niche 3650 and its boreholes. The mesh is created in several steps as
follows (SN YMP-LBNL-SAF-1, pp. 100–102):

1. A basic mesh is generated with X-Y-Z dimensions of $6 \times 1.5 \times 5$ m, respectively,
   discretized into regular, square gridblocks with a side length of 0.1 m. Given the small
   amount of water being injected, a model thickness of 1.5 m is sufficient to avoid
   unwanted boundary effects. This was confirmed by the simulations, in which the
   saturation plumes did not reach the model boundaries at Y=0.0 m and Y=1.5 m. As
   discussed in Section 5.3.6, the estimated parameters are affected by grid resolution, i.e.,
   the values given in Table 10 below strictly refer to the discretization chosen here.

2. The heterogeneous permeability field (see Section 6.3.2) is mapped onto the mesh using
   program Perm2Mesh (Perm2Mesh, V1.0, ACC: MOL.19990721.0554).

3. A niche is cut from the mesh using program CutNiche (CutNiche, V1.1,
   ACC: MOL.19990721.0557). The niche is rectangular (4 m wide and 2.5 m high) with a
   circular ceiling (radius 3 m, crown at Z = 3.25 m, axis parallel to the Y direction). A very

small nodal distance is defined from the element representing the niche to the first layer of formation elements, allowing us to set boundary conditions right at the niche wall. The length of the last vertical connection is thus 0.05 m, i.e., no horizontal flow diversion can occur closer than 0.05 m from the niche wall. (For more details, see SN YMP-LBNL-SAF-1, p. 39, 101.)

4. Boundary elements are added to the top and bottom of the model domain using program AddBound (AddBound, V1.0, ACC: MOL.19990721.0553). The bottom boundary element is assigned to rock type DRAIN to allow specifying a free-drainage boundary condition (Section 6.3.4).

5. Boreholes, injection intervals, and packers are included by modifying the material name of the corresponding elements (for details, see SN YMP-LBNL-SAF-1, pp. 100–101).

The final grid and log-permeability field of the 3D heterogeneous SCM is shown in Figure 18. Submodels of the SCM include a 2D X-Z cross section at Y = 0.75 and homogeneous versions of the model in two and three dimensions.
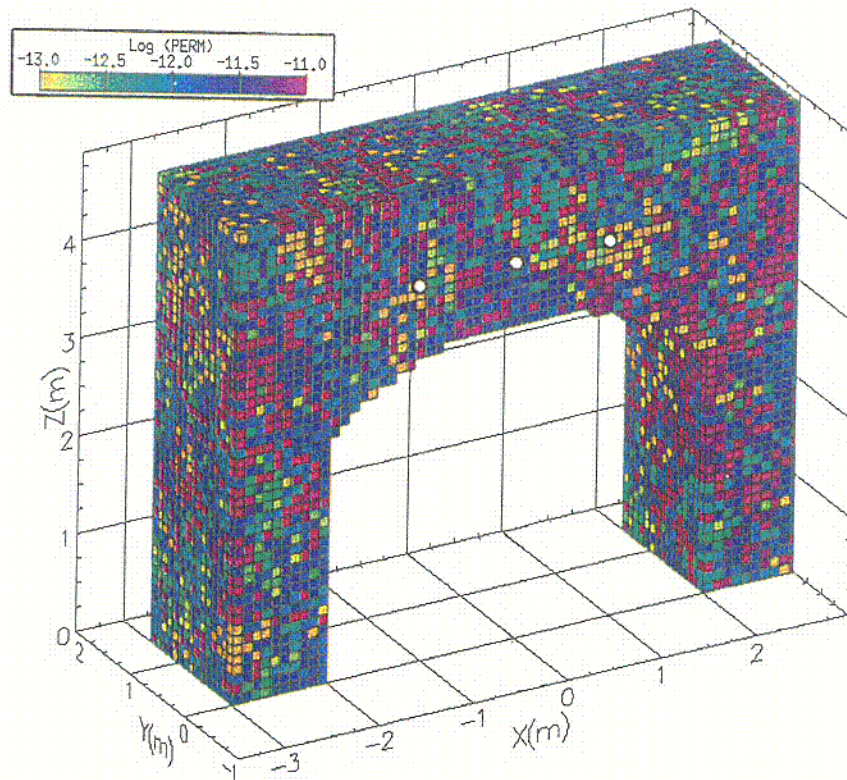
(based on data submitted with this AMR under DTN: LB990831012027.001)

Figure 18. 3D Seepage Calibration Model with Log-Permeability Field

6.3.4   Initial and Boundary Conditions

The present-day percolation flux at Niche 3650 is unknown or highly uncertain. The uncertainty is a result of uncertainties in the infiltration rates, and the channeling effects on account of larger scale flow diversions and local heterogeneities. Nevertheless, percolation flux on the scale of the niche is expected to be on the order of a few millimeters per year (see also Section 5.2, Assumption No. 7). It is considered reasonable to apply a constant rate of 3 mm/year at the top of the model domain. Since this flux is significantly lower than the fluxes induced by the liquid-release tests to be modeled with the SCM, it is not expected that the simulation results are strongly affected by the uncertainty in the assumed percolation flux. Moreover, this flux is believed to be below the seepage threshold, an assumption that is tested and confirmed after calibration of the SCM (see Section 6.6). A free-drainage boundary condition (Finsterle 1998, pp. 14–15) is applied at the bottom of the model. The niche itself is at a reference pressure of 1 bar. No capillary suction is applied in the niche, i.e., it is assumed that the air directly at the niche wall is of 100% relative humidity (see discussion of Assumption No. 6 in Section 5.2). Water is allowed to enter, but is prevented from exiting the niche. Thus, the temporal change of water in the niche element represents the cumulative seepage collected in the capture system installed during the liquid-release tests in Niche 3650. No-flow boundary conditions are specified at the left, right, back, and front sides of the model.

The initial saturation distribution is given by the steady-state flow field under natural percolation. Since the steady-state flow field changes if some of the input parameters are updated during the inversion, a steady-state simulation should precede each transient simulation of the liquid-release test. This approach is implemented for the homogeneous cases. For the heterogeneous cases, however, reaching steady state is computationally very time consuming. The initial saturation in the fracture continuum is generally low and is likely to have only a small impact on the simulation results. Moreover, the need for an accurate reproduction of a steady-state saturation distribution cannot be justified given the fact that initial conditions are under a transient regime as a result of ESF and niche excavation as well as dry-out from ventilation. Consequently, steady-state calculations are performed only once for the heterogeneous cases, assuming initial parameter values (see Section 6.3.5), and each transient run is preceded by a 2-year natural-state simulation to allow some redistribution of water as parameters are updated.

6.3.5   Initial Parameter Set

Table 8 summarizes the initial parameter set for the SCM. Reference permeability is taken from the post-excavation air-injection tests (see Section 6.2.3). The permeability used in the UZ Flow and Transport Model is given for comparison and is used to test the predictability of an uncalibrated, unconditioned SCM (see discussion in Section 6.4). Porosity and the reference van Genuchten parameter $1/\alpha$ will be varied during the inversion. All the other parameters are taken from the calibrated property set (DTN: LB997141233129.001) for the middle nonlithophysal unit of the Topopah Spring Tuff (hydrogeologic model layer TSw34), under base-case infiltration conditions. Since the SCM is a fracture-continuum model, no matrix properties are needed. Recall that the heterogeneous models include a spatially correlated permeability field, i.e., each gridblock has its own permeability value; the capillary strength parameter $1/\alpha$ is also considered heterogeneous, correlated to the permeabilities according to the Leverett scaling rule (see Section 6.3.2).

Table 8. Initial Parameter Set

Parameter	Value	Units	Reference
fracture permeability, k_f	2.18E-12	m^2	from post-excavation air-injection tests, see Section 6.2.3, Table 5.
fracture permeability, k_f	1.70E-11	m^2	DTN: LB997141233129.001
porosity, ϕ	0.01	-	DTN: LB997141233129.001; will be estimated.
van Genuchten α	5.16E-4	Pa^{-1}	DTN: LB997141233129.001; will estimate $1/\alpha$.
van Genuchten m	0.608	-	DTN: LB997141233129.001
van Genuchten n	2.551	-	$n=1/(1-m)$
residual saturation, S_{lrf}	0.01	-	DTN: LB997141233129.001
satiated saturation, S_{lsf}	1.0	-	DTN: LB997141233129.001

6.4 MODEL CALIBRATION

Calibrating the SCM against seepage data from liquid-release tests provides model-related, effective parameters relevant to the processes involved in drift seepage. The fact that seepage-relevant parameters are determined using flow data from a seepage experiment is a key aspect of our modeling approach. Determining parameters from flow experiments rather than from geometric information such as fracture density and aperture has significant advantages. Fracture mappings are strongly biased because of the selection of an arbitrary cut-off length, which filters out the smaller fractures and microfractures. The latter are believed to be of great importance for seepage. Small fractures and microfractures, if interconnected, are critical for seepage because they have sufficient capillary strength to hold the water, preventing it from seeping into the opening. At the same time they have—unlike the matrix—sufficient permeability to facilitate flow diversion around the drift. Furthermore, deriving flow properties from geometric fracture information must rely on simplified models, such as the parallel plate assumption, leading to highly uncertain and systematically biased estimates. In general, we believe that there is only a weak correlation between fracture mapping information and seepage-relevant hydrogeologic parameters, i.e., flow and seepage behavior cannot be reliably predicted from geometric fracture information alone.

If parameters are estimated by inverse modeling using flow data from seepage experiments, seepage-relevant processes are automatically reflected in the estimated parameters. Moreover, the estimates are able to partly compensate for processes and features not explicitly accounted for in the model. For example, an estimate of matrix permeability determined by inverse modeling is automatically increased if microfractures are present. Or—more relevant for the current study—the tendency for increased seepage from poorly connected, discrete fractures intersecting the drift can be accounted for by an appropriately reduced van Genuchten $1/\alpha$ value (see discussion in Section 5.3). The simplification made by the model (discrete fractures are not explicitly included) can be partly compensated by estimating effective parameters. It should be acknowledged that the estimated parameters are not hydrologic properties *per se*, but are related to the conceptual model. Determining model-related parameters from data that reveal seepage-relevant processes results in a model suitable for seepage predictions.

We employed inverse modeling techniques implemented into the code iTOUGH2 for automatic calibration of the SCM. As described in Section 6.2.4, a sequence of five liquid-release tests was selected for calibration. The five tests from interval UM 4.27–4.57 m were conducted at various injection rates with different lengths of inactivity between individual test events. The seepage data are thus expected to reveal a number of seepage-relevant processes, including storage, memory effects and the approach of a seepage threshold.

In a transient seepage experiment with only a small volume released, the amount of water seeping into the niche mainly depends on three factors:

1. The potential of the formation to hold the water by capillary forces, here expressed through an effective van Genuchten parameter $1/\alpha$.

2. The potential of the formation to store the finite amount of water released, here expressed through an effective porosity ϕ, which may include effects of matrix imbibition.

3. The potential of the formation to divert water around the opening, here expressed through an effective permeability k, which may include contributions from microfractures and the matrix.

The simulated seepage percentage can be increased by decreasing either capillary strength $1/\alpha$, porosity ϕ, or permeability k. Consequently, all parameter pairs are negatively correlated when inversely determined from seepage data. If only seepage-percentage data are available for calibration, the parameter correlations are expected to be strong, i.e., it is unlikely that they can be determined independently from one another and with a reasonably low estimation uncertainty.

Unfortunately, each liquid-release test provides only one data point for calibration, which is the total amount of water collected in the capture system at the end of each test event. No time-dependent seepage rates are available from Niche 3650. As a result of this limited data basis and the expected strong correlations, the number of parameters to be estimated must be kept as small as possible.

We choose to determine the porosity ϕ and the van Genuchten parameter $1/\alpha$ while fixing permeability k at the value estimated from the post-excavation air-injection tests (see Section 6.2.3). The rationale for this selection is as follows:

1. The capillary strength $1/\alpha$ is both sensitive and uncertain, i.e., the reliability of subsequent seepage predictions depends to a large extent on the value of $1/\alpha$, which cannot be deduced from independent information (such as fracture mapping). The estimated value will be an effective parameter describing the capillary barrier in a drift-scale fracture continuum model.

2. Since only a relatively small amount of water (approximately 1 kg, see Table 6) is released in each test event, fracture and matrix storage effects are expected to be significant. It should be noted that porosity is not important for seepage predictions under near-steady-state conditions. The fact that porosity must be estimated here is a result of the particular liquid-release test design. Liquid-release test were restricted to the use of a

small amount of water, which made the tests highly transient and increased the importance of storage effects.

3. Permeability is excluded from the estimation process because there is independent information available from the air-injection tests (for further discussion, see Section 5.2, Assumption No. 3). Furthermore, flow diversion is expected to play a minor role during these tests as a result of the small amount of water released. Nevertheless, permeability should be included and considered uncertain in any steady-state seepage prediction exercise.

The need to estimate porosity is unfortunate because porosity will not affect steady-state seepage predictions. Moreover, estimating porosity increases the uncertainty in the estimate of $1/\alpha$ to which it is strongly correlated. Future liquid-release tests should be designed as long-term experiments, with a sufficient amount of water being released so that porosity becomes insensitive, and conversely flow diversion around the niche becomes important, enabling the estimation of seepage-relevant permeability values on the drift scale.

Transient information is needed to better determine porosity. The obvious memory effect seen between Test #1 12-3-97 and Test #2 12-3-97 helps identify the storage capacity in a joint inversion of data from both tests. Moreover, the time when seepage starts and ends has been recorded (see Table 6). This information—even though highly dependent on the specific features of the fractures encountered by the water on its path from the injection point to the niche ceiling—is included in the inversion in an approximate way. Two dummy data points are added to each test event. The first dummy data point of zero seepage is specified at the time when seepage starts, and the total seepage amount is given as a second dummy data point at the time when seepage stopped, along with the actual point which is assigned at the end of the test event. For example, for Test #1 12-3-97 (see Table 6), a calibration point with a seepage mass of zero is specified at time 1,721,804 s and assigned a standard deviation of 0.03 kg; the second dummy calibration point has a value of 0.2354 kg at time 1,724,389 s, also with a standard deviation of 0.03 kg; finally, the third calibration point with the measured seepage mass of 0.2354 kg is set at time 1,729,520 s (i.e., shortly before the next test event) and is more strongly weighted by assigning a lower standard deviation of 0.01 kg. The first two calibration points penalize both early water breakthrough and long seepage tails, thus introducing some transient information for a better constraint of porosity. More details can be found in YMP-LBNL-SAF-1, pp. 103–109, 146.

Using the initial parameter set of Table 8 would lead to zero seepage in all simulated liquid-release tests as a result of the relatively low α value. Recall that initial α was determined based on air-permeability data, fracture density information, and a parallel-plate assumption, and by calibration against matrix saturation and water-potential measurements, i.e., they are not expected to be representative of seepage-related processes.

A joint inversion of all five test events was performed using homogeneous and heterogeneous, 2D and 3D representations of the SCM. The resulting matches are summarized in Table 9 and visualized in Figure 19.
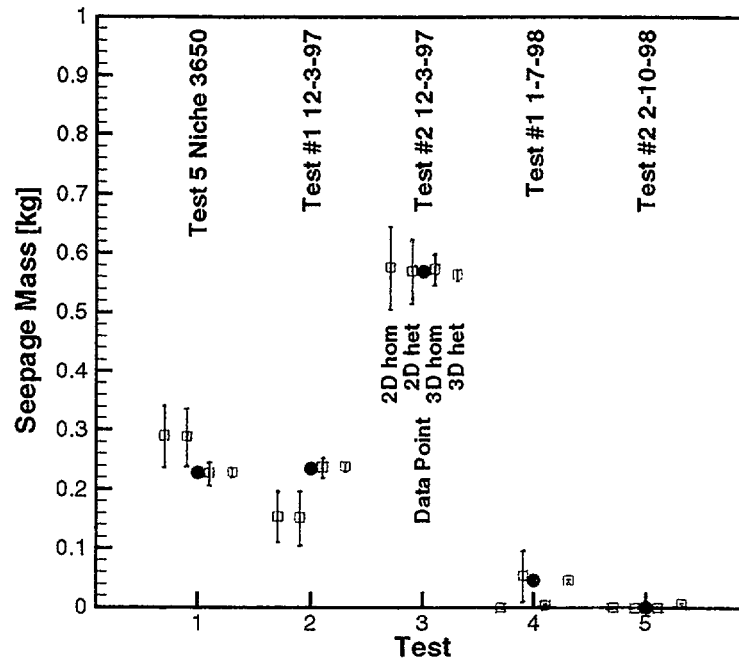
(based on DTN: LB980001233124.003 and on data submitted with this AMR
under DTN: LB990831012027.001)

NOTE: 95%-error bands indicate prediction uncertainty of calibrated SCM.

Figure 19. Comparison Between Measured (Circles) and Calculated (Squares) Seepage Mass

All models show the following general behavior:

1. Even though the total amount of water released during each test event is approximately the same, less seepage is observed if the water is released at a lower rate, suggesting the existence of a seepage threshold, which is defined as a rate below which no seepage occurs. This fundamental behavior is seen in both the data and the corresponding simulation results.

2. If a liquid-release test is followed by another test at a similar rate but with little inactive time between them (e.g., Tests #1 and #2 conducted on 12-3-97) the second test leads to significantly more seepage. This is a result of the fact that a certain amount of water is stored in the formation before seepage is initiated; this storage volume is reduced or not available for the second test event. The resulting memory effect can be seen in both the data and the simulation.

3. The two effects described above overlap, making it sometimes difficult to clearly separate and identify them. For example, Test #1 12-3-97 yielded a seepage mass comparable to that measured in Test 5 Niche 3650 despite its lower rate and despite a long inactive time between them. A potential explanation for this behavior is that storage

effects are much stronger and last longer for the first in a sequence of liquid-release tests. Water from the first test is used mainly to fill up dead-end fractures and to saturate the matrix; the seepage rate is correspondingly low. For all subsequent tests, storage is restricted to saturation increases in the flowing fractures, i.e., the memory effect is expected to be much weaker. A second explanation could be that—considering the rate and measured air permeability—the test is performed at a rate close to or exceeding the saturated hydraulic conductivity in the vicinity of the tested interval, conditions for which seepage is almost constant regardless of injection rate.

The matches obtained with the SCM can be considered acceptable given the uncertainty in the data and the parsimony of the models. The 3D models perform slightly better than the 2D alternatives; the differences in the matches obtained with homogeneous and heterogeneous models are insignificant. A notable exception is Test #1 1-7-98, in which a higher seepage mass is predicted with the heterogeneous models compared to the homogeneous models. The heterogeneous models are in better agreement with the measured data point.

The 2D models fail to reproduce the relatively high seepage mass in Test #1 12-3-97, which indicates that the strong memory effect from the initial injection (Test 5 Niche 3650) is not appropriately represented in the model because features such as dead-end fractures and processes such as matrix imbibition are not explicitly represented. As a result, seepage from the first test is overpredicted, whereas the calculated seepage mass for the second test—performed at a lower rate—is underpredicted. This inability of the 2D model to reproduce the initial memory effect may slightly bias the estimates. Since initial memory effects are insignificant if the flow field is near steady state, they are of little importance for seepage predictions under natural percolation conditions and should be eliminated by matching data of long-term liquid-release tests.

The 3D models simulate the temporal and spatial spreading of the liquid plume more accurately than the 2D models. The initial storage of water and its distribution is better represented, and as a result, the 3D models are capable of matching all test events very accurately. Note that the 3D heterogeneous model is the only one that leads to seepage for the last test, which was conducted at a very low rate. It is therefore expected that the 3D heterogeneous model will predict a lower seepage threshold than the other models.

Table 9. Comparison Between Measured and Calculated Seepage Mass in kg

Model	Test 5 Niche 3650		Test #1 12-3-97		Test #2 12-3-97		Test #1 1-7-98		Test #2 2-10-98	
	Meas.	Calc.	Meas.	Calc.	Meas.	Calc.	Meas.	Calc.	Meas.	Calc.
2D-homogeneous	0.228	0.290	0.235	0.155	0.569	0.577	0.046	0.000	0.000	0.000
2D-heterogeneous	0.228	0.289	0.235	0.153	0.569	0.571	0.046	0.055	0.000	0.000
3D-homogeneous	0.228	0.228	0.235	0.238	0.569	0.574	0.046	0.004	0.000	0.000
3D-heterogeneous	0.228	0.229	0.235	0.239	0.569	0.564	0.046	0.046	0.000	0.001

(based on DTN: LB980001233124.003 and on data submitted with this AMR under DTN: LB990831012027.001)

The parameter estimates and their uncertainties are summarized in Table 10. The standard deviation is the square root of the diagonal element of the estimation covariance matrix (Carrera and Neuman 1986, p. 205); the correlation coefficient is calculated from the variances and the covariance between the two estimated parameters (Finsterle 1999, p. 63).

Table 10. Parameter Estimates, Estimation Uncertainty, and Correlation Coefficient

Model	$\log(1/\alpha$ [Pa] $)^*$		$\log(\phi)$		Corr. Coeff.
	Estimate	Std. Dev.	Estimate	Std. Dev.	
2d-homogeneous	2.25	0.09	-2.46	0.06	-0.75
2d-heterogeneous	2.95	0.06	-2.49	0.05	-0.63
3d-homogeneous	1.50	0.03	-2.87	0.02	-0.74
3d-heterogeneous	1.82	0.01	-2.89	0.01	-0.77

(based on data submitted with this AMR under DTN: LB990831012027.001)

* In the heterogeneous models, $1/\alpha$ is the reference capillary strength, which is related to the reference permeability $k = 10^{-12}$ m^2 through Leverett's scaling rule (Leverett 1941, p. 159).

The following comments can be made:

1. The estimated seepage-related capillary strength parameter $\log(1/\alpha)$ is much lower than the initial value of 3.29 (see Table 8). The difference can be explained as a result of the fact that the initial guess refers to the large-scale behavior of intact rock, whereas the estimate from the liquid-release tests characterizes the excavation-distrurbed zone and includes the seepage-specific effects from discrete fractures near the niche wall.

2. The capillary strength parameter $1/\alpha$ is lower for the homogenous than for the heterogeneous model. This is expected because the explicitly modeled heterogeneity leads to some flow channeling, resulting in higher seepage. The absence of flow channeling in the homogeneous model is compensated for by reducing the capillary barrier effect, i.e., by making $1/\alpha$ smaller.

3. The capillary-strength parameter $1/\alpha$ is lower for the 3D than for the 2D models. The 3D models provide additional possibilities for flow diversion, reducing seepage. Consequently, the capillary strength must be reduced to induce seepage comparable to that obtained with the 2D models and the observed data, leading to relatively low $1/\alpha$ estimates.

4. The porosity estimates for the 2D homogeneous and heterogeneous models are consistent with one another. They are higher than the estimates from the 3D models, indicating that the liquid plume was somewhat confined by the two-dimensionality of the model.

5. The correlation coefficient between capillary strength and porosity is negative because reducing $1/\alpha$ leads to an increase in seepage, which can be partly compensated by an increase in the pore volume available for storage. The correlation coefficient is consistently estimated for all four models considered.

As demonstrated here, the differences and similarities in the estimated parameter sets can be explained and related to the structure of the respective conceptual models, illustrating the need to determine and to use process-specific and model-related parameters. As a result of effective parameter estimation, all models are able to reproduce the same effective behavior.

6.5 MODEL VALIDATION

According to AP-3.10Q/Rev. 1/ICN 0, p. 5, model validation is the "process that demonstrates that a model is an acceptable representation of the process or system for which it is intended." This usually involves blind predictions of the calibrated model and comparison with independent data. The ultimate purpose of drift-scale seepage models is to predict seepage under natural flow conditions, which involve generally lower percolation fluxes over longer time periods than those encountered during a liquid-release test. Since no seepage data under natural percolation are currently available, the SCM cannot be validated. However, the SCM can be partly validated using seepage data from liquid-release tests different from those used in the calibration of the model. The prediction of transient seepage data from a local liquid-release test may be considered more difficult than predictions of average seepage under steady-state conditions because it includes additional uncertainty from the highly sensitive porosity estimate. On the other hand, predictions of natural seepage must be based on an extrapolation to significantly lower percolation rates.

In this section, we predict seepage from four liquid-release tests and compare the results to the corresponding data, taking into account the prediction uncertainty. The four tests selected for validation are believed to be the most difficult ones to be simultaneously reproduced by the calibrated SCM. They were performed using a wide range of injection rates, and they show a seepage threshold and potentially storage effects. The majority of liquid-release tests performed showed zero seepage, a result that is believed to be reproducible with the calibrated SCM.

The four tests were conducted in Interval UM 5.49–5.79 m as described in Section 6.2.4; the data are summarized in Table 7. We consider the validation successful if the data lie within the 95% error band calculated by the calibrated SCM. This means that the seepage calculated with the best-estimate parameter set is not required to match the data precisely, but with reasonable accuracy, where "reasonable" is defined by the prediction uncertainty. The question whether this prediction uncertainty is acceptable for future model applications does not need to be answered to validate the SCM. The uncertainty will simply be taken as input to the Seepage Models for PA and propagated through applicable PA models. A probabilistic acceptance criterion is adopted to ensure that prediction uncertainty is included in the validation process as well as in future model predictions. This should reduce misinterpretations and the misuse of the SCM.

Several methods can be employed to assess the uncertainty of model predictions as a result of parameter uncertainty. When computationally feasible, Monte Carlo simulations (Finsterle 1999, pp. 76–78) are the method of choice because they automatically account for nonlinearities in the model. A simplified linear uncertainty-propagation analysis (Finsterle 1999, pp. 74–76) can be chosen in cases where running many simulations is prohibitive. Monte Carlo simulations are performed for the 2D models, whereas linear uncertainty-propagation analysis is applied for the 3D models.

For the Monte Carlo simulations using the 2D models, a standard deviation of 0.1 is assigned to $\log(1/\alpha)$, $\log(\phi)$, and $\log(k)$. This value represents a 25% uncertainty in each of the parameters, which are assumed to be uncorrelated. The parameter uncertainty is slightly increased over the standard deviation given in Table 10 to account for the fact that the prediction is performed at a different location. Moreover, permeability is included as an additional uncertain parameter.

Note that these small standard deviations lead to relatively small prediction uncertainties, making it difficult to meet the validation acceptance criteria. The standard deviations should be appropriately increased for probabilistic seepage predictions that involve a change in conditions such as a different location or unit with potentially changed formation characteristics, changes in spatial or temporal scale, or changes in governing processes (e.g., unmodeled thermal or geochemical effects). Heterogeneities that are not explicitly represented in the model or other conceptual uncertainties should also be accounted for by increasing parameter standard deviations in probabilistic seepage predictions.

The histogram of the seepage predictions from four liquid-release tests for the 2D homogeneous and heterogeneous models are shown in Figures 20 and 21, respectively. The prediction with the best-estimate parameter set (see Table 10) is shown as a thin red line, whereas the long shaded bar indicates the measured value (see Table 7). For the 2D homogeneous model, the measured value is always within the range predicted by the Monte Carlo simulations, i.e., a correct statement regarding seepage was made with the calibrated SCM.

The 2D heterogeneous model overpredicts seepage for the first two tests of the series. Predictions made with a heterogeneous model should include multiple realizations of the heterogeneous permeability field. Probabilistic simulations with multiple stochastic realizations are beyond the scope of this study.
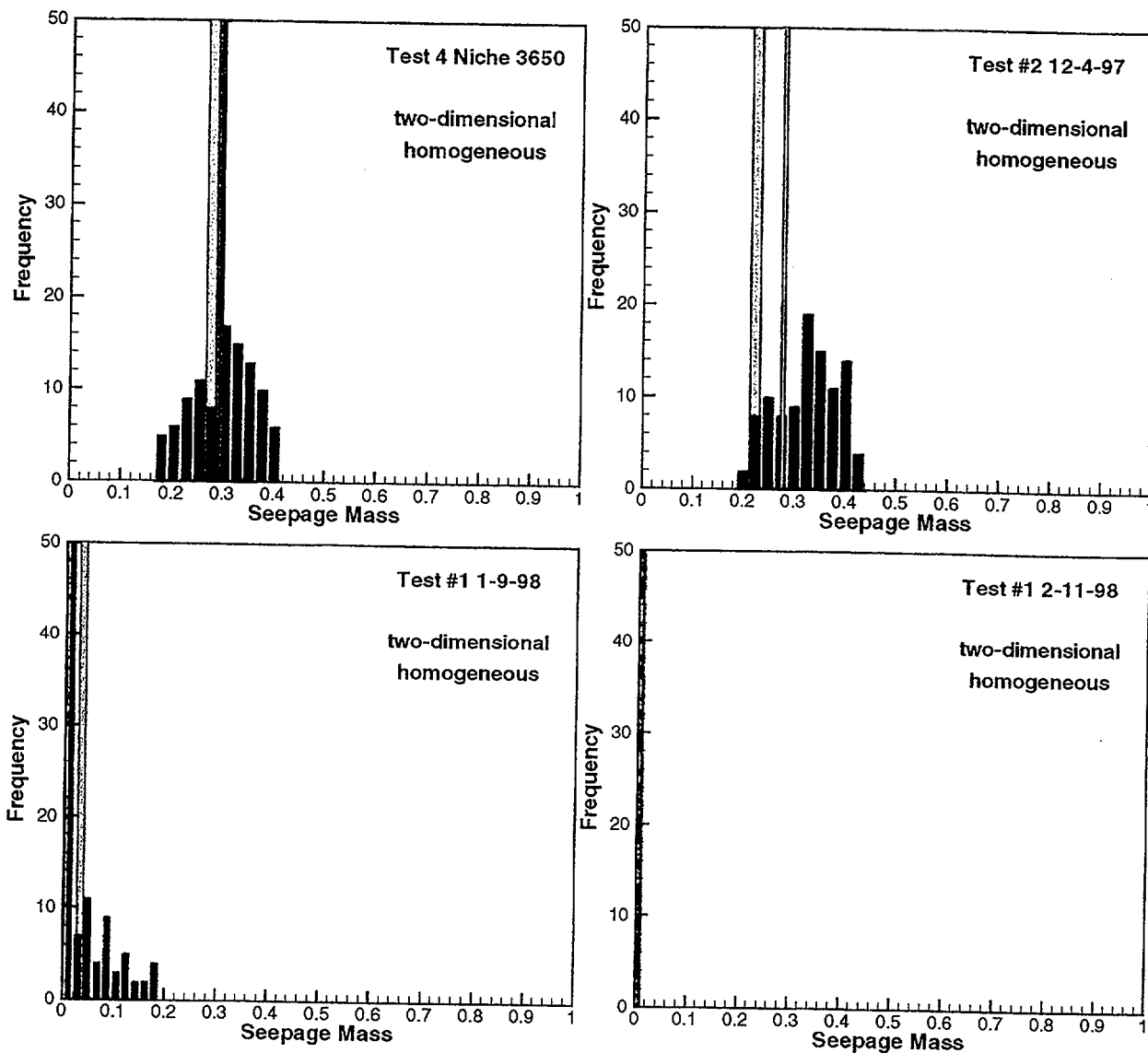
(based on DTN: LB980001233124.003 and on data submitted with this AMR under DTN: LB990831012027.001)

NOTE: The seepage mass predicted with the best-estimate parameter set is shown as a thin red line; the measured value is represented by the long shaded bar.

Figure 20. Histograms of Model Predictions with 2D Homogeneous Seepage Calibration Model
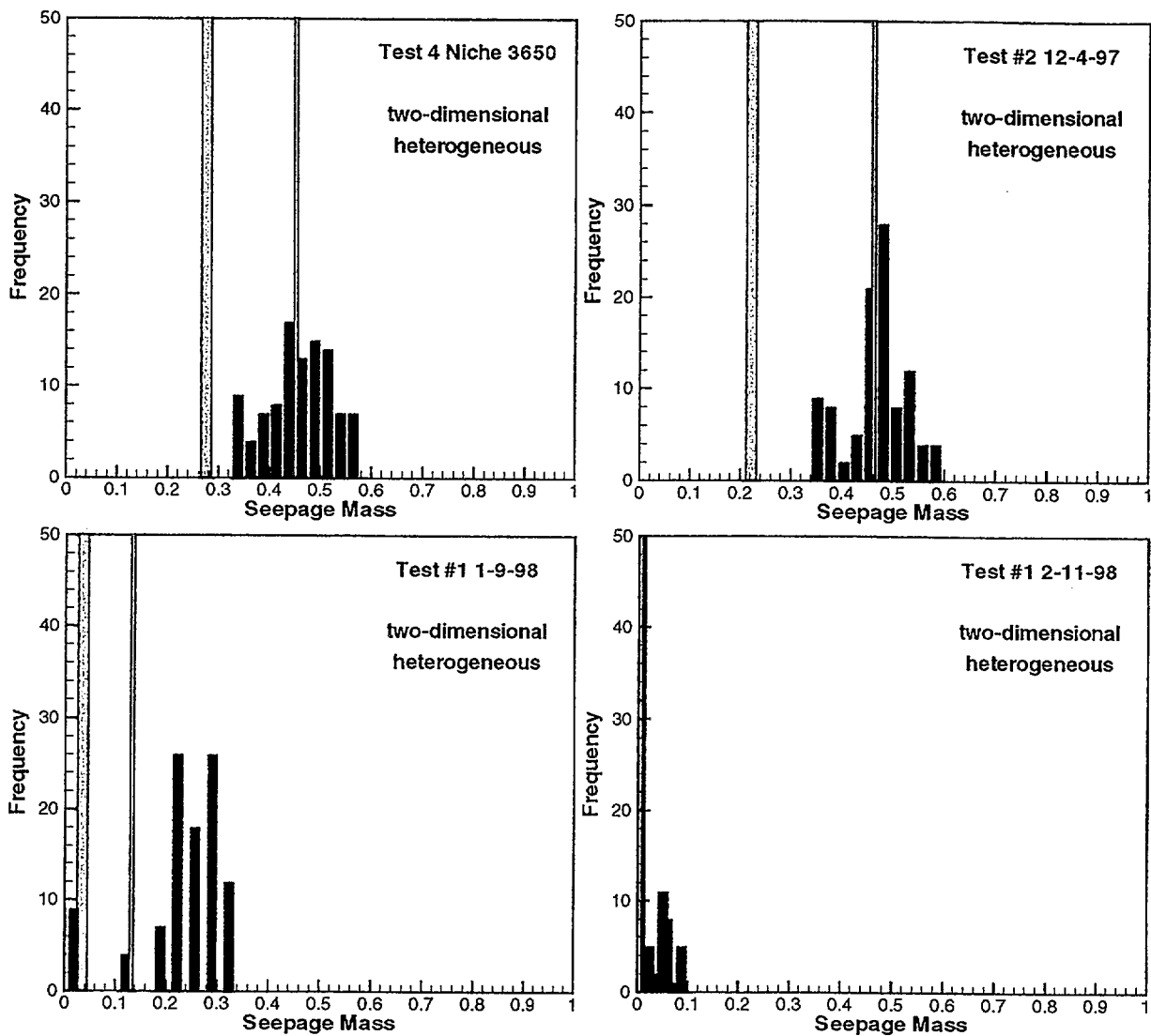
(based on DTN: LB980001233124.003 and on data submitted with this AMR under DTN: LB990831012027.001)

NOTE: The seepage mass predicted with the best-estimate parameter set is shown as a thin red line; the measured value is represented by the long shaded bar.

Figure 21. Histograms of Model Predictions with 2D Heterogeneous Seepage Calibration Model

The seepage predictions with the 3D homogeneous model are very accurate, i.e., the measured value is very close to the simulation result and always within the error band (see Figure 22). The uncertainties of the model predictions were calculated on the basis of a linearity and normality assumption with a very small parameter standard deviation of 0.05 for $\log(1/\alpha)$ and $\log(\phi)$, which corresponds to as little as 12% variation in these estimates. The standard deviations are chosen

smaller than those used for the 2D models because the estimation uncertainties were also smaller (see Table 10).

The 3D heterogeneous model also meets the validation criteria with the exception of the first event, Test 4 Niche 3650, where seepage was underpredicted (see Figure 23). As in the 2D heterogeneous case, the additional uncertainty resulting from multiple realizations of random permeability fields is not included here.
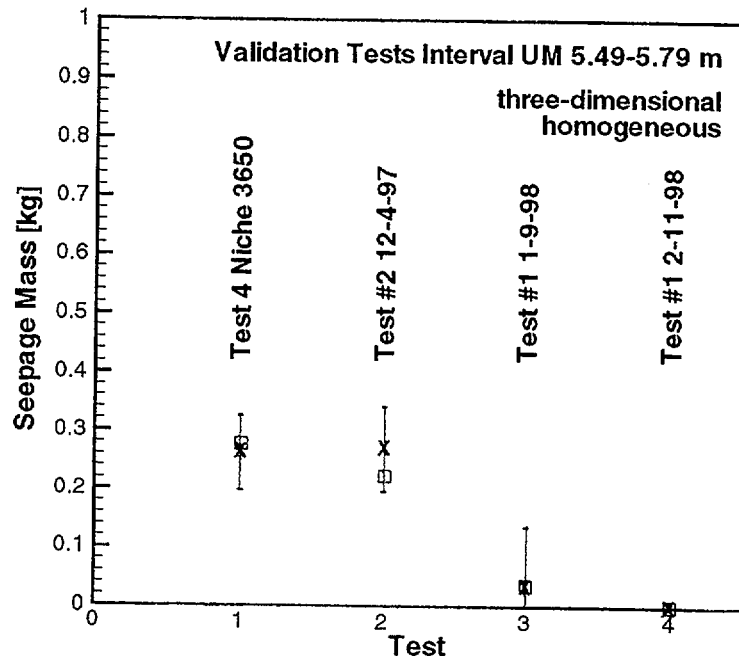
(based on DTN: LB980001233124.003 and on data submitted with this AMR
under DTN: LB990831012027.001)

NOTE: The seepage mass predicted with the best-estimate parameter set is shown as a cross; the measured value is represented by a square; 95% error bars are determined by linear uncertainty-propagation analysis.

Figure 22. Validation of 3D Homogeneous Seepage Calibration Model
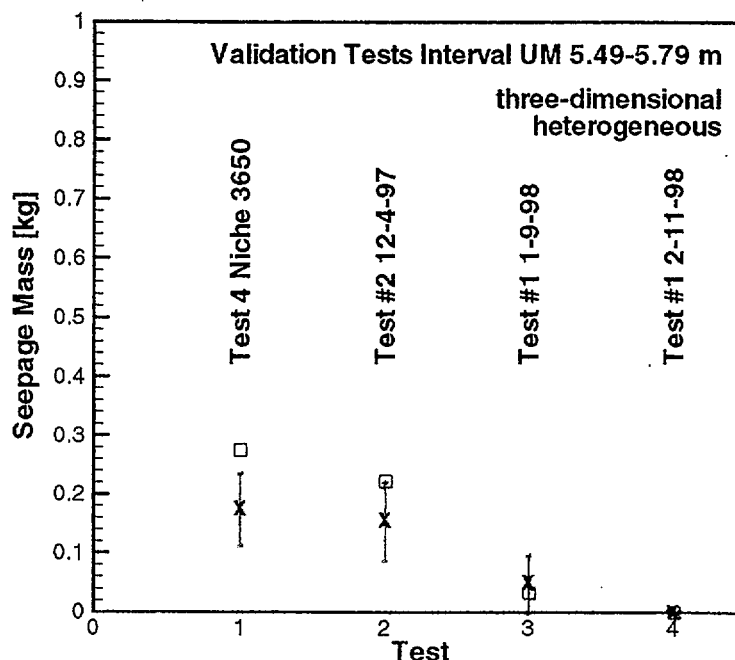
(based on DTN: LB980001233124.003 and on data submitted with this AMR
under DTN: LB990831012027.001)

NOTE: The seepage mass predicted with the best-estimate parameter set is shown as a cross; the
measured value is represented by a square; 95% error bars are determined by linear uncertainty
propagation analysis

Figure 23. Validation of 3D Heterogeneous Seepage Calibration Model

In summary, the model predictions are consistent with the measured seepage mass in most cases, despite rigorous assumptions regarding the uncertainty of the input parameters. The homogeneous models unconditionally meet the stringent validation criteria. Since only a single realization of the random permeability field was used to test the heterogeneous models, the predictions are outside the 95% error band in certain test events. Multiple realizations should be generated, which will provide a larger, more realistic spread of seepage predictions. Furthermore, blind predictions of future long-term seepage tests should be made and compared to the data to gain additional confidence into the SCM prediction capability. Instructions for reproducing the simulations discussed in this section can be found in SN YMP-LBNL-SAF-2, pp. 2–7.

6.6 SEEPAGE THRESHOLD PREDICTIONS

Steady-state simulations are performed to calculate seepage for a large range of percolation fluxes. The percolation flux below which no seepage occurs is termed "seepage threshold." Note that the percolation fluxes examined here are significantly higher than the average infiltration rate considered reasonable at Yucca Mountain. These fluxes can be interpreted as being local and relevant to drift-scale studies. They are assumed to be significantly larger than average infiltration or percolation fluxes as a result of flow channeling effects (Birkholzer and Tsang 1997). The

development and characteristics of such weeps are not investigated here; we simply extend our seepage predictions to very high percolation fluxes to cover potential channeling effects. Also note that the seepage threshold and seepage percentages determined here are for a niche with a circular, smooth ceiling (see Figure 18), located in the middle nonlithophysal zone of the Topopah Spring welded tuffs, in an area of relatively competent rock mass and low fracture density. Extrapolations to other drift geometries and hydrogeologic units are not valid.

Figures 24 and 25 show the seepage percentages as a function of percolation flux as predicted by the 2D homogeneous and heterogeneous models, respectively. The results with the best-estimate parameter set (see Table 10) are shown as a solid line, revealing a seepage threshold of 3,150 and 1,000 mm/year, respectively. It is interesting to note that a new seepage location becomes available for percolation fluxes higher than 5,000 mm/year, leading to a kink in the predicted seepage percentage for the heterogeneous model (Figure 25).

For the 2D models, Monte Carlo simulations were performed; the results are depicted as short dashes. The capillary strength parameter $1/\alpha$ and absolute permeability k are assumed uncorrelated and log-normally distributed with a standard deviation of 0.1. Percolation flux is sampled uniformly between 1 and 10,000 mm/year. The uniform distribution is not supposed to reflect the assumption about percolation uncertainty, but is chosen to cover a wide range of fluxes as part of a sensitivity analysis. The results would have to be weighted with the assumed percolation probability before making any probabilistic statements about drift seepage.

The 3D homogeneous and heterogeneous model results (see Figures 26 and 27) yield a seepage threshold of approximately 700 and 250 mm/year, respectively. No Monte Carlo simulations could be performed to assess prediction uncertainty. Future seepage studies should include Monte Carlo simulations in which not only parameters are sampled from a distribution, but also a large number of random permeability fields are generated.

The Monte Carlo simulations performed with the 2D models and the implied variability and uncertainty in the 3D models indicate significant uncertainty in seepage percentage predictions. Nevertheless, there seems to be a low seepage probability for percolation fluxes below 100 mm/year. The calculation of this probability is beyond the scope of this AMR.

Instructions for reproducing the simulations discussed in this section can be found in SN YMP-LBNL-SAF-2, pp. 10–15.
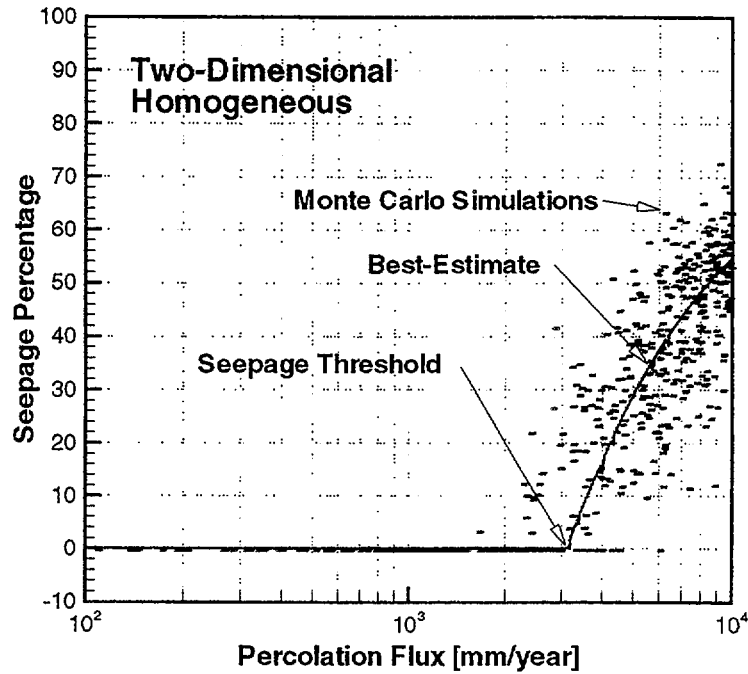
(based on data submitted with this AMR under DTN: LB990831012027.001)

NOTE: Solid line shows result obtained with best-estimate parameter set; short dashes depict Monte Carlo simulation results.

Figure 24. Seepage Percentage as a Function of Percolation Flux for 2D Homogeneous Model
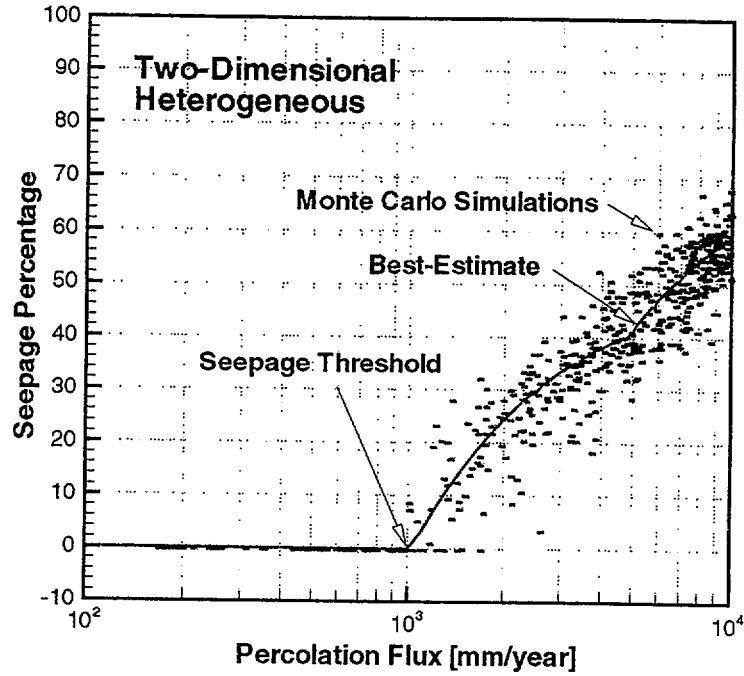
(based on data submitted with this AMR under DTN: LB990831012027.001)

NOTE: Solid line shows result obtained with best-estimate parameter set; short dashes depict Monte Carlo simulation results.

Figure 25. Seepage Percentage as a Function of Percolation Flux for 2D Heterogeneous Model
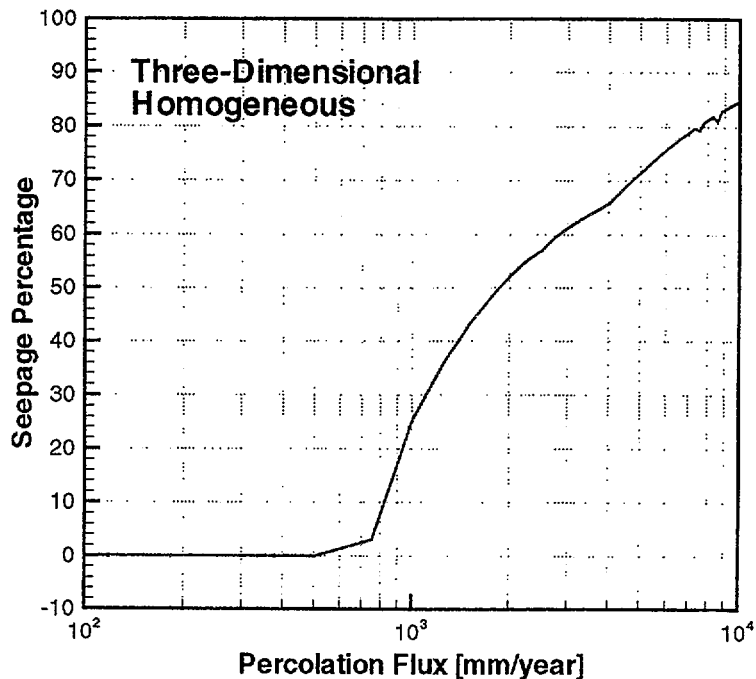
(based on data submitted with this AMR under DTN: LB990831012027.001)

Figure 26. Seepage Percentage as a Function of Percolation Flux for 3D Homogeneous
Model
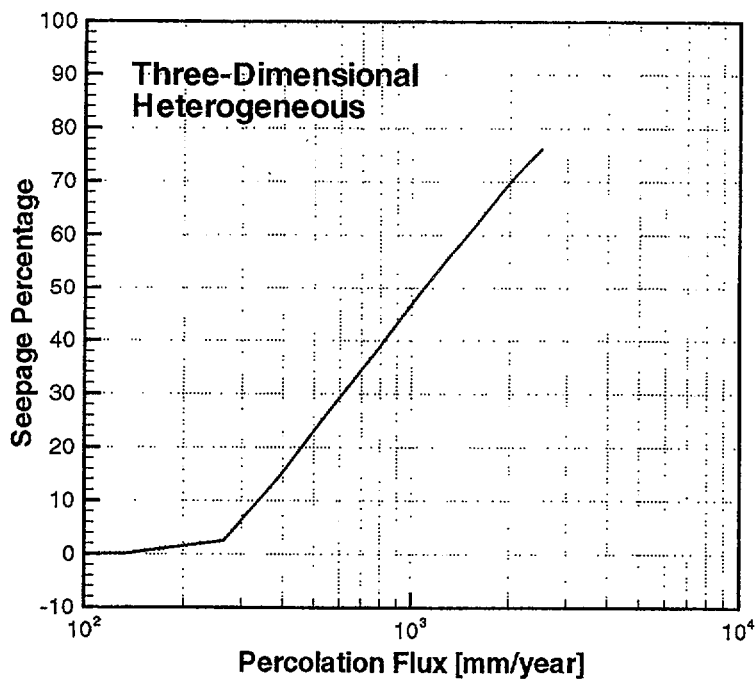
(based on data submitted with this AMR under DTN: LB990831012027.001)

Figure 27. Seepage Percentage as a Function of Percolation Flux for 3D Heterogeneous
Model

6.7 ALTERNATIVE CONCEPTUAL MODELS AND SENSITIVITY ANALYSES

6.7.1 Alternative Conceptual Models

Using a discrete fracture network model (DFNM) as an alternative to the fracture continuum model presented here is a valid option that should be studied in detail. The DFNM has the advantage of being intuitively more appropriate for seepage predictions. The reasons for not using a DFNM can be summarized as follows:

1. A very large amount of geometric and unsaturated hydrologic property data would be required for the development of a defensible DFNM. While part of the geometric information can be obtained from fracture mappings, the description of the network remains incomplete and potentially biased. Moreover, unsaturated hydrologic parameters on the scale of individual fractures would be required, along with conceptual models and simplifying assumptions regarding unsaturated flow within fractures and across fracture intersections. The required data basis is not available. As a result, the cumulative effect of all the input uncertainties is likely to outweigh the apparent advantage of a detailed representation of the fracture network.

2. Considering a DFNM more appropriate for seepage predictions is based on the premise that all physical processes relevant for seepage are well understood, well characterized, and appropriately described in the model, and that the accurate geometric representation of the fracture network is the only aspect that needs refinement. We believe that the complexity of seepage cannot be described, characterized, and simulated on the scale of individual water droplets. However, we maintain that the effects can be reasonably well accounted for in a model that acknowledges its limitations, and for which effective parameters are determined *based on seepage-relevant data.*

3. The incorporation of a DFNM into the current framework of nested continuum models would be problematic.

4. The appropriateness of using a fracture continuum model for the prediction of effective seepage quantities such as seepage percentage was demonstrated in Section 5.3 of this AMR.

5. To our knowledge, no sophisticated fracture network code is currently available that would be capable of simulating unsaturated flow through complex, heterogeneous, three-dimensional fracture networks and seepage into underground openings.

6. The FCM can be developed based on less information than would be required for the development of a DFNM.

In general, the choice of a conceptual model for seepage predictions should be based on a careful consideration of the study objectives, the available data basis in comparison with the data needs, the uncertainties in the input parameters and the corresponding prediction uncertainties, as well as computational aspects.

6.7.2   Sensitivity Analysis

This AMR is concerned with the development and calibration of the Seepage Calibration Model (SCM). Extensive sensitivity analyses for seepage into drifts of varying geometry and flow conditions will be performed with the Seepage Model for PA. Nevertheless, many simulations were performed during the calibration process and to generate distributions of model output during validation and seepage threshold predictions. These simulations provided insight into the variability of the model result as parameters are changed within the range of their expected uncertainty. The results of these extensive sensitivity analyses were visualized and discussed in Sections 6.5 and 6.6.

INTENTIONALLY LEFT BLANK

7. CONCLUSIONS

2D and 3D homogeneous and heterogeneous versions of the Seepage Calibration Model (SCM) were developed based on post-excavation air-permeability data, which showed little spatial correlation (see Sections 6.2 and 6.3). The SCM models were calibrated against seepage data from liquid-release tests performed at various injection rates and with different inactive periods between individual test events. Effective values for the capillary strength parameter $1/\alpha$ and porosity ϕ were determined (Section 6.4). Permeability was fixed at the values estimated from the air-injection tests. The inverse modeling results can be summarized as follows:

1. While zero seepage would be predicted with an uncalibrated model using initial parameter values (see Table 8), the seepage data were reasonably well matched by the calibrated models considered in this study (see Table 9).

2. The capillary strength parameter $1/\alpha$ is reduced relative to the initial value. The smallest value was obtained with the 3D homogeneous model, and the highest value was estimated for the 2D heterogeneous model (see discussion of Table 10).

3. It was necessary to estimate porosity as a parameter representing the storage capacity of the formation despite storage effects being of little concern for seepage predictions under natural, near-steady-state conditions. Liquid-release tests should be designed as long-term experiments with a sufficient amount of water being released. The transient and steady-state seepage rate should be measured. In such an experiment, porosity, which does not affect steady-state seepage predictions, becomes insensitive, i.e., it does not need to be determined from the liquid-release test data. This greatly reduces the uncertainty of the concurrently estimated parameters. On the other hand, flow diversion around the niche becomes important, potentially enabling the estimation of seepage-relevant permeability values on the scale of a drift. If possible, one should try to capture water near the spring line of the drift as independent evidence of flow diversion.

4. The differences and similarities in the estimated parameter sets can be explained and related to the structure of the respective conceptual models, illustrating the need to determine and use model-related parameters. As a result of effective parameter estimation, all models are able to reproduce the same effective behavior.

The SCM was tested in a validation exercise against liquid-release test data that were not used for the calibration of the model (Section 6.5). A probabilistic acceptance criterion was adopted to ensure that prediction uncertainty is included in the validation process as well as in future model predictions. Simulations of four liquid-release tests were performed, and the uncertainties of the predicted seepage values were determined. The model predictions were consistent with the measured seepage mass in most cases. Blind predictions of future long-term seepage tests should be made and compared to the data to gain additional confidence into the SCM prediction capability.

Seepage threshold was determined and sensitivity studies were performed (Section 6.6). The calibrated SCM predicts a low seepage probability for a wide range of percolation fluxes. Detailed seepage predictions will be performed with the Seepage Model for PA.

The calibration, validation, and prediction studies reported in this AMR demonstrate that:

1. The methodology outlined in this AMR yields drift-scale seepage models that are capable of reproducing and predicting seepage data from liquid-release tests (Sections 6.4 and 6.5).

2. The parameters estimated by calibrating the SCM against liquid-release test data are (a) seepage related and (b) model dependent (Sections 5.3 and 6.4).

3. Seepage predictions performed with a homogeneous SCM are consistent with those of a heterogeneous fracture continuum model (Section 6.6). Predictions with a fracture continuum model are consistent with simulated data from a model that displays discrete flow and seepage behavior (Section 5.3).

A homogeneous model is capable of determining integral measures such as seepage percentage. If the distribution of dripping locations is requested in addition to average seepage rates, a heterogeneous or discrete fracture network model must be developed. Higher model sophistication comes at the expense of increased data needs and often leads to the need to estimate a large number of strongly correlated parameters (i.e., overparameterization), which results in reduced prediction reliability. Extrapolations and applications of the calibrated model to different locations, units, time scales, and processes must be performed with great care and may require the development of more sophisticated models, including an extended characterization effort to satisfy additional or changed data needs.

A consistently high seepage threshold on the order of 200 mm/year or more was predicted. These estimates remain uncertain and are only valid for seepage under ambient temperature conditions into an uncollapsed opening with a circular, smooth ceiling, located in the middle nonlithophysal zone of the Topopah Spring welded tuffs, in an area of relatively competent rock mass and low fracture density. Extrapolations to other drift geometries and hydrogeologic units are not valid.

All software routines as well as input and output files pertinent to this AMR (see Attachment II) were submitted to the TDMS under DTN: LB990831012027.001. All input data residing in the TDMS were designated "To Be Verified (TBV)" until further verification. It is anticipated that the data, which were previously considered Q, will remain Q after the re-verification process is complete. The status of all the inputs for this AMR is available by referring to the DIRS database; the most recent version of the DIRS is included in Attachment I.

8. REFERENCES

8.1 DOCUMENTS CITED

Birkholzer, J. and Tsang, C.F. 1997. "Solute Channeling in Unsaturated Heterogeneous Porous Media." *Water Resources Research*, *33* (10), 2221–2238. Washington, D.C.: American Geophysical Union. TIC: 235675.

Carrera, J. and Neuman, S.P. 1986. "Estimation of Aquifer Parameters Under Transient and Steady State Conditions: 1. Maximum Likelihood Method Incorporating Prior Information." *Water Resources Research*, *22* (2), 199–210. Washington, D.C.: American Geophysical Union. TIC: 245915.

CRWMS M&O (Civilian Radioactive Waste Management System Management & Operating Contractor) 1999a. *M&O Site Investigations*. Activity Evaluation. Las Vegas, Nevada: CRWMS M&O. ACC: MOL.19990317.0330.

CRWMS M&O 1999b. *M&O Site Investigations*. Activity Evaluation. Las Vegas, Nevada: CRWMS M&O. ACC: MOL.19990928.0224.

CRWMS M&O 1999c. *Analysis & Modeling Development Plan (DP) for U0080 Seepage Calibration Model and Seepage Testing Data, Rev 00*. TDP-NBS-HS-000005. Las Vegas, Nevada: CRWMS M&O. ACC: MOL.19990826.0109.

Deutsch, C.V. and Journel, A.G. 1992. *GSLIB–Geostatistical Software Library and User's Guide*. New York, New York: Oxford University Press. TIC: 224174.

Dyer, J.R. 1999. "Revised Interim Guidance Pending Issuance of New U.S. Nuclear Regulatory Commission (NRC) Regulations (Revision 01, July 22, 1999), for Yucca Mountain, Nevada." Letter from J.R. Dyer (DOE) to D.R. Wilkins (CRWMS M&O), September 9, 1999, OL&RC:SB-1714, with enclosure, "Interim Guidance Pending Issuance of New U.S. Nuclear Regulatory Commission (NRC) Regulations (Revision 01)." ACC: MOL.19990910.0079.

Finsterle, S. 1997. *ITOUGH2 Command Reference, Version 3.1*. LBNL-40041. Berkeley, California: Lawrence Berkeley National Laboratory. ACC: MOL.19981008.0015.

Finsterle, S. 1998. *ITOUGH2 V3.2 Verification and Validation Report*. LBNL-42002. Berkeley, California: Lawrence Berkeley National Laboratory. ACC: MOL.19981008.0014.

Finsterle, S. 1999. *ITOUGH2 User's Guide*. LBNL-40040. Berkeley, California: Lawrence Berkeley National Laboratory. TIC: 243018.

LeCain, G.D. 1995. *Pneumatic Testing in 45-Degree-Inclined Boreholes in Ash-Flow Tuff Near Superior, Arizona*. Water-Resources Investigations Report 95-4073. Denver, Colorado: U.S. Geological Survey. TIC: 221220.

Leverett, M.C. 1941. "Capillary Behavior in Porous Solids." *AIME Transactions, Tulsa Meeting, October 1940, 142,* 152–169. New York, New York: American Institute of Mining, Metallurgical, and Petroleum Engineers. TIC: 240680.

Luckner, L.; van Genuchten, M.T.; and Nielsen, D.R. 1989. "A Consistent Set of Parametric Models for the Two-Phase Flow of Immiscible Fluids in the Subsurface." *Water Resources Research, 25* (10), 2187–2193. Washington, D.C.: American Geophysical Union. TIC: 224845.

Pruess, K. 1991. "Grid Orientation and Capillary Pressure Effects in the Simulation of Water Injection into Depleted Vapor Zones." *Geothermics, 20* (5-6), 257–277. Elmsford, New York: Pergamon Press. TIC: 245139.

Pruess, K. 1999. "A Mechanistic Model for Water Seepage through Thick Unsaturated Zones in Fractured Rocks of Low Matrix." *Water Resources Research, 35* (4), 1039–1051. Washington, D.C.: American Geophysical Union. TIC: 244913.

Richards, L.H. 1931. "Capillary Conduction of Liquids through Porous Media." *Physics, 1,* 218–233. Washington, D.C.: American Physical Society. TIC: 225383.

Wang, J.S.Y. and Elsworth, D. 1999. "Permeability Changes Induced by Excavation in Fractured Tuff." *Rock Mechanics for Industry, Proceedings of the 37th U.S. Rock Mechanics Symposium, Vail, Colorado, June 6-9, 1999, 2,* 751–757. Alexandria, Virginia: The American Rock Mechanics Association. TIC: 245246.

Wemheuer, R.F. 1999. "First Issue of FY00 NEPO QAP-2-0 Activity Evaluations." Interoffice correspondence from R.F. Wemheuer (CRWMS M&O) to R.A. Morgan (CRWMS M&O), October 1, 1999, LV.NEPO.RTPS.TAG.10/99-155, with attachments, Activity Evaluation for Work Package #1401213UM1. ACC: MOL.19991028.0162.

Software Cited

Software Code: iTOUGH2 V.4.0. STN: 10003-4.0-00.

Software Code: GSLIB Module SISIM V.1.203. STN: 10001-1.0MSISIMV1.203-00.

Software Code: GSLIB Module GAMV2 V.1.201. STN: 10087-1.0MGAMV2V1.201-00.

Software Code: EXT V.1.0. STN: 10047-1.0-00.

Macro/Routine: MoveMesh V.1.0. ACC: MOL.19990721.0552.

Macro/Routine: AddBound V.1.0. ACC: MOL.19990721.0553.

Macro/Routine: Perm2Mesh V.1.0. ACC: MOL.19990721.0554.

Macro/Routine: DelMatrix V.1.0. ACC: MOL.19990721.0555.

Macro/Routine: Eos9Eos3 V.1.0. ACC: MOL.19990721.0556.

Macro/Routine: CutNiche V.1.1. ACC: MOL.19990721.0557.

Macro/Routine: userobs V.1.01. ACC: MOL.19990721.0558.

8.2 STANDARDS, REGULATIONS AND PROCEDURES CITED

64 FR (Federal Register) 8640. Disposal of High-Level Radioactive Waste in a Proposed Geologic Repository at Yucca Mountain. Proposed rule 10 CFR 63. Readily available.

AP-3.10Q, Rev. 1, ICN 0. *Analysis and Models.* Washington, D.C.: U.S. Department of Energy, Office of Civilian Radioactive Waste Management. ACC: MOL.19990702.0314.

AP-SI.1Q, Rev. 1, ICN 0. *Software Management.* Washington, D.C.: U.S. Department of Energy, Office of Civilian Radioactive Waste Management. ACC: MOL.19990630.0395.

DOE (U.S. Department of Energy) 1998. *Quality Assurance Requirements and Description.* DOE/RW-0333P, REV 8. Washington D.C.: DOE OCRWM. ACC: MOL.19980601.0022.

QAP-2-0, Rev. 5. *Conduct of Activities.* Las Vegas, Nevada: CRWMS M&O. ACC: MOL.19980826.0209.

8.3 SOURCE DATA, LISTED BY DATA TRACKING NUMBER

DTN: LB980001233124.002. Air Permeability Testing in Niches 3566 and 3650. Submittal date: 04/23/1998.

DTN: LB980001233124.003. Liquid Release Tests Performed to Determine if a Capillary Barrier Exists in Niches 3566 and 3650. Submittal date: 04/23/1998.

DTN: LB997141233129.001. Calibrated Basecase Infiltration 1-D Parameter Set for the UZ Flow and Transport Model, FY99. Submittal date: 07/21/1999.

8.4 AMR OUTPUT DATA LISTED BY DATA TRACKING NUMBER

DTN: LB990831012027.001. Input to Seepage Calibration Model AMR U0080. Submittal date: 08/26/1999.

8.5 SUPPORTING BIBLIOGRAPHY

Birkholzer, J.; Li, G.; Tsang, C.F.; and Tsang, Y. 1999. "Modeling Studies and Analysis of Seepage into Drifts at Yucca Mountain." *Journal Of Contaminant Hydrology, 38* (1-3), 349–384. Amsterdam, The Netherlands: Elsevier Science. TIC: 244160.

Birkholzer, J.; Li, G.; Tsang, C.F.; and Tsang, Y. 1998. *Drift Scale Modeling: Studies of Seepage into a Drift.* Milestone Report SP4CKLM4. Berkeley, California: Lawrence Berkeley National Laboratory. ACC: MOL.19980825.0204.

Birkholzer, J.; Li, G.; Tsang, C.F.; Tsang, Y; Trautz, R.C.; and Wang, J. 1998. *Drift Scale Modeling: Studies of Seepage into a Drift.* Milestone Report SP3CKLM4. Berkeley, California: Lawrence Berkeley National Laboratory. ACC: MOL.19980908.0282.

Birkholzer, J.T.; Tsang, C.F.; Tsang, Y.W.; and Wang, J.S.Y. 1996. "Drift Scale Modeling, FY96 Project Report." Chapter 4 of *Multi-Scale Modeling to Evaluate Scaling Issues, Percolation Flux and Other Processes for PA Recommendations.* Altman S.J. et al., eds. Milestone Report T6540. Albuquerque, New Mexico: Sandia National Laboratories. ACC: MOL.19970320.0116.

Cook, P.J.; Trautz, R.C.; and Wang, J.S.Y. 1998. "Compilation of Borehole Permeability Values from the Pre- and Post-Excavation Air Injection Tests." Chapter 3 of *Drift Seepage and Niche Moisture Study: Phase 1 Report on Flux Threshold Determination, Air Permeability Distribution, and Water Potential Measurement,* Version 1.0. Wang, J.S.Y. et al. Milestone Report SPC315M4. Berkeley, California: Lawrence Berkeley National Laboratory. ACC: MOL.19980806.0713.

Cook, P.J.; Trautz, R.C.; and Wang, J.S.Y. 1997. "Cross-hole Pneumatic Tests of Fracture Flow Paths." Chapter 2 of *Field Testing and Observation of Flow Paths in Niches, Phase 1 Status Report of the Drift Seepage Test and Niche Moisture Study.* Wang, J.S.Y et al. Milestone Report SPC314M4. Berkeley, California: Lawrence Berkeley National Laboratory. ACC: MOL.19980121.0078.

Finsterle, S. and James, A.L. 1998. "Sensitivity Analysis of Drift Seepage with Two-Dimensional and Three-Dimensional Models." Chapter 3 of *Testing and Modeling of Seepage into Drift: Input of Exploratory Study of Facility Seepage Test Results to Unsaturated Zone Models.* Wang, J.S.Y. et al. Milestone Report SP33PLM4. Berkeley, California: Lawrence Berkeley National Laboratory. ACC: MOL.19980508.0004.

Finsterle, S.; James, A.L.; Ritcey, A.C.; and Wang, J.S.Y. 1998. *Model Prediction of Cross-Drift Impact on Moisture.* Milestone Report SP33T1M4. Berkeley, California: Lawrence Berkeley National Laboratory. ACC: MOL.19980507.0177.

Finsterle, S. 1997. *ITOUGH2 Sample Problems.* Report LBNL-40042. Berkeley, California: Lawrence Berkeley National Laboratory. TIC: 244009.

Flint, A. L. and Flint, L. E. 1997. "Niche Moisture Analysis." Chapter 5 of *Field Testing and Observation of Flow Paths in Niches, Phase 1 Status Report of the Drift Seepage Test and Niche Moisture Study.* Wang, J.S.Y. et al. Milestone Report SPC314M4. Berkeley, California: Lawrence Berkeley National Laboratory. ACC: MOL.19980121.0078.

Flint, L.E. 1998. *Characterization of Hydrogeologic Units Using Matrix Properties, Yucca Mountain, Nevada.* Water Resources Investigations Report 97–4243. Denver, Colorado: U.S. Geological Survey. ACC: MOL.19980429.0512.

Geller, J.T.; Su, G.; and Pruess, K. 1996. *Preliminary Studies of Water Seepage through Rough-Walled Fractures.* Report LBNL-38810. Berkeley, California: Lawrence Berkeley National Laboratory. TIC: applied for.

James, A.L. and Finsterle, S. 1997. "Fracture Flow Models for Niche Liquid Release Tests." Chapter 4 of *Field Testing and Observation of Flow Paths in Niches, Phase 1 Status Report of the Drift Seepage Test and Niche Moisture Study*. Wang, J.S.Y. et al. Milestone Report SPC314M4. Berkeley, California: Lawrence Berkeley National Laboratory. ACC: MOL.19980121.0078.

Hvorslev, M.J. 1951. "Time Lag and Soil Permeability in Ground-Water Observations." *U.S. Army Corps of Engineers Bulletin, 36*. Vicksburg, Mississippi: U.S. Army Corps of Engineers. TIC: 238956.

Li, G.; Tsang, C.F.; and Birkholzer, J. 1998. *Calculation of Drift Seepage for Alternative Emplacement Designs*. BB0000000-01717-0200-00011. Berkeley, California: Lawrence Berkeley National Laboratory. ACC: MOL.19990323.0138

Philip, J.R. 1989. "The Seepage Exclusion Problem for Sloping Cylindrical Cavities." *Water Resources Research*, 25 (6), 1447–1448. Washington, D.C.: American Geophysical Union. TIC: 239729.

Philip, J.R. 1989. "Asymptotic Solutions for the Seepage Exclusion Problem for Elliptic-Cylindrical, Spheroidal, and Strip- and Disc-Shaped Cavities." *Water Resources Research*, 25 (7), 1531–1540. Washington, D.C.: American Geophysical Union. TIC: 239858.

Philip, J.R.; Knight, J.H. and Waechter, R.T. 1989. "Unsaturated Seepage and Subterranean Holes: Conspectus, and Exclusion Problem for Cylindrical Cavities." *Water Resources Research*, 25 (1), 16–28. Washington, D.C.: American Geophysical Union. TIC: 239117.

Philip, J.R.; Knight, J.H; and Waechter, R.T. 1989. "The Seepage Exclusion Problem for Parabolic and Paraboloidal Cavities." *Water Resources Research*, 25 (4), 605–618. Washington, D.C.: American Geophysical Union. TIC: 239116.

Pruess, K. 1998. "On Water Seepage and Fast Preferential Flow in Heterogeneous, Unsaturated Rock Fractures." *Journal of Contaminant Hydrology*, 30 (3–4), 333–362. Amsterdam, The Netherlands: Elsevier Science. TIC: 238921.

Pruess, K.; Faybishenko, B.; and Bodvarsson, G.S. 1997. "Alternative Concepts and Approaches for Modeling Unsaturated Flow and Transport in Fractured Rocks." Chapter 5 of *The Site-Scale Unsaturated-Zone Model of Yucca Mountain, Nevada, for the Viability Assessment*. Bodvarsson, G.S.; Bandurraga, T.M.; and Wu, Y.S., eds. LBNL-40376. Berkeley, California: Lawrence Berkeley National Laboratory. ACC: MOL.19971014.0232.

Rasmussen, T.C.; Evans, D.D.; Sheets, P.J.; and Blanford, J.H. 1993. "Permeability of Apache Leap Tuff: Borehole and Core Measurements Using Water and Air." *Water Resources Research*, 29 (7), 1997–2006. Washington, D.C.: American Geophysical Union. TIC: 245278.

Salve, R. and Wang, J.S.Y. 1998. "Compilation of Water Potentials Measured in the Niches." Chapter 4 of *Drift Seepage Test and Niche Moisture Study: Phase 1 Report on Flux Threshold Determination, Air Permeability Distribution, and Water Potential Measurement*. Wang, J.S.Y. et

al. Milestone Report SPC315M4. Berkeley, California: Lawrence Berkeley National Laboratory. ACC: MOL.19980806.0713.

Trautz, R.C.; Wang, J.S.Y.; and Cook, P.J. 1998. "Compilation of Seepage Results From the Pre- And Post-Excavation Liquid-Release Tests." Chapter 2 of *Drift Seepage Test and Niche Moisture Study: Phase 1 Report on Flux Threshold Determination, Air Permeability Distribution, and Water Potential Measurement.* Wang, J.S.Y. et al. Milestone Report SPC315M4. Berkeley, California: Lawrence Berkeley National Laboratory. ACC: MOL.19980806.0713.

Trautz, R.C.; Cook, P.J.; and Wang, J.S.Y. 1997. "Liquid Migration Along Fracture Flow Paths." Chapter 3 of *Field Testing and Observation of Flow Paths in Niches.* Milestone Report SPC314M4. Wang, J.S.Y. et al. Berkeley, California: Lawrence Berkeley National Laboratory. ACC: MOL.19980121.0078.

Tsang, C.F.; Li, G.; Birkholzer, J.T.; and Tsang, Y.W. 1998 . *Abstraction Modeling of Drift Seepage for TSPA/VA.* Milestone Report SLX01LB4. Berkeley, California: Lawrence Berkeley National Laboratory. ACC: MOL.19980730.0607.

Tsang, C.F. 1997. *Drift-Scale Heterogeneous Permeability Field Conditioned to Field Data.* Milestone Report SP331BM4. Berkeley, California: Lawrence Berkeley National Laboratory. ACC: MOL.19971125.0915.

Tsang, C.F.; Birkholzer, J.T.; and Li, G. 1997. *Drift Scale Modeling: Progress in Studies of Seepage into a Drift.* Milestone Report SP331CM4. Berkeley, California: Lawrence Berkeley National Laboratory. ACC: MOL.19971204.0420.

Tsang, C.F.; Birkholzer, J.T.; Li, G; and Tsang, Y.W. 1997. *Drift Scale Modeling: Studies of Seepage into a Drift.* Milestone Report SP331DM4. Berkeley, California: Lawrence Berkeley National Laboratory. ACC: MOL.19971208.0369.

Tsang, C.F.; Li, G.; Birkholzer, J.T.; and Tsang, Y.S. 1997. *Drift Scale Abstraction: Evaluation of Seepage into Drifts.* Milestone Report NWD98–1. Berkeley, California: Lawrence Berkeley National Laboratory. ACC: MOL.19980423.0388.

Tsang, C.F.; Li, G.; Birkholzer, J.; and Tsang, Y. S 1997. *Drift Scale Abstraction: Additional Results on Seepage into Drifts and Model Testing against Niche Liquid Release Test.* Milestone Report NWD98–2. Berkeley, California: Lawrence Berkeley National Laboratory. ACC: MOL.19980506.0008.

Wang, J.S.Y.; Trautz, R.C.; Salve, R.; Oldenburg, C.M.; Ahlers, C.F.; Finsterle, S.; Cook, P.J.; Doughty, C.; Fairley, J.P.; James, A. Hu, M.Q.; Guell, M.A.; and Freifeld, B. 1998. *Progress Report on Fracture Flow, Drift Seepage, and Matrix Imbibition Tests in the Exploratory Studies Facility.* Milestone Report SP33PBM4. Berkeley, California: Lawrence Berkeley National Laboratory.

Wang, J.S.Y.; Trautz, R.C.; Cook, P.J.; Finsterle, S.; James, A.L.; Birkholzer J.; and Ahlers, C.F. 1998. *Testing and Modeling of Seepage into Drift: Input of Exploratory Study of Facility Seepage*

Test Results to Unsaturated Zone Model. Milestone Report SP33PLM4. Berkeley, California: Lawrence Berkeley National Laboratory. ACC: MOL.19980508.0004.

Wang, J.S.Y.; Trautz, R.C.; Cook, P.J.; and Salve, R. 1998. *Drift Seepage Test and Niche Moisture Study: Phase 1 Report on Flux Threshold Determination, Air Permeability Distribution, and Water Potential Measurement.* Milestone Report SPC315M4. Berkeley, California: Lawrence Berkeley National Laboratory. ACC: MOL.19980806.0713.

Wang, J.S.Y, Cook, P.; Trautz, R.; James, A.; Finsterle, S. Sonnenthal, E.; Salve, R.; Hesler, G.; and Flint, A. 1997. *Drift Seepage Test and Niche Moisture Study: Phase 1 Progress Report on Data Interpretation and Model Prediction.* Milestone Report SPC31DM4. Berkeley, California: Lawrence Berkeley National Laboratory. ACC: MOL.19980501.0484.

Wang, J.S.Y., Cook, P.J.; Trautz, R.C.; Salve, R.; James, A.L.; Finsterle, S.; Tokunaga, T.K.; Solbau, R.; Clyde, J.; Flint, A.L.; and Flint, L.E. 1997. *Field Testing and Observation of Flow Paths in Niches, Phase 1 Status Report of the Drift Seepage Test and Niche Moisture Study.* Milestone Report SPC314M4. Berkeley, California: Lawrence Berkeley National Laboratory. ACC: MOL.19980121.0078.

INTENTIONALLY LEFT BLANK

9. ATTACHMENTS

Attachment I – Document Input Reference Sheet

Attachment II – Software Routines, Input and Output Files

INTENTIONALLY LEFT BLANK

ATTACHMENT I-DOCUMENT INPUT REFERENCE SHEET

OFFICE OF CIVILIAN RADIOACTIVE WASTE MANAGEMENT DOCUMENT INPUT REFERENCE SHEET									
1. Document Identifier No./Rev.: MDL-NBS-HS-000004/Rev. 00 *NOH 02-11-00*		Change:	Title: Seepage Calibration Model & Seepage Testing Data						
Input Document		4. Input Status	5. Section Used in	6. Input Description		7. TBV/TBD Priority	8. TBV Due To		
2. Technical Product Input Source Title and Identifier(s) with Version	3. Section						Unqual.	From Uncontrolled Source	Un-confirmed
1. DTN: LB980001233124.002. Wang, J. Air permeability testing in Niches 3566 and 3650. Submittal date: 04/23/1998. Initial use.	File S98131_002, Rows 247-277, 309-339	TBV-3094	6.2, 6.3	Post-excavation air permeability data for conditioning of Seepage Calibration Model		1	N/A	N/A	X
2. DTN: LB980001233124.003. Wang, J. Liquid Release Tests Performed to Determine if a Capillary Barrier Exists in Niches 3566 and 3650. Submittal date: 04/23/1998. Initial Use.	File S98132_005, Rows 10-14, 20-23	TBV-3093	6.2, 6.4	Liquid release test data for calibration and validation		1	N/A	N/A	X
3. DTN: LB997141233129.001. Wu, Y.S. Calibrated Basecase Infiltration 1-D Parameter Set for the UZ Flow and Transport Model FY99. Submittal date: 07/21/1999. Initial use.	IDbasecase R1wodis.xls.	TBV-3095	6.3	Fracture properties for Seepage Calibration Model		1	N/A	N/A	X

OFFICE OF CIVILIAN RADIOACTIVE WASTE MANAGEMENT

DOCUMENT INPUT REFERENCE SHEET

1. Document Identifier No./Rev.: NO4 02-11-00 MDL-NBS-HS-000004/Rev. 00E		Change:	Title: Seepage Calibration Model & Seepage Testing Data					
Input Document		4. Input Status	5. Section Used in	6. Input Description	7. TBV/TBD Priority	8. TBV Due To		
2. Technical Product Input Source Title and Identifier(s) with Version	3. Section					Unqual.	From Uncontrolled Source	Un-confirmed
4. Birkholzer, J. and Tsang, C.F. 1997. "Solute Channeling in Unsaturated Heterogeneous Porous Media." *Water Resources Research, 33* (10), 2221–2238. Washington, D.C.: American Geophysical Union. TIC: 235675.	Entire	N/A - Reference only	6.6	Channeling effect	N/A	N/A	N/A	N/A
5. Carrera, J. and Neuman, S.P. 1986. "Estimation of Aquifer Parameters Under Transient and Steady State Conditions: 1. Maximum Likelihood Method Incorporating Prior Information." *Water Resources Research, 22* (2), 199–210. Washington, D.C.: American Geophysical Union. TIC: 245915.	205	N/A - Reference only	6.4	Estimation covariance matrix	N/A	N/A	N/A	N/A

U0080

OFFICE OF CIVILIAN RADIOACTIVE WASTE MANAGEMENT

DOCUMENT INPUT REFERENCE SHEET

1. Document Identifier No./Rev.: New 02-11-00 MDL-NBS-HS-000004/Rev. 00		Change:	Title: Seepage Calibration Model & Seepage Testing Data						
Input Document		4. Input Status	5. Section Used in	6. Input Description	7. TBV/TBD Priority	8. TBV Due To			
2. Technical Product Input Source Title and Identifier(s) with Version	3. Section					Unqual.	From Uncontrolled Source	Un-confirmed	
6. CRWMS M&O (Civilian Radioactive Waste Management System Management & Operating Contractor) 1999a. *M&O Site Investigations.* Activity Evaluation. Las Vegas, Nevada: CRWMS M&O. ACC: MOL.19990317.0330.	Entire	N/A - Reference only	2	Standards, Codes & Regulations	N/A	N/A	N/A	N/A
7. CRWMS M&O 1999b. *M&O Site Investigations.* Activity Evaluation. Las Vegas, Nevada: CRWMS M&O. ACC: MOL. 19990928.0224.	Entire	N/A - Reference only	2	Standards, Codes & Regulations	N/A	N/A	N/A	N/A

OFFICE OF CIVILIAN RADIOACTIVE WASTE MANAGEMENT
DOCUMENT INPUT REFERENCE SHEET

1. Document Identifier No./Rev.: 104 02-11-00 MDL-NBS-HS-000004/Rev. 00		Change:	Title: Seepage Calibration Model & Seepage Testing Data						
Input Document		4. Input Status	5. Section Used in	6. Input Description	7. TBV/TBD Priority	8. TBV Due To			
2. Technical Product Input Source Title and Identifier(s) with Version	3. Section					Unqual.	From Uncontrolled Source	Un-confirmed
8. CRWMS M&O 1999c. *Analysis & Modeling Development Plan (DP) for U0080 Seepage Calibration Model and Seepage Testing Data, Rev 00.* TDP-NBS-HS-000005. Las Vegas, Nevada: CRWMS M&O. ACC: MOL.19990826.0109.	Entire	N/A - Reference only	2	Standards, Codes & Regulations	N/A	N/A	N/A	N/A
9. Deutsch, C.V. and Journel, A.G. 1992. *GSLIB—Geostatistical Software Library and User's Guide.* New York, New York: Oxford University Press. TIC: 224174.	53-55 151	N/A - Reference only	5.3, 6.2.3 6.3.2	Use of modules GAMV2 and SISIM	N/A	N/A	N/A	N/A

U0080

OFFICE OF CIVILIAN RADIOACTIVE WASTE MANAGEMENT
DOCUMENT INPUT REFERENCE SHEET

1. Document Identifier No./Rev.: Not 02-11-00 MDL-NBS-HS-000004/Rev. 00E		Change:	Title: Seepage Calibration Model & Seepage Testing Data						
Input Document		4. Input Status	5. Section Used in	6. Input Description	7. TBV/TBD Priority	8. TBV Due To			
2. Technical Product Input Source Title and Identifier(s) with Version	3. Section					Unqual.	From Uncontrolled Source	Un-confirmed	
10.	Dyer, J.R. 1999. "Revised Interim Guidance Pending Issuance of New U.S. Nuclear Regulatory Commission (NRC) Regulations (Revision 01, July 22, 1999), for Yucca Mountain, Nevada." Letter from J.R. Dyer (DOE) to D.R. Wilkins (CRWMS M&O), September 9, 1999, OL&RC:SB-1714, with enclosure, "Interim Guidance Pending Issuance of New U.S. Nuclear Regulatory Commission (NRC) Regulations (Revision 01)." ACC: MOL.19990910.0079.	Entire	N/A-Reference only	4.2	Interim Guidance	N/A	N/A	N/A	N/A
11.	Finsterle, S. 1997. *ITOUGH2 Command Reference, Version 3.1.* Report LBNL-40041. Berkeley, California: Lawrence Berkeley National Laboratory. ACC: MOL.19981008.0015.	Entire	N/A - Reference only	5.2 6.3	Supports software use	N/A	N/A	N/A	N/A

OFFICE OF CIVILIAN RADIOACTIVE WASTE MANAGEMENT
DOCUMENT INPUT REFERENCE SHEET

1. Document Identifier No./Rev.: 新 02-11-00 MDL-NBS-HS-000004/Rev. 00E		Change:	Title: Seepage Calibration Model & Seepage Testing Data						
Input Document		4. Input Status	5. Section Used in	6. Input Description	7. TBV/TBD Priority	8. TBV Due To			
2. Technical Product Input Source Title and Identifier(s) with Version	3. Section					Unqual.	From Uncontrolled Source	Un-confirm ed	
12. Finsterle, S. 1998. *ITOUGH2 V3.2 Verification and Validation Report*. Report LBNL-42002. Berkeley, California: Lawrence Berkeley National Laboratory. ACC: MOL.19981008.0014.	p. 14-15	N/A - Reference only	5.3.2 6.3.4	Instructions for application of free-drainage boundary condition	N/A	N/A	N/A	N/A	
13. Finsterle, S. 1999. *ITOUGH2 User's Guide*. Report LBNL-40040. Berkeley, California: Lawrence Berkeley National Laboratory. TIC: 243018.	Entire	N/A - Reference only	5.3.4 6.3.5 6.5	Objective function, minimization algorithm and error analysis	N/A	N/A	N/A	N/A	
14. LeCain, G. D. 1995. *Pneumatic Testing in 45-Degree-Inclined Boreholes in Ash-Flow Tuff near Superior, Arizona*. Water Resources Investigations Report 95-4073. Denver, Colorado: U.S. Geological Survey. ACC: MOL.19960416.0160.	p. 32	N/A - Reference only	5.3.3	Analytical solution for permeability from steady-state air-injection data.	N/A	N/A	N/A	N/A	

OFFICE OF CIVILIAN RADIOACTIVE WASTE MANAGEMENT
DOCUMENT INPUT REFERENCE SHEET

1. Document Identifier No./Rev.: MDL-NBS-HS-000004/Rev. 00 *JCH 02-11-00*		Change:	Title: Seepage Calibration Model & Seepage Testing Data						
Input Document		4. Input Status	5. Section Used in	6. Input Description	7. TBV/TBD Priority	8. TBV Due To			
2. Technical Product Input Source Title and Identifier(s) with Version	3. Section					Unqual.	From Uncontrolled Source	Un-confirmed	
15. Leverett, M.C. 1941. "Capillary Behavior in Porous Solids." *AIME Transactions, Tulsa Meeting, October 1940, 142*, 152-169. New York, New York: American Institute of Mining, Metallurgical, and Petroleum Engineers. TIC: 240680.	Entire	N/A - Reference only	5.2 6.3	Leverett Scaling Rule	N/A	N/A	N/A	N/A	
16. Luckner, L.; van Genuchten, M.T.; and Nielsen, D.R. 1989. "A Consistent Set of Parametric Models for the Two-Phase Flow of Immiscible Fluids in the Subsurface." *Water Resources Research, 25* (10), 2187–2193. Washington, D.C.: American Geophysical Union. TIC: 224845.	pp. 2191-2192	N/A - Reference only	5.2 6.3	Relative permeability and capillary pressure function	N/A	N/A	N/A	N/A	

OFFICE OF CIVILIAN RADIOACTIVE WASTE MANAGEMENT

DOCUMENT INPUT REFERENCE SHEET

1. Document Identifier No./Rev.: MDL-NBS-HS-000004/Rev. 00 *NW 02-11-00*		Change:	Title: Seepage Calibration Model & Seepage Testing Data						
Input Document		4. Input Status	5. Section Used in	6. Input Description	7. TBV/TBD Priority	8. TBV Due To			
2. Technical Product Input Source Title and Identifier(s) with Version	3. Section					Unqual.	From Uncontrolled Source	Un-confirmed
17. Pruess, K. 1991. "Grid Orientation and Capillary Pressure Effects in the Simulation of Water Injection into Depleted Vapor Zones." *Geothermics, 20* (5–6), 257–277. Elmsford, New York: Pergamon Press. TIC: 245139.	pp. 272-274	N/A - Reference only	5.3.6	Description of phase dispersion effects	N/A	N/A	N/A	N/A
18. Pruess, K. 1999. "A Mechanistic Model for Water Seepage through Thick Unsaturated Zones in Fractured Rocks of Low Matrix." *Water Resources Research, 35* (4), 1039–1051. Washington, D.C.: American Geophysical Union. TIC: 244913.	pp. 1039-1051	N/A - Reference only	5.3	Alternative conceptual model description	N/A	N/A	N/A	N/A

OFFICE OF CIVILIAN RADIOACTIVE WASTE MANAGEMENT DOCUMENT INPUT REFERENCE SHEET									
1. Document Identifier No./Rev.: ꞰꞴꝎ 02-11-00 MDL-NBS-HS-000004/Rev. 00		Change:	Title: Seepage Calibration Model & Seepage Testing Data						
Input Document		4. Input Status	5. Section Used in	6. Input Description	7. TBV/TBD Priority	8. TBV Due To			
2. Technical Product Input Source Title and Identifier(s) with Version	3. Section					Unqual.	From Uncontrolled Source	Un-confirmed	
19. Richards, L.H. 1931. "Capillary Conduction of Liquids Through Porous Media." *Physics, 1*, 218–233. Washington, D.C.: American Physical Society. TIC: 225383.	pp. 218-233	N/A - Reference only	5.2 6.3	Concept of unsaturated flow through porous media	N/A	N/A	N/A	N/A	
20. Wang, J. S. Y., and Elsworth, D. 1999. "Permeability Changes Induced by Excavation in Fractured Tuff." *Proceedings, 37th U.S. Rock Mechanics Symposium, Rock Mechanics for Industry, 2,* 751–757. Alexandria, Virginia: The American Rock Mechanics Association. TIC: 245246.	pp. 751-757	N/A - Reference only	5.3.2	Description of excavation-disturbed zone around niches	N/A	N/A	N/A	N/A	

OFFICE OF CIVILIAN RADIOACTIVE WASTE MANAGEMENT
DOCUMENT INPUT REFERENCE SHEET

1. Document Identifier No./Rev.: MDL-NBS-HS-000004/Rev. 00E 02-11-00		Change:	Title: Seepage Calibration Model & Seepage Testing Data						
Input Document		4. Input Status	5. Section Used in	6. Input Description	7. TBV/TBD Priority	8. TBV Due To			
2. Technical Product Input Source Title and Identifier(s) with Version	3. Section					Unqual.	From Uncontrolled Source	Un-confirmed	
21. Wemheuer, R.F. 1999. "First Issue of FY00 NEPO QAP-2-0 Activity Evaluations." Interoffice correspondence from R.F. Wemheuer (CRWMS M&O) to R.A. Morgan (CRWMS M&O), October 1, 1999, LV.NEPO.RTPS.TAG.10/99-155, with attachments, Activity Evaluation for Work Package #1401213UM1. ACC: MOL.19991028.0162.	WP#1401 213UM1	N/A-Reference only	2	Activity Evaluation	N/A	N/A	N/A	N/A	
22. Software Code: iTOUGH2 v 4.0, STN: 10003-4.0-00	Entire	N/A-Qualified/ Verified/ Confirmed	5.3, 6.4, 6.5, 6.6	General software use	N/A	N/A	N/A	N/A	
23. Software Code: GSLIB Module SISIM v 1.203, STN: 10001-1.0MSISIMV1.203-00	Entire	N/A-Qualified/ Verified/ Confirmed	5.3, 6.3	General software use	N/A	N/A	N/A	N/A	
24. Software Code: GSLIB Module GAMV2 v 1.201, STN: 10087-1.0MGAMV2V1.201-00	Entire	N/A-Qualified/ Verified/ Confirmed	6.2	General software use	N/A	N/A	N/A	N/A	

OFFICE OF CIVILIAN RADIOACTIVE WASTE MANAGEMENT
DOCUMENT INPUT REFERENCE SHEET

1. Document Identifier No./Rev.: NOW 02-11-00 MDL-NBS-HS-000004/Rev. 00E		Change:	Title: Seepage Calibration Model & Seepage Testing Data						
Input Document		4. Input Status	5. Section Used in	6. Input Description	7. TBV/TBD Priority	8. TBV Due To			
2. Technical Product Input Source Title and Identifier(s) with Version	3. Section					Unqual.	From Uncontrolled Source	Un-confirmed	
25.	Software Code: EXT v 1.0, STN: 10047-1.0-00	Entire	N/A-Qualified/ Verified/ Confirmed	5.3, 6	General software use	N/A	N/A	N/A	N/A
26.	Software Code: MoveMesh v. 1.0. ACC: MOL.19990721.0552	Entire	N/A-Qualified/ Verified/ Confirmed	5.3, 6.3	General software use	N/A	N/A	N/A	N/A
27.	Software Code: AddBound v. 1.0. ACC: MOL.19990721.0553.	Entire	N/A-Qualified/ Verified/ Confirmed	5.3, 6.3	General software use	N/A	N/A	N/A	N/A
28.	Software Code: Perm2Mesh v. 1.0. ACC: MOL.19990721.0554.	Entire	N/A-Qualified/ Verified/ Confirmed	5.3, 6.3	General software use	N/A	N/A	N/A	N/A
29.	Software Code: DelMatrix v 1.0. ACC: MOL.19990721.0555.	Entire	N/A-Qualified/ Verified/ Confirmed	5.3, 6.3	General software use	N/A	N/A	N/A	N/A
30.	Software Code: Eos9Eos3 v 1.0. ACC: MOL.19990721.0556.	Entire	N/A-Qualified/ Verified/ Confirmed	5.3, 6.3	General software use	N/A	N/A	N/A	N/A

OFFICE OF CIVILIAN RADIOACTIVE WASTE MANAGEMENT DOCUMENT INPUT REFERENCE SHEET								
1. Document Identifier No./Rev.: MDL-NBS-HS-000004/Rev. 00 *KH 02-11-00*		Change:	Title: Seepage Calibration Model & Seepage Testing Data					
Input Document		4. Input Status	5. Section Used in	6. Input Description	7. TBV/TBD Priority	8. TBV Due To		
2. Technical Product Input Source Title and Identifier(s) with Version	3. Section					Unqual.	From Uncontrolled Source	Un-confirmed
31. Software Code: CutNiche v 1.1. ACC: MOL.19990721.0557.	Entire	N/A-Qualified/ Verified/ Confirmed	5.3, 6.3	General software use	N/A	N/A	N/A	N/A
32. Software Code: userobs v 1.01. ACC: MOL.19990721.0558.	Entire	N/A-Qualified/ Verified/ Confirmed	5.3, 6.3	General software use	N/A	N/A	N/A	N/A

AP-3.15Q.1

Rev. 06/30/1999

308840

YUCCA MOUNTAIN SITE CHARACTERIZATION PROJECT
TECHNICAL DATA INFORMATION FORM

YMP-023-R6
04/99

Page 1 of 2

☐ ACQUIRED DATA

☒ DEVELOPED DATA

DTN: __LB990831012027.001__

Preliminary Data: _____

PART I Identification of Data

Title of Data: __INPUT TO SEEPAGE CALIBRATION MODEL AMR U0080, REV. 00A.__

Description of Data: __SOFTWARE ROUTINES AND FILES NECESSARY FOR REPRODUCTION OF RESULTS PRESENTED IN__ __AMR U0080, REV. 00A, "SEEPAGE CALIBRATION MODEL AND SEEPAGE TESTING DATA," ANL-NBS-HS-000004,__

Data Originator/Preparer: __FINSTERLE, S A__
                          Last Name   First and Middle Initials

Data Originator/Preparer Organization: __LAWRENCE BERKELEY NATIONAL LABORATORY__

Qualification Status: ☒ Q ☐ Un-Q ☐ Accepted   Governing Plan: __SCP__

SCP Activity Number(s): __8.3.1.2.2.4__

WBS Number(s): __1.2.3.3.1.2.4__

PART II Data Acquisition/Development Information

Method: __ITOUGH2, VERSION 4.0 SOFTWARE.__

Location(s): __MODEL DEVELOPED AT LBNL.__

Period(s): __4/28/1999 to 8/31/1999__
            From: MM/DD/YY   To: MM/DD/YY

Sample ID Number(s): _____

PART III Source Data DTN(s)

LB980001233124.002

LB980001233124.003

LB997141233129.001

Comments

SEE INSTRUCTIONS IN FILE "MAKETAR" SUBMITTED WITH THE INPUT FILES.

Checked by: _Suzanne M. Link_   _August 26, 1999_
                    Signature   Date

AP-SIII.3Q

308840

YMP-023-R6 04/99	YUCCA MOUNTAIN SITE CHARACTERIZATION PROJECT TECHNICAL DATA INFORMATION CONTINUATION SHEET	Page _2_ of 2___

Description of Data (continued)

  MOL.19990721.0521.

AP-SIII.3Q

```
#! /bin/sh
#
# file "maketar" ceates compressed tar file U0080.tar.Z.
# DTN: LB990831012027.001, TDIF 308840
#
# Contains input and output files that allow reproduction of all simulations pertinent to AMR U0080,
# "Seepage Calibration Model and Seepage Testing Data," ANL-NBS-HS-000004, MOL.19990721.0521
#
# To extract files from U0080_00B.tar.Z on a Unix workstation, type:
# uncompress U0080.tar.Z; tar xvf U0080.tar
# Requires about 150 MB of disk space.
#
# All commands can be found in the sh.* script files;
# consult Scientific Notebooks YMP-LBNL-SAF-1, YMP-LBNL-SAF-2, and YMP-LBNL-RCT-DSM-1.
#
# S. Finsterle, September 1999
#
tar -cvf - \
\
./maketar                          \ the file creating the tar file
                                   \
./Codes/AddBound.f                 \ FORTRAN77 source code
./Codes/CutNiche.f                 \ FORTRAN77 source code
./Codes/DelMatrix.f                \ FORTRAN77 source code
./Codes/Eos9Eos3.f                 \ FORTRAN77 source code
./Codes/MoveMesh.f                 \ FORTRAN77 source code
./Codes/Perm2Mesh.f                \ FORTRAN77 source code
./Codes/sisim.f                    \ FORTRAN77 source code
./Codes/sisimm.f                   \ FORTRAN77 source code
./Codes/sisim.inc                  \ include file for SISIM
./Codes/ext.f                      \ FORTRAN77 source code
./Codes/catalog.f                  \ FORTRAN77 source code
./Codes/inspect.f                  \ FORTRAN77 source code
./Codes/rmesh.f                    \ FORTRAN77 source code
./Codes/gamv2m.f                   \ FORTRAN77 source code
./Codes/gamv2.f                    \ FORTRAN77 source code
./Codes/gamv2.inc                  \ include file for GAMV2
./Codes/userobs.f                  \ link to iTOUGH2 V4.0
./Codes/xAddBound                  \ Executable for Sun SPARC multiprocessor, Solaris
./Codes/xCutNiche                  \ Executable for Sun SPARC multiprocessor, Solaris
./Codes/xDelMatrix                 \ Executable for Sun SPARC multiprocessor, Solaris
./Codes/xEos9Eos3                  \ Executable for Sun SPARC multiprocessor, Solaris
```

```
./Codes/xExt                    \ Executable for Sun SPARC multiprocessor, Solaris
./Codes/xGamv2                  \ Executable for Sun SPARC multiprocessor, Solaris
./Codes/xMoveMesh               \ Executable for Sun SPARC multiprocessor, Solaris
./Codes/xPerm2Mesh              \ Executable for Sun SPARC multiprocessor, Solaris
./Codes/xSisim                  \ Executable for Sun SPARC multiprocessor, Solaris
./Codes/sh.compile              \ Unix shell script file used to compile all codes
                                \
./Codes/gamv2/cluster.dat       \ Input data for gamv2 validation case 1
./Codes/gamv2/gamv2.par1        \ Input parameter file for gamv2 validation case 1
./Codes/gamv2/gamv2.par2        \ Input parameter file for gamv2 validation case 2
./Codes/gamv2/gamv2.var1        \ Ouput variogram for gamv2 validation case 1
./Codes/gamv2/gamv2.var2        \ Ouput variogram for gamv2 validation case 2
./Codes/gamv2/randfield.f       \ FORTRAN77 source code to generate random numbers
./Codes/gamv2/random.dat        \ Input data for gamv2 validation case 2
                                \
./ContDisc/DFNMairk             \ TOUGH2 input file air-k test with DFNM, Section 5.3.3
./ContDisc/DFNMairki            \ iTOUGH2 input file air-k test with DFNM, Section 5.3.3
./ContDisc/DFNMairki.out        \ iTOUGH2 output file air-k test with DFNM, Section 5.3.3, Figure 4
./ContDisc/DFNMlrt              \ TOUGH2 input file liquid-release test with DFNM, Section 5.3.4, Table 4
./ContDisc/DFNMlrt.out          \ TOUGH2 output file liquid-release test with DFNM, Section 5.3.4, Figure 5.
./ContDisc/DFNMlrti             \ iTOUGH2 input file liquid-release test with DFNM, Section 5.3.4, Table 4
./ContDisc/DFNMlrti.out         \ iTOUGH2 output file liquid-release test with DFNM, Section 5.3.4, Figure 6
./ContDisc/DFNMperm             \ TOUGH2 input file for saturated steady-state run with DFNM, Section 5.3.2
./ContDisc/DFNMperm.out         \ TOUGH2 output file for saturated steady-state run with DFNM, Section 5.3.2, Figure 1a
./ContDisc/DFNMpred             \ TOUGH2 input file for prediction run with DFNM, Section 5.3.7
./ContDisc/DFNMpredi            \ iTOUGH2 input file for prediction run with DFNM, Section 5.3.7
./ContDisc/DFNMpredi.out        \ iTOUGH2 output file for prediction run with DFNM, Section 5.3.7, Figure 10
./ContDisc/DFNMseep             \ TOUGH2 input file for seepage threshold determination with DFNM, Section 5.3.7
./ContDisc/DFNMseepi            \ iTOUGH2 input file for seepage threshold determination with DFNM, Section 5.3.7
./ContDisc/DFNMseepi.out        \ iTOUGH2 output file for seepage threshold determination with DFNM, Section 5.3.7, Figure 11
./ContDisc/DFNMss               \ TOUGH2 input file for steady-state run with DFNM, Section 5.3.2
./ContDisc/DFNMss.out           \ TOUGH2 output file for steady-state run with DFNM, Section 5.3.2, Figures 2, 3
./ContDisc/DFNM.inc             \ Initial condition file (output from DFNMss run), Section 5.3.2
./ContDisc/DFNMairk.inc         \ Initial condition file for DFNMairk run (converted output from DFNMss run), Section 5.3.2
./ContDisc/FCMlrt               \ TOUGH2 input file for liquid-release test with FCM, Section 5.3.6
./ContDisc/FCMlrt.out           \ TOUGH2 output file for liquid-release test with FCM, Section 5.3.6, Figures 7, 9
./ContDisc/FCMlrti              \ iTOUGH2 input file for liquid-release test with FCM, Section 5.3.6
./ContDisc/FCMlrti.out          \ iTOUGH2 output file for liquid-release test with FCM, Section 5.3.6, Figure 8
./ContDisc/FCMpred              \ TOUGH2 input file for prediction run with FCM, Section 5.3.7
./ContDisc/FCMpredi             \ iTOUGH2 input file for prediction run with FCM, Section 5.3.7
./ContDisc/FCMpredi.tec         \ iTOUGH2 output file for prediction run with FCM, Section 5.3.7, Figure 10
./ContDisc/FCMseep              \ TOUGH2 input file for seepage threshold determination with FCM, Section 5.3.7
```

```
./ContDisc/FCMseepi              \ iTOUGH2 input file for seepage threshold determination with FCM, Section 5.3.7
./ContDisc/FCMseepi.out          \ iTOUGH2 output file for seepage threshold determination with FCM, Section 5.3.7, Figure 11
./ContDisc/FCMseepMC             \ TOUGH2 input file for seepage threshold determination with FCM, Section 5.3.7
./ContDisc/FCMseepMCi            \ iTOUGH2 input file for seepage threshold determination with FCM, Section 5.3.7
./ContDisc/FCMseepMCi.tec        \ iTOUGH2 output file for seepage threshold determination with FCM, Section 5.3.7, Figure 11
./ContDisc/sh.DFNM               \ Unix shell script file for all DFNM runs
./ContDisc/sh.FCM                \ Unix shell script file for all FCM runs
                                 \
./Heterogeneity/N2xyk_2-dpost.prn \ Input data for gamv2-4.par, all post-excavation data, Section 6.2.3
./Heterogeneity/N2xyk_2-dp_tr.prn \ Input data for gamv2-8.par, truncated post-excavation data, Section 6.2.3, Table 5, Figure 16
./Heterogeneity/gamv2-4.par      \ Input parameter file for gamv2, all post-excavation data, Section 6.2.3
./Heterogeneity/gamv2-4.var      \ Output variogram from gamv2, all post-excavation data, Section 6.2.3, Figure 15
./Heterogeneity/gamv2-8.par      \ Input parameter file for gamv2, truncated post-excavation data, Section 6.2.3
./Heterogeneity/gamv2-8.var      \ Output variogram from gamv2, truncated  post-excavation data, Section 6.2.3, Figures 15, 17
./Heterogeneity/condUM442_post.dat \ Conditioning points for test UM 4.42, Section 6.3.2
./Heterogeneity/UM442_3.par      \ Input parameter file for gamv2, permeability field for test UM 4.42, Section 6.3.2
./Heterogeneity/UM442_3.dat      \ Output permeability field for test UM 4.42, Section 6.3.2
./Heterogeneity/condUM564_post.dat \ Conditioning points for test UM 5.64, Section 6.5
./Heterogeneity/UM564_1.par      \ Input parameter file for gamv2, permeability field for test UM 5.64, Section 6.5
./Heterogeneity/UM564_1.dat      \ Output permeability field for test UM 5.64, Section 6.5
./Heterogeneity/conditioning.dat \ Conditioning points for FCM model, Section 5.3.5
./Heterogeneity/fract2dc.par     \ Input parameter file for gamv2, FCM, Section 5.3.5
./Heterogeneity/fract2dc.dat     \ Output permeability field, FCM, Section 5.3.5
./Heterogeneity/fract0.par       \ Input parameter file for gamv2, 0-degree fracture set, Section 5.3.2
./Heterogeneity/fract0.dat       \ Output permeability field, 0-degree fracture set, Section 5.3.2
./Heterogeneity/fract45.par      \ Input parameter file for gamv2, 45-degree fracture set, Section 5.3.2
./Heterogeneity/fract45.dat      \ Output permeability field, 45-degree fracture set, Section 5.3.2
./Heterogeneity/fract90.par      \ Input parameter file for gamv2, 90-degree fracture set, Section 5.3.2
./Heterogeneity/fract90.dat      \ Output permeability field, 90-degree fracture set, Section 5.3.2
./Heterogeneity/fractm45.par     \ Input parameter file for gamv2, -45-degree fracture set, Section 5.3.2
./Heterogeneity/fractm45.dat     \ Output permeability field, -45-degree fracture set, Section 5.3.2
./Heterogeneity/sh.2dcont        \ Unix shell script file used to generate permeability field for FCM
./Heterogeneity/sh.2dfract       \ Unix shell script file used to generate permeability field for DFNM
./Heterogeneity/var              \ Dummy TOUGH2 input file used for variogram model matching, Section 6.3.2
./Heterogeneity/vari             \ iTOUGH2 input file used for variogram model matching, Section 6.3.2
./Heterogeneity/vari.out         \ iTOUGH2 input file used for variogram model matching, Section 6.3.2, Figure 17
                                 \
./LRT/ThresGS_het-2d             \ TOUGH2 input file for 2d-heterogeneous grid search of seepage threshold, Section 6.6
./LRT/ThresGS_het-2di            \ iTOUGH2 input file for 2d-heterogeneous grid search of seepage threshold, Section 6.6
./LRT/ThresGS_het-2di.out        \ iTOUGH2 output file for 2d-het. grid search of seepage threshold, Section 6.6, Figure 25
./LRT/ThresGS_hom-2d             \ TOUGH2 input file for 2d-homogeneous grid search of seepage threshold, Section 6.6
./LRT/ThresGS_hom-2di            \ iTOUGH2 input file for 2d-homogeneous grid search of seepage threshold, Section 6.6
```

```
./LRT/ThresGS_hom-2di.out    \ iTOUGH2 output file for 2d-hom. grid search of seepage threshold, Section 6.6, Figure 24
./LRT/ThresGS_hom-3d         \ TOUGH2 input file for 3d-homogeneous grid search of seepage threshold, Section 6.6
./LRT/ThresGS_hom-3di        \ iTOUGH2 input file for 3d-homogeneous grid search of seepage threshold, Section 6.6
./LRT/ThresGS_hom-3di.out    \ iTOUGH2 output file for 3d-hom. grid search of seepage threshold, Section 6.6, Figure 26
./LRT/ThresGS_het-3d         \ TOUGH2 input file for 3d-heterogeneous grid search of seepage threshold, Section 6.6
./LRT/ThresGS_het-3di        \ iTOUGH2 input file for 3d-heterogeneous grid search of seepage threshold, Section 6.6
./LRT/ThresGS_het-3di.out    \ iTOUGH2 output file for 3d-het. grid search of seepage threshold, Section 6.6, Figure 27
./LRT/Thres_het-2d           \ TOUGH2 input file for 2d-heterogenous MC simulations of threshold, Section 6.6
./LRT/Thres_het-2di          \ iTOUGH2 input file for 2d-heterogenous MC simulations of threshold, Section 6.6
./LRT/Thres_het-2di.out      \ iTOUGH2 output file for 2d-heterogenous MC simulations of threshold, Section 6.6, Figure 25
./LRT/Thres_hom-2d           \ TOUGH2 input file for 2d-homogeneous MC simulations of threshold, Section 6.6
./LRT/Thres_hom-2di          \ iTOUGH2 input file for 2d-homogeneous MC simulations of threshold, Section 6.6
./LRT/Thres_hom-2di.out      \ iTOUGH2 output file for 2d-homogeneous MC simulations of threshold, Section 6.6, Figure 24
./LRT/UM442_0-2d             \ TOUGH2 input file for 2d-homogeneous liquid-release test UM 4.42, Section 6.4
./LRT/UM442_0-2di            \ iTOUGH2 input file for 2d-homogeneous liquid-release test UM 4.42, Section 6.4
./LRT/UM442_0-2di.out        \ iTOUGH2 output file for 2d-homogeneous liquid-release test UM 4.42, Section 6.4, Tables 9, 10
./LRT/UM442_0-3d             \ TOUGH2 input file for 3d-homogeneous liquid-release test UM 4.42, Section 6.4
./LRT/UM442_0-3di            \ iTOUGH2 input file for 3d-homogeneous liquid-release test UM 4.42, Section 6.4
./LRT/UM442_0-3di.out        \ iTOUGH2 output file for 3d-homogeneous liquid-release test UM 4.42, Section 6.4, Tables 9, 10
./LRT/UM442_3ss-2d           \ TOUGH2 input file for 2d-heterogeneous steady-state run, Section 6.4
./LRT/UM442_3-2d.inc         \ Initial condition file for 2d-heterogeneous runs (output from UM442_3ss-2d), Section 6.4
./LRT/UM442_3-2d             \ TOUGH2 input file for 2d-heterogeneous liquid-release test UM 4.42, Section 6.4
./LRT/UM442_3-2di            \ iTOUGH2 input file for 2d-heterogeneous liquid-release test UM 4.42, Section 6.4
./LRT/UM442_3-2di.out        \ iTOUGH2 output file for 2d-het. liquid-release test UM 4.42, Section 6.4, Tables 9, 10
./LRT/UM442_3ss-3d           \ TOUGH2 input file for 3d-heterogeneous steady-state run, Section 6.4
./LRT/UM442_3-3d.inc         \ Initial condition file for 3d-heterogeneous runs (output from UM442_3ss-2d), Section 6.4
./LRT/UM442_3-3d             \ TOUGH2 input file for 3d-heterogeneous liquid-release test UM 4.42, Section 6.4
./LRT/UM442_3-3di            \ iTOUGH2 input file for 3d-heterogeneous liquid-release test UM 4.42, Section 6.4
./LRT/UM442_3-3di.out        \ iTOUGH2 output file for 3d-het. liquid-release test UM 4.42, Section 6.4, Tables 9, 10
./LRT/UM564_0-2d             \ TOUGH2 input file for 2d-homogeneous validation run, Section 6.5
./LRT/UM564_0-2di            \ iTOUGH2 input file for 2d-homogeneous validation run, Section 6.5
./LRT/UM564_0-2di.out        \ iTOUGH2 output file for 2d-homogeneous validation run, Section 6.5, Figure 20
./LRT/UM564_0-2di.tec        \ iTOUGH2 output file for 2d-homogeneous validation run, Section 6.5, Figure 20
./LRT/UM564_1-2d             \ TOUGH2 input file for 2d-heterogeneous validation run, Section 6.5
./LRT/UM564_1-2d.inc         \ Initial condition file for 2d-heterogeneous validation run, Section 6.5
./LRT/UM564_1-2di            \ iTOUGH2 input file for 2d-heterogeneous validation run, Section 6.5
./LRT/UM564_1-2di.out        \ iTOUGH2 output file for 2d-heterogeneous validation run, Section 6.5, Figure 21
./LRT/UM564_1-2di.tec        \ iTOUGH2 output file for 2d-heterogeneous validation run, Section 6.5, Figure 21
./LRT/UM564_0-3d.inc         \ Initial condition file for 3d-homogeneous validation run, Section 6.5
./LRT/UM564_0-3d             \ TOUGH2 input file for 3d-homogeneous validation run, Section 6.5
./LRT/UM564_0-3di            \ iTOUGH2 input file for 3d-homogeneous validation run, Section 6.5
./LRT/UM564_0-3di.out        \ iTOUGH2 output file for 3d-homogeneous validation run, Section 6.5, Figure 22
```

```
./LRT/UM564_0-3di.tec          \ iTOUGH2 output file for 3d-homogeneous validation run, Section 6.5, Figure 22
./LRT/UM564_1-3dss             \ TOUGH2 input file for 3d-heterogeneous steady-state run, Section 6.5
./LRT/UM564_1-3d.inc           \ Initial condition file for 3d-heterogeneous validation run, Section 6.5
./LRT/UM564_1-3d               \ TOUGH2 input file for 3d-heterogeneous validation run, Section 6.5
./LRT/UM564_1-3di              \ iTOUGH2 input file for 3d-heterogeneous validation run, Section 6.5
./LRT/UM564_1-3di.out          \ iTOUGH2 output file for 3d-heterogeneous validation run, Section 6.5, Figure 23
./LRT/UM564_1-3di.tec          \ iTOUGH2 output file for 3d-heterogeneous validation run, Section 6.5, Figure 23
./LRT/sh.LRT2d                 \ Unix shell script file used for running 2d liquid-release test calibrations
./LRT/sh.LRT3d                 \ Unix shell script file used for running 3d liquid-release test calibrations
./LRT/sh.THR2d                 \ Unix shell script file used for running 2d MC simulations of seepage threshold
./LRT/sh.THRGS2d               \ Unix shell script file used for running 2d grid searches of seepage threshold
./LRT/sh.THRGS3d               \ Unix shell script file used for running 3d grid searches of seepage threshold
./LRT/sh.VAL2d                 \ Unix shell script used for running 2d validation cases
./LRT/sh.VAL3d                 \ Unix shell script used for running 3d validation cases
                               \
./Meshgeneration/MESH2d        \ 2d mesh file for FCM
./Meshgeneration/MESH2dSS      \ 2d mesh file for FCM, for steady-state runs
./Meshgeneration/MESH2dUM442_0 \ 2d mesh file for test UM 4.42, homogeneous
./Meshgeneration/MESH2dUM442_0SS \ 2d mesh file for test UM 4.42, homogeneous, for steady-state runs
./Meshgeneration/MESH2dUM442_3 \ 2d mesh file for test UM 4.42, heterogeneous
./Meshgeneration/MESH2dUM442_3SS \ 2d mesh file for test UM 4.42, heterogeneous, for steady-state runs
./Meshgeneration/MESH2dUM564_0 \ 2d mesh file for test UM 5.64, homogeneous
./Meshgeneration/MESH2dUM564_0SS \ 2d mesh file for test UM 5.64, homogeneous, for steady-state runs
./Meshgeneration/MESH2dUM564_1 \ 2d mesh file for test UM 5.64, heterogeneous
./Meshgeneration/MESH2dUM564_1SS \ 2d mesh file for test UM 5.64, heterogeneous, for steady-state runs
./Meshgeneration/MESH2dfract   \ 2d mesh file for DFNM
./Meshgeneration/MESH2dfractAK \ 2d mesh file for DFNM, for air injection simulations
./Meshgeneration/MESH2dfractNoNiche \ 2d mesh file for DFNM, for run DFNMperm
./Meshgeneration/MESH2dfractSS \ 2d mesh file for DFNM, for steady-state runs
./Meshgeneration/MESH3dUM442_0 \ 3d mesh file for test UM 4.42, homogeneous
./Meshgeneration/MESH3dUM442_0SS \ 3d mesh file for test UM 4.42, homogeneous, for steady-state runs
./Meshgeneration/MESH3dUM564_0 \ 3d mesh file for test UM 5.64, homogeneous
./Meshgeneration/MESH3dUM564_0SS \ 3d mesh file for test UM 5.64, homogeneous, for steady-state runs
./Meshgeneration/mesh2d        \ TOUGH2 input file to generate basic 2d mesh for FCM
./Meshgeneration/mesh2dfract   \ TOUGH2 input file to generate basic 2d mesh for DFNM
./Meshgeneration/mesh2dlrt     \ TOUGH2 input file to generate basic 2d mesh for calibration/validation
./Meshgeneration/mesh3d        \ TOUGH2 input file to generate basic 3d mesh
./Meshgeneration/onestep       \ TOUGH2 input file to run a single time step
./Meshgeneration/sh.mesh2d     \ Unix shell script file used to generate 2d-mesh for FCM
./Meshgeneration/sh.mesh2dfract \ Unix shell script file used to generate 2d-mesh for DFNM
./Meshgeneration/sh.mesh2dlrt  \ Unix shell script file used to generate 2d-mesh for calibration/validation
./Meshgeneration/sh.mesh3d     \ Unix shell script file used to generate 3d-mesh for calibration/validation
```

```
./Meshgeneration/sh.onestep          \ Unix shell script file used to run a single time step
                                     \
| compress > U0080.tar.Z            \ Compressed tar file containg all files listed above
```